Applications of practical process modeling based on statistics, multivariate analysis, and simulation in pharmaceutical development

Doctoral thesis submitted in the partial fulfilment of the requirements for the degree of Doctor in Natural Sciences at Kiel University, Germany

By

Shuichi Tanabe

Kiel 2018

Referee	Prof. Dr. Regina Scherließ
Co-Referee	PD Dr. Nora Anne Urbanetz
Date of Exam	20.11.2018
Accepted for Publication	20.11.2018

sgd. Prof. Dr. Frank Kempken

List of publications contributing to the present thesis

Shuichi Tanabe, Srikanth Gopireddy, Hidemi Minami, Shuichi Ando, Nora A. Urbanetz, Regina Scherließ. Qualitative and quantitative prediction of blend uniformity based on discrete element method. Eur. J. Pharm. Sci. (under peer reviewing)

Shuichi Tanabe, Hiroshi Nakagawa, Tomoyuki Watanabe, Hidemi Minami, Shuichi Ando, Nora A. Urbanetz, Regina Scherließ. Selection of a round convex tablet shape that mitigates the risk of chipping and capping based on systematic evaluation by utilizing multivariate analysis. Eur. J. Pharm. Sci. (2018) 120, 212-221

Shuichi Tanabe, Hiroshi Nakagawa, Tomoyuki Watanabe, Hidemi Minami, Manabu Kano, Nora A. Urbanetz. Setting the process parameters for the coating process in order to assure tablet appearance based on multivariate analysis of prior data. Int. J. Pharm. (2016) 511, 341–350

Shuichi Tanabe, Takuya Miyano, Jin Maeda, Hiroshi Nakagawa, Tomoyuki Watanabe, Hidemi Minami, Nora A. Urbanetz. Scientific rationale for sampling regimen and acceptance criteria of blend uniformity based on Monte Carlo simulation. Powder Technol. (2016) 301, 336–341

Conference participation – oral presentations

Shuichi Tanabe, Srikanth R. Gopireddy, Shuichi Ando, Hidemi Minami, Nora A. Urbanetz, Regina Scherlieβ. Prediction of Blend Uniformity by utilizing Discrete Element Method simulation. 2018 AIChE Annual Meeting, Pittsburgh, United States (2018)

Shuichi Tanabe, Srikanth R. Gopireddy, Hidemi Minami, Shuichi Ando, Nora A. Urbanetz, Regina Scherließ. Qualitative evaluation of blend uniformity by discrete element method simulation. The 34th Symposium on Particulate Preparations and Designs, Kitakyushu, Japan (2017)

Shuichi Tanabe, Hiroshi Nakagawa, Tomoyuki Watanabe, Naoki Wakiyama. Process parameters optimization for the coating process in order to assure tablet appearance based on multivariate analysis of prior data. 134th Annual Meeting of the Pharmaceutical Society of Japan, Kumamoto, Japan (2014)

Conference participation – poster presentations

Shuichi Tanabe, Srikanth R. Gopireddy, Hidemi Minami, Shuichi Ando, Regina Scherlieβ, Nora A. Urbanetz. Blend uniformity prediction based on discrete element method simulation. 11th World Meeting on Pharmaceutics, Biopharmaceutics and Pharmaceutical Technology, Granada, Spain (2018)

Shuichi Tanabe, Nora A. Urbanetz. Scientific rationale for sampling procedure and acceptance criteria of blend uniformity based on Monte Carlo simulation. 10th World Meeting on Pharmaceutics, Biopharmaceutics and Pharmaceutical Technology, Glasgow, Scotland (2016)

Shuichi Tanabe, Hiroshi Nakagawa, Tomoyuki Watanabe, Hidemi Minami. Multivariate analysis for coating process optimization. AAPS Annual Meeting, San Diego, United States (2014)

Awards

Hiroshi Nakagawa, Yoshito Kikkawa, Kazuhiro Matsuura, Shuichi Tanabe, Tomoyuki Watanabe. Implementation of Enhanced QbD to Drug Product Development. The 15th NAKAI Award of the Japan Society of Pharmaceutical Machinery and Engineering (2015)

Shuichi Tanabe, Satoko Yoshimatsu, Kenjirou Higashi, Kunikazu Moribe, Keiji Yamamoto. Solid state NMR investigation into the mechanism of indomethacin nanoparticle formation by co-grinding with β-cyclodextrin. The Asian Federation for Pharmaceutical Sciences (AFPS) Nagai-Shukri Pre-Doctoral Oral and Poster Presentation Award (2009)

List of publications not contributing to the present thesis

Kensaku Matsunami, Shuichi Tanabe, Hiroshi Nakagawa, Masahiko Hirao, Hirokazu Sugiyama. Economic Evaluation of Batch and Continuous Manufacturing Technologies for Solid Drug Products during Clinical Development. Computer Aided Chemical Engineering. (2018) 44, 2131-2136

Ryosuke Yoshizaki, Manabu Kano, Shuichi Tanabe, Takuya Miyano. Process Parameter Optimization based on LW-PLS in Pharmaceutical Granulation Process. IFAC-PapersOnLine. (2015) 48-8, 303–308

Shuichi Tanabe, Kenjirou Higashi, Makoto Umino, Waree Limwikrant, Keiji Yamamoto, Kunikazu Moribe. Yellow coloration phenomena of incorporated indomethacin into folded sheet mesoporous materials. Int. J. Pharm. (2012) 429, 38-45

Table of contents

Introduction

Pharmaceutical oral solid dosage forms such as tablets, capsules, and granules are generally mass-produced. The manufacture of the drug products include blending of one or more active ingredients and functional excipients, granulation of the powder blend to provide a better handling in the following unit operations, unit dosing of the final blend, i.e., tableting, encapsulating, or bottle filling, and coating of the tablets if needed. Manufacturing process development of drug products has to be based on a scientific rationale as the process conditions do affect the drug product quality. Traditionally, process validation is performed by demonstrating a successful manufacture of three consecutive commercial scale batches at the target manufacturing conditions. However, from a process control point of view, the traditional process validation approach is insufficient as to ensure consistency of quality in commercial production runs. Regulatory agencies, universities, and pharmaceutical industries acknowledged that a comprehensive understanding of the relationship between manufacturing conditions and the resultant drug product quality should be investigated prior to selecting target manufacturing conditions, and a systematic control strategy of the process should be established based on the identified relationship between the manufacturing conditions and drug product quality[1, 2].

In 2010, a guideline regarding a systematic approach on establishing the control strategy of the pharmaceutical drug product manufacturing process, defined as Quality by Design (QbD) approach, was published by the International Conference on Harmonisation of Technical Requirements for Registration of Pharmaceuticals for Human Use (ICH); ICH Q8 (R2)[3]. The systematic approach to the manufacturing process development should begin with defining the objectives as the Quality Target Product Profile (QTPP), and proceed with product and process understanding and process control to satisfy the target quality, based on a scientific rationale including quality risk management. A typical example of this activity is to control process risk factors selected by preliminary risk assessment on the drug product quality based on a process model, typically derived from a Design of Experiments (DoE). DoE is defined as a structured, organized method for determining the relationship between

[1] Food and Drug Administration, 2011. Guidance for Industry, Process Validation: General Principles and Practices.

[2] European Medicines Agency, 2016. Guideline on process validation for finished products - information and data to be provided in regulatory submissions.

[3] International Conference on Harmonisation of Technical Requirements for Registration of Pharmaceuticals for Human Use, 2009. Pharmaceutical Development Q8 (R2).

factors affecting a process and the output of that process[3, 4]. This process modeling approach can provide a comprehensive understanding of the process by providing a numerical relationship between the process condition and the resultant drug product quality[5]. Setting acceptable ranges of process parameters based on the process model, e.g., design space or normal operating ranges (NORs) by ensuring the desired drug product quality, should provide a higher assurance of the drug product quality.

Currently, DoE is a common and standard approach in developing a process model in pharmaceutical industry because of its simplicity and the recommendation from authorities. In general, it starts with the selection of input parameters that potentially affect the output parameters to be controlled. Following to the first step a screening DoE, which is to distinguish which of the many input parameters really affect the output parameters, is performed as the second step by using a highly fractionated design, e.g., focus on the main effect of the input parameters, to reduce the number of experiments. And in the third step, a less fractionated DoE, i.e., factorial or response surface experiments, are performed where the effect of interaction and quadratic terms of the input parameters on the output parameters can be analyzed in addition to the main effects. Less fractionated DoEs can capture the curvilinear correlations between the input and output parameters by considering the quadratic terms though it cannot capture the nonlinearity in a general sense, therefore it will provide a higher prediction accuracy compared to the model developed in the screening DoE. In general, the least squares regressions derived from the third step are utilized for process development and control. Due to the simplicity in analyzing the cause and effect relationship, the DoE based process modeling is being the first option in the pharmaceutical industry[6, 7, 8].

One common drawback of the DoE based approach is the resources required to develop a reliable model for commercial manufacture. Even at a fractionated DoE, a response surface experiment such

---

[4] Yu, L.X., 2008. Pharmaceutical Quality by Design: Product and Process Development, Understanding, and Control. Pharm. Res. 25, 4, 781–791.

[5] Huang, J., Kaul, G., Cai, C., Chatlapalli, R., Hernandez-Abad, P., Ghosh, K., Nagi, A., 2009. Quality by design case study: An integrated multivariate approach to drug product and process development. Int. J. Pharm. 382, 23–32.

[6] Rajalahti, T., Kvalheim, O.M., 2011. Multivariate data analysis in pharmaceutics: a tutorial review. Int. J. Pharm. 417, 280–290.

[7] Teckoe, J., Mascaro, T., Farrell, T.P., Rajabi-Siahboomi, A.R., 2013. Process optimization of a novel immediate release film coating system using QbD principles. AAPS Pharm. Sci. Technol. 14, 531–540.

[8] Zacour, B.M., Drennen, J.K., Anderson, C.A., 2012. Development of a fluid bed granulation design space using critical quality attribute weighted tolerance intervals. J. Pharm. Sci. 101, 2917–2929.

as Box-Behnken design requires 15 runs for 3 input parameters[9, 10]. While it is also possible to develop a DoE based process model based on experiments conducted at laboratory or pilot scale, it needs to be verified at commercial scale in setting the NORs based on the process model[11]. If the input parameters and output parameters are scale-independent, the verification studies at commercial scale can be minimized. However, the scalability of input and output parameters, i.e., the degree of scale dependency, has to be taken into account in most of the industrial processes. For example, in a fluid bed granulation process where binder solution is sprayed onto the powders fluidized by a heated airflow, the heat loss efficiency from the surface of the equipment, which is critical to the process performance, is dependent on the size and design of the fluid bed granulator[12, 13]. The spraying time and spray rate are also scale-dependent, and are known to affect the particle size distribution. Further, the location of the heat sensor is different between equipment, which can affect the monitored inlet and exhaust air temperatures. The other processes also tend to show scale-dependent relationships, and even though a scale-independent monitoring parameter, e.g., in-line NIR monitoring of the materials properties, is selected as outputs, the challenge of scale dependency remain. Hence in setting the design space and NORs of the process parameters to assure the desired quality in a scale-dependent process, the process parameters need to be challenged even the process model was developed in a laboratory or pilot scale, which require huge resources in general.

The other problem in utilizing a DoE is that it cannot solve multicollinearity problems. Multicollinearity, which is a common issue in industrial processes when having multiple input parameters, is defined as the situation where the input parameters are interdependent. Under a multicollinearity situation, an effect of an input parameter on the output parameter is not attributed solely to the contribution of that single input parameter. This is because the change of the input parameter restricted the other input parameters' range at the same time. As a result, it can increase the

---

[9] Ferreira, S.L.C., Bruns, R.E., Ferreira, H.S. Matos, G.D., David, J.M., Brandão, G.C., da Silva, E.G.P., Portugal, L.A., dos Reis, P.S., Souza, A.S., dos Santos, W.N.L., 2007. Box-Behnken design: An alternative for the optimization of analytical methods. Anal. Chim. Acta 597, 179–186.

[10] Candioti, L.V., De Zan, M.M., Cámara, M.S., Goicoechea, H.C., 2014. Experimental design and multiple response optimization. Using the desirability function in analytical methods development. Talanta124, 123–138.

[11] Food and Drug Administration and European Medicines Agency, 2013. Questions and Answers on Design Space Verification.

[12] Larsen, C.C., Sonnergaard, J.M., Bertelsen, P., Holm, P., 2003. A new process control strategy for aqueous film coating of pellets in fluidised bed. Eur. J. Pharm. Sci. 20, 273–283.

[13] am Ende, M.T., Berchielli, A., 2005. A thermodynamic model for organic and aqueous tablet film coating. Pharm. Dev. Technol. 1, 47–58.

variance of the coefficient estimates and make the outputs highly responsive to slight changes of the inputs in the model, which can deteriorate prediction accuracy[14, 15]. Even when developing a process model using independent process parameters only to avoid the overfitting, the effect of the excluded process parameters that are correlated with the input process parameters in the model cannot be described although it affect to the outputs. In addition to that, performing DoE at a sufficiently wide range to assure the robustness of the process is often not applicable due to the practical manufacturability if multicollinearity of the process parameters exists.

Computer-aided process modeling such as population balance models and numerical models are alternative approaches that potentially reduce the resources required in process modeling. In the population balance model, phenomena to describe changes in physical and chemical properties of materials are expressed and the dynamic changes are calculated by first principles under a conservation law. For example, a thermodynamic model to predict moisture content of materials in fluid bed granulation and tablet film coating processes is one of the population balance models described in solid oral dosage form manufacturing[12, 13]. While a population balance model is usually independent of equipment and formulation, in order to improve the prediction accuracy in a given equipment and formulation fitting parameters are sometimes added in the first principles[13, 16, 17]. The numerical model approach is an emerging, compute-intensive technique computing motions, deformations, and heat transfers of a large number of small particles, fluids, or a continuum on the basis of forces acting on each component and gas flow. With the increasing computational capabilities over the last years, the computationally intensive in-silico experiments using Discrete Element Method (DEM) are becoming an important tool to understand production processes containing particles such as particle packing, particle flow, and particle-fluid flow[18, 19]. The advantage of DEM is that it is able to capture

---

[14] Burnham, A.J., Viveros, R., MacGregor, J.F., 1996. Frameworks for latent variable multivariate regression. J. Chemom. 10, 31–45.

[15] Höskuldsson, A., 1988. PLS regression methods. J. Chemom. 2, 211–228.

[16] Sen, M., Singh, R., Vanarase, A., John, J., Ramachandran R., 2012. Multi-dimensional population balance modeling and experimental validation of continuous powder mixing processes. Chem. Eng. Sci. 80, 349–360.

[17] Barrasso, D., El Hagrasy, A, Litster, J.D., Ramachandran, R., 2015. Multi-dimensional population balance model development and validation for a twin screw granulation process. Powder Technol. 270, 612–621.

[18] Zhu, H.P., Zhou, Z.Y., Yang, R.Y., Yu, A.B., 2007. Discrete particle simulation of particulate systems: theoretical developments. Chem. Eng. Sci. 62, 3378–3396.

[19] Zhu, H.P., Zhou, Z.Y., Yang, R.Y., Yu, A.B., 2008. Particle simulation of particulate systems: A review of major applications and findings. Chem. Eng. Sci. 63, 5728–5770.

the trajectory of each individual particle in the system through Newton's equation of motion, by calculating the new positions and velocities of the particles based on the forces acting on them at a defined time step. However, in most of the previous studies the particle size and the geometry of equipment were far away from the practical manufacturing process[19, 20]. As a matter of fact, it is still not feasible to simulate >1 kg scale processes containing particles of ~100 μm in diameter ending up with more than ca. 10^8 particles, since it requires huge computational time. It was reported that even a simulation of a blending process containing 225,000 particles over a span of 2 minutes in a V-blender required a few weeks of CPU time on a Beowulf cluster[20]. Due to the fact that DEM simulation is a compute-intensive technique, prediction models typically are limited to the evaluation of laboratory scale experiments. Up to now the quantitative prediction of larger scales by DEM, which is required to utilize the model for identifying the acceptable ranges of the process conditions, i.e., NORs, is not addressed yet.

Further statistical process modeling approaches based on the experimental data set are also available and they have a potential to resolve the multicollinearity problem. Among the chemometric techniques, partial least squares regression (PLSR) has been utilized for description and control of multivariate processes in the pharmaceutical industry because of the high prediction accuracy[21, 22, 23]. The advantage of the PLSR is that it can generate latent variables, which are independent of each other, and cope with mutually correlated input variables[24]. By selecting appropriate latent variables a multivariate problem that existed in the dataset can be avoided in the PLSR, resulting in a higher prediction accuracy compared to the least squares regression used in DoE based process modeling. Further, as it can avoid multicollinearity problem by selecting appropriate latent variables, a fixed experimental design required in DoE is not necessarily needed in the PLSR model. Therefore it has the potential to provide a commercial scale process model with sufficiently wide parameter ranges

---

[20] Lemieux, M., Léonard, G., Doucet, J., Leclaire, L.A., Viens, F., Chaouki, J., Bertrand, F., 2008. Large-scale numerical investigation of solids mixing in a V-blender using the discrete element method. Powder Technol. 181, 205–216.

[21] Gabrielsson, J., Lindberg, N, Lundstedt, T., 2002. Multivariate methods in pharmaceutical applications. J. Chemometrics 16, 141-160.

[22] Haware, R.V., Tho, I., Bauer-Brandl, A., 2009. Multivariate analysis of relationships between material properties, process parameters and tablet tensile strength for a-lactose monohydrates. 73, 424–431.

[23] Muteki, K., Yamamoto, K., Reid, G.L., Krishnan, M., 2011. De-risking scale-up of a high shear wet granulation process using latent variable modeling and near-infrared spectroscopy. J. Pharm. Innov. 6, 142–156.

[24] Kano, M., Nakagawa, Y., 2008. Data-based process monitoring, process control, and quality improvement: recent developments and applications in steel industry. Comput. Chem. Eng. 32, 12–24.

even at a process where a multicollinearity problem exists. While the higher prediction accuracy and the utilization of the prediction model such as the sensitivity analysis of the input parameters have been demonstrated, its applicability to pharmaceutical process development studies such as the optimization of a commercial scale process and its control, i.e., setting of acceptable process parameter ranges, has not been reported in literature. To facilitate the use of the PLSR model in the pharmaceutical development, further understanding of the PLSR modeling including its benefit and limitation is required.

When it comes to the process modeling method selection, it becomes important whether it is possible to prepare a large number of manufacturing data performed at different manufacturing conditions with reasonable cost, especially at commercial scale, or not. In general, a large-scale batch process such as wet granulation, blending, and coating requires a huge amount of resources to prepare manufacturing results performed at different conditions, which would be needed to develop a process model based on a conventional DoE approach. As resources are limited such a huge number of experiments is sometimes unacceptable even when leveraging the benefit of the factorial design to reduce the number of experiments, therefore a practicable, cost-effective process modeling approach is needed to implement the QbD concept in large-scale batch processes. One alternative and innovative process modeling approach to the DoE in order to reduce the amount of experiments is the process simulation based on numerical methods such as DEM. However, in a process that can provide several manufacturing data performed at different manufacturing conditions with reasonable cost, e.g., a small-scale batch process and a continuous process such as dry granulation, tableting, and encapsulation, actual experiments still have an advantage over the simulation as they can provide faster development speed due to the currently limited computing capacity. In these cases, a statistical process modeling based on the PLSR could be a practicable alternative to the conventional DoE based process modeling, since it can avoid the multicollinearity problems and hence it is expected to provide a higher prediction accuracy and a wider assurance range of the process parameters. However, the actual application has not been reported yet.

In summary, currently there are two challenges in process modeling and the utilization for process development and control:

- First, a method to develop a quantitative process model which does not require a huge amount of data or computational time needs to be established for a practicable, cost-effective process modeling of a large-scale batch process.
- Second, while a method to develop a prediction model based on multivariate analysis that can cope with the multivariate process is already available, the practical utilization for process optimization and control needs to be developed for a small-scale batch process and a continuous process.

In order to facilitate process modeling and utilization, this thesis is addressing those two challenges

through four case studies; two case studies in a batch blending process, one case study in a continuous tableting process, and one case study in a batch coating process.

Aim of work and thesis outline

This thesis aims at providing practicable, reliable, and cost-effective process modeling approaches applied to both a large-scale batch process and a continuous process. As the challenges in process modeling are different between a large-scale batch and a small-scale batch or a continuous process, different process modeling approaches are explored through the four case studies.

In **case study 1**, process modeling is demonstrated in a batch blending process utilizing DEM. A batch blending process can be expressed as the reorientation of each and every particle existing in a blender container caused by the mechanical forces and intended to assure the desired blend uniformity of active ingredient to satisfy the critical quality attribute (CQA) of content uniformity. As the blending process is known to have a high scalability[25], the numerical process modeling and simulation utilizing DEM can be potentially a beneficial approach in understanding the process cost-effectively. Adam et al. suggested a potential to predict blend uniformity qualitatively based on DEM simulation[26]. Also, the quantitative prediction of blend uniformity, which is a key output parameter of the blending process has not been addressed yet, due to the huge computational time in simulating >1 kg blending process containing particles of ~100 μm in diameter. Herein for the first time, a quantitative prediction model for blend uniformity with reduced computational time was developed for the blending process understanding and controls.

To provide a reasonable process control of the blending process in order to assure the blend uniformity, the sampling regimen, which is the combination of sampling locations and the number of samples from each sampling location, and the acceptance criteria need to be defined with a scientific rationale together with the process model derived from case study 1. However, there are little publication how to correlate the key factors, i.e., the sampling regimen and the acceptance criteria in blend uniformity analysis, and the resultant assurance level of the bulk blend homogeneity, even the regulatory agencies emphasized to provide a scientific rationale of the sampling regimen and the acceptance criteria in blend uniformity analysis (BUA)[27, 28]. Therefore in **case study 2** the relationship between the sampling regimen and acceptance criteria on the assurance level of the content uniformity

---

[25] Levin, M., 2001. Pharmaceutical Process Scale-Up. Marcel Dekker Inc..

[26] Adam, S., Suzzi, D., Radeke, C., Khinast, J.G., 2011. An integrated Quality by Design (QbD) approach towards design space definition of a blending unit operation by Discrete Element Method (DEM) simulation. Eur. J. Pharm. Sci. 42, 106–115.

[27] Food and Drug Administration, 2013. Questions and Answers on Current Good Manufacturing Practices, Good Guidance Practices, Level 2 Guidance—Production and Process Controls.

[28] Bergum, J.S., Prescott, J.K., Tejwani, R.W., Garcia, T.P., Clark, J., Brown, W., 2014. Current event in blend and content uniformity, Pharm. Eng. 34, 1–10.

is evaluated based on Monte Carlo simulation and the resultant conditional probability analysis.

In contrast, for the small-scale batch process and the continuous process with multicollinearity problem, an alternative statistical process modeling needs to be developed as the multicollinearity can deteriorate the prediction accuracy and interfere with the comprehensive evaluation of the process by limiting the species and range of input parameters. Hence to facilitate a process development and control comprehensively with an accurate process model even in a process where multicollinearity exists, statistical process modeling based on PLSR was demonstrated for the continuous tableting process in **case study 3**. While the tableting process is well understood already, an effect of tablet shape on the tablet's physical robustness, which is a critical quality attribute of the tablet appearance, is not well addressed due to the multicollinearity problem. Tablet shape parameters, i.e., diameter, cup depth, surface radius, determine the tablet shape. At the same time, the tablet shape parameters have constraints in order to build a smooth convex cup portion. Herein the practicability of the PLSR model and the application for multivariate process optimization is demonstrated through the tablet shape design in case study 3.

Further, an innovative, cost-effective approach of statistical process modeling was demonstrated in **case study 4**. A common drawback of the statistical process modeling, e.g., DoE and PLSR, is the resources required to generate a sufficient amount of experimental data to build a model with high prediction accuracy. The coating process is a typical batch process, where coating suspension is sprayed onto tablet cores in a rotating drum that are in turn blown dry with a heated drying airflow. The moisture content of the spray mist and/or the tablets are considered most decisive for the quality such as tablet appearance in the coating process. As the input parameters such as inlet air temperature, inlet air volume, and spray rate are mutually correlated to the moisture content, the coating process is considered as a process with a multicollinearity problem. Theoretically, exhaust air temperature, which is known to correlate with moisture content during the coating process, can be modeled based on thermodynamics[13]. Although this thermodynamics based modeling should be cost-effective compared to the DoE based modeling or PLSR modeling, as the heat transfer coefficient from the drying air to the droplets and/or tablets depends on equipment and the operating conditions, a couple of experiments to estimate the heat transfer coefficient of a given coating equipment at the target condition is needed to predict the moisture content in the existing thermodynamic model. Because of this, the semi-empirical thermodynamic model does not contribute to decreasing the cost required to develop a prediction model. A significant workload reduction could be attained if prior knowledge (such as existing product batch records) is fully utilized for product-independent process modeling and optimization if the multicollinearity problem is appropriately managed. Since the PLSR does not require a fixed experimental design like DoE, prior knowledge such as the past manufacturing data of other drug products using similar equipment might be applicable for the product independent process modeling. Herein, in case study 4 a PLSR model that uses process conditions to predict exhaust air

temperature was developed based on prior knowledge and the prediction accuracy was compared with that of the conventional semi-empirical thermodynamic model. At the same time, the practicability of the PLSR model for process optimization was demonstrated.

The thesis is finished by an overall discussion emphasizing advantages and limitations of the described methods for implementation in pharmaceutical development and will give an outlook into future opportunities to speed up and create lean development and validation procedures.

Case study 1 - Qualitative and quantitative prediction of blend uniformity in a binary granular mixture based on DEM simulation

Submitted to European Journal of Pharmaceutical Sciences on 18 July 2018, current status: under review (responsible editor: Martin Brandl, Dr. rer. nat. habil, Editor In Chief)

Outline

Efficient and effective, product-independent process modeling that uses process parameters to predict the CQAs is addressed in a batch blending process utilizing DEM simulation. The advantage of a theoretical model compared to an experimental model derived from regression analysis of existing data is that it could explain the cause and the effect clearly without a large quantity of experimental data. As heat production and/or absorption can be neglected in a diffusion blending where a gentle powder flow is generated by the rotation of the blender bin, a process model that uses the physical properties of particles and the process parameters such as rotation speed and blending time to predict the blend uniformity might be able to develop by utilizing DEM. The aim of this case study is to develop a quantitative process model of a blending process to predict blend uniformity by DEM, which has never been addressed before. Potential applications of the DEM process model of the blending process for the efficient process development and validation are also discussed together with the outcomes obtained through the second case study.

Abstract

The blending process of a binary granular mixture, active and placebo granules, in a bin blender was simulated using the Discrete Element Method (DEM). Three 10 kg blending experiments differentiated by the physical properties specifically particle size of granules were performed as reference for DEM simulations. Segregation of active granules in the blender was observed during diffusion blending. The segregation behavior was common for all blends, while the sample Blend Uniformity (BU), i.e., standard deviation of active ingredient content % was different among the three blends reflecting segregation due to the particle size differences between the components. Quantitative prediction of the sample BU probability density distribution in reality based on the DEM simulation results was successfully demonstrated. The average root mean square error normalized by the mean (nRMSE) of the mean sample BU in the blends was 0.228. In this study, it was demonstrated that the sample BU at given granule properties can be predicted with feasible prediction accuracy. Therefore, these in-silico experiments through DEM simulations would help in setting a reliable "edge of failure" specification with respect to the particle size and in a broader sense with respect to the physical properties in general.

Keywords: Specification setting, In-silico experiments, Segregation, Bin blender, Granules

Introduction

The blending process is a common and a critical manufacturing process and critically impacts the quality of finished dosage units such as the uniformity of active ingredients´ content in tablets, capsules, powder filled bottles, etc., which is defined as content uniformity (CU) in pharmaceutical industry. Numerous mechanisms are known that play a role when blending particles and granules, including convection, diffusion, shear, and percolation, while a diffusion mixer (tumbling) is the most common blender[29]. In general, samples are taken from various locations of the bulk powder blend to estimate the homogeneity of the active ingredients in the powder blend; i.e., blend uniformity (BU). The physical properties of components in the blend, the sampling regimen that defines sampling locations and the number of samples taken from each sampling location, and the acceptance criteria are the key factors in blend uniformity analysis to check the homogeneity of the bulk powder blend[27, 28]. Usually, the acceptable ranges of the physical properties of the components to assure the desired BU at the given sampling regimen and acceptance criteria are confirmed based on experiments. However, as resources are limited, it has been considered practically difficult to conduct large numbers

[29] Paul E.L., Atiemo-Obeng V.A., Kresta S.M., 2004. Handbook of industrial mixing science and practice. Wiley & Sons, Inc..

of commercial scale experimental studies, even with the benefit of sophisticated design of experiments (DoEs) to reduce the amount of experimentation. With the increasing computational capabilities over the last years, in-silico experiments using the discrete element method (DEM) are becoming an important tool to understand production processes such as blending. The advantage of the DEM compared to other simulation techniques is that it is able to capture the trajectory of each and every particle in the system through Newton's equation of motion. The forces acting on each particle which may be due to particle-particle or particle-wall contacts or the non-contact forces such as gravity, cohesion etc. enter as source terms in the equation of motion[18]. A large number of studies have been reported to understand blending of granular materials and estimate the homogeneity of components in several types of blenders[26, 30, 31, 32]. Sudah et al.[30] and Arratia et al.[31, 32] reported the qualitative effect of fill level and loading pattern of granules to the blender on the time-series sample BU and granules velocity during blending. Adam et al.[26] demonstrated a qualitative sample BU evaluation based on DEM simulation in a diffusion mixer. However, particle size and the geometry of equipment as described in the previous studies are far away from the practical manufacturing process in pharmaceutical industry. As a matter of fact it is still not feasible to simulate >1 kg scale blending processes containing particles of ~100 μm in diameter, since it requires huge computational time. Increasing the particle size from actual values and decreasing the geometry of the equipment are common practices in DEM simulations to reduce computational time by reducing the number of particles in a system[26]. The DEM simulation with the changes to reduce the computational time differentiate the simulated sample BU from the reality. In addition, the distribution of sample BU in consideration of the sampling regimen is not addressed in the previous studies, although it is important to identify the sample BU probability density distribution to estimate a probability to satisfy the BU requirement[33]. Herein for the first time, this study aims at predicting the sample BU probability density distribution quantitatively for given physical properties and sampling regimens by using DEM simulation, while considering the effect of the particle size expansion and blender geometry reduction. Once this quantitative prediction is demonstrated it will facilitate an effective blending process

[30] Sudah, O.S., Coffin-Beach, D., Muzzio, F.J., 2002. Quantitative characterization of mixing of free-flowing granular material in tote (bin)-blenders. Powder Technol. 126, 191– 2002.

[31] Arratia, P.E., Duong, N., Muzzio, F.J., Godbole, P., Lange, A., Reynolds, S., 2006. Characterizing mixing and lubrication in the Bohle Bin blender. Powder Technol. 161, 202 – 208.

[32] Arratia, P.E., Duong, N-H., Muzzio, F.J., Godbole, P., Reynolds, S., 2006. A study of the mixing and segregation mechanisms in the Bohle Tote blender via DEM simulations. Powder Technol. 164, 50–57.

[33] Tanabe, S., Miyano, T., Maeda, J., Nakagawa, H., Watanabe, T., Minami, H., Urbanetz, N.A., 2016. Scientific rationale for sampling regimen and acceptance criteria of blend uniformity based on Monte Carlo simulation. Powder Technol. 301, 336–341.

development by describing the relationship between the input parameters such as physical properties of components and the sample BU in-silico including possible “edge of failure” conditions comprehensively. Those conditions leading to failure need to be verified experimentally, which will ensure a higher quality of pharmaceutical drug product finally by setting a reliable “edge of failure” specification for the given physical properties.

Materials and Methods

A binary granular mixture formulation composed of active granules and placebo granules (active : placebo = 14 : 86 wt/wt%) is considered. The DEM simulation was performed for the blending process using a bin blender to develop a quantitative sample BU prediction procedure. Verification studies were performed by comparing the experimental sample BU with the corresponding DEM simulations data.

2.1. Manufacturing of the binary mixtures formulation

Active granules composed of active ingredients, mannitol, pregelatinized starch, crospovidone, and hydroxypropyl cellulose and placebo granules composed of xylitol and carboxymethyl cellulose sodium salt were manufactured separately by fluid bed granulation followed by screening. The fluid bed granulator S2-B5-F2 (Aeromatic Fielder AG, Bubendorf, Switzerland) and the screening mill QC-197s (Quadro Comil, Ontario, Canada) were used for the granulation and screening, respectively. A 50 L bin blender (Limitec GmbH, Keckum, Germany) was used to mix the active and the placebo granules (Figure 1). Fill mass was 10 kg which is equivalent to around 25% fill level and corresponds to ca. 3650 dosage units. The rotation radius of the 50 L blender is 0.583 m. Blending was performed for 20 min at the rotation speed of 6 rpm, the Froude number is 0.02, in an oscillating mode: clockwise and anticlockwise rotation repeated alternately every minute. After 20 min blending the binary mixture was discharged and part of the granules was bottled with the bottle filling equipment SW 703 (Collischan GmbH & Co. KG, Nürnberg, Germany), as a unit dose package. Three different binary mixtures having different particle size distributions of the active granules and the placebo granules were manufactured as shown in Table 1 by varying the granulation and screening conditions.

Figure 1 Bin blender used in the experiment. (a) Front view. (b) Top view. (c) Blender geometry. (d) Rotation of blender.

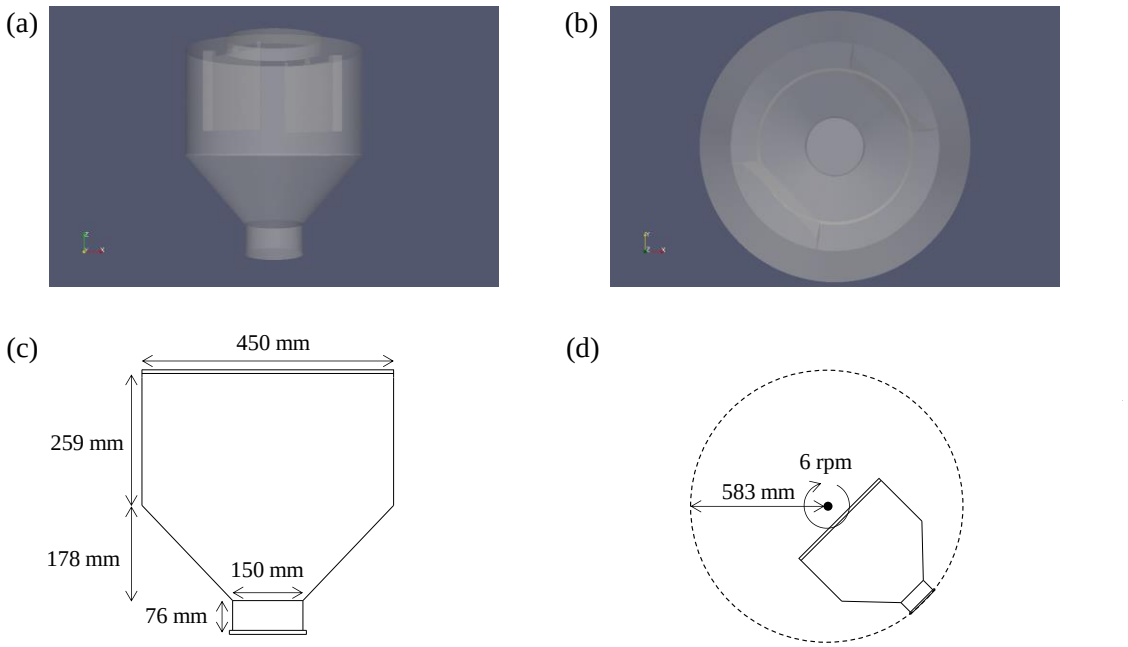

Table 1 Granule properties used in the actual experiments. NA: not available

Sample	*PSD X10* µm	*PSD X50* µm	*PSD X90* µm	*Bulk density* g/mL	*Tapped density* g/mL	*LoD* %	*Sphericity S50* -	*ffc* -
A1	69	137	232	0.30	0.40	2.2	0.88	9.04
A2	76	177	310	0.36	0.51	2.0	0.88	10.00
A3	58	212	466	0.36	0.50	2.0	0.88	8.81
P1	105	234	346	0.47	0.61	0.5	0.88	15.56
P2	65	179	267	0.53	0.74	0.5	0.88	8.13
P3	62	181	292	0.56	0.78	0.5	0.88	8.61
FB1 (A1+P1)	101	225	344	0.46	0.60	0.8	NA	12.00
FB2 (A2+P2)	83	185	292	0.52	0.69	0.7	NA	10.30
FB3 (A3+P3)	77	192	317	0.54	0.72	1.0	NA	9.41

2.2. Sample analysis

Particle size distribution

The mass based particle size distributions of the active and the placebo granules were evaluated using a vibratory sieve shaker AS 200 (Retsch GmbH, Haan, Germany). Stainless steel sieves with 200 mm in diameter and 50 mm in height were used. The mesh sizes of the sieve stack were 1000 µm, 500 µm, 355µm, 250 µm, 180 µm, 150 µm, 106 µm, and 75 µm. 50 g of the granules were used for the analyses. The amplitude, which means the vertical vibration height of the sieves was fixed at 1.5 mm and the sieving duration was 5 min. The x_{10}, x_{50} and x_{90} of the blends and the individual components are given in Table 1.

Particle flowability, friction, and cohesiveness

A Ring Shear Tester RST-XS.s (Dr.-Ing. Dietmar Schulze, Wolfenbuettel, Germany) was used for the evaluation of flowability, internal friction, and wall friction. A bulk sample of 30 mL was prepared in a shear cell and the shear cell was covered with a lid. The sample was consolidated at the vertical normal stress σ_c of 2000 Pa, which is called pre-shear stress σ_{pre}, and sheared by rotating the cell to identify the maximum shear stress. After the pre-shearing procedure, the sample was consolidated at specific normal stresses σ_{sh} (300 Pa, 950 Pa, and 1600 Pa). At each normal stress the powder was sheared to find the corresponding shear stress which is then used to describe the yield locus. The flowability, ffc, of the granules was characterized by σ_c as a function of the vertical consolidation stress σ_1 shown in equation 1, based on the yield locus. All measurements were done in triplicate. The ffc values of all blends including individual components are provided in Table 1.

$$ffc = \sigma_1 / \sigma_c \qquad (1)$$

Particle shape analysis

The particle shape of the active and placebo granules was analyzed using the QICPIC RODOS (dry dispersion method) (Sympatec GmbH, Clausthal-Zellerfeld, Germany). Equipped with a high-speed image analysis sensor, QIPIC captures the particle shapes in an extremely short exposure time of 1 ns. A sufficient amount of granules (about 1 g) was poured into the dispersing system inlet delivering a stream of particles into the image-capturing zone. As soon as the particles appeared in this zone, their images were captured at a rate of up to 500 frames per second (fps). These images were then summarized as a gallery with multiple filter functions by the attached software WINDOX. The software also calculates the sphericity, aspect ratio, shape distribution of particles, and other shape characteristics. Additional details about the instrument are given by Witt et. al.[34]. All measurements were done in triplicate and a summary of these measurements is reported in Table 1.

Moisture analysis

The halogen moisture analyzer HR73 of Mettler Toledo GmbH (Giessen, Germany) was used. About 1 g of sample was heated at 80°C (active granules) or 90°C (placebo granules) at the switch-off mode 5, i.e., drying was finished when a weight variation of less than 1 mg for 140 seconds occurred. The loss of water is quantified and called "Loss on Drying (LoD)". The measured data of different blends, active and placebo granules, is listed in Table 1.

[34] Witt, W., Kohler, U., List, J., 2004. Direct Imaging of Very Fast Particles Opens the Application of the Powerful (Dry) Dispersion for Size and Shape Characterization. In Proceedings of the PARTEC 2004, 16–18 March, Nuremberg, Germany.

Blend and Content Uniformity Analysis, Assay in PSD fractions

Samples were taken from 10 different locations in the blender as depicted in Figure 2 at blending times of 10, 15, and 20 min to evaluate the sample BU. A sampling spoon having a 2 mL hollow cylinder (Figure 3) was used for the sampling. The sample amount was equivalent to one unit dose of 2.75 g. The sample CU, defined as the standard deviation of active ingredient content % to the label claim in the unit dose package was evaluated using 10 samples taken following the stratified sampling approach during the bottle filling process[35]. The assays of the samples were evaluated by UPLC Acquity (Waters, Massachusetts, US). The analytical validation of the assay measurement revealed that the analytical error of the intermediate precision was 0.4% SD. The sample BU and sample CU as the standard deviation of assay *s* (%) were calculated by the following equation.

$$s(\%) = \sqrt{\frac{\sum_{n=1}^{10}(y_n - \bar{y})^2}{n-1}} \qquad (2)$$

Where y_n denotes the assay of individual sample as the ratio to the label claim (%), $\bar{y}$ denotes the mean assay (%). The assays of the active granules in the five particle size fractions: over 250 μm, 250 μm - 180 μm, 180 μm - 106 μm, 106 μm - 75 μm, and under 75 μm were also analyzed.

Figure 2 Sampling points for blend uniformity analysis. (a) Top view. (b) Side view.

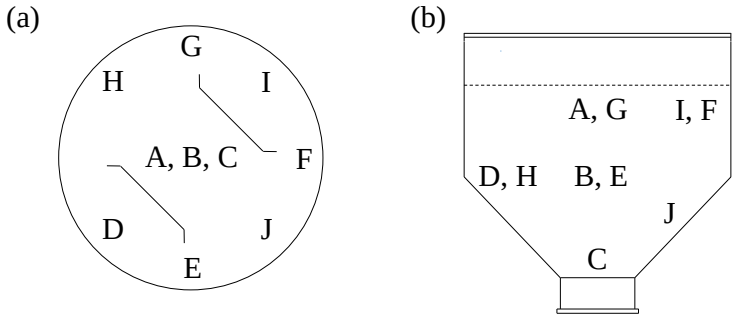

[35] Bergum, J.S., Parks, T., Prescott, J.K., Tejwani, R.W., Clark, J., Brown, W., Muzzio, F., Patel, S., Hoiberg, C., 2015. Assessment of blend and content uniformity. Technical discussion of sampling plans and application of ASTM E2709/E2810. J. Pharm. Innov. 10, 84–97.

Figure 3 Sampling spoon. (a) Top view. (b) Side view.

(a)

(b)

2.3. Numerical approach

Discrete element method (DEM)

All computations were performed using the open source DEM software known as LIGGGHTS[36]. LIGGGHTS has been developed based on the molecular dynamic simulation tool known as LAMMPS, which in turn has been developed by Sandia National Laboratories[37]. In this study, LIGGGHTS version 3.2.1 was used for all DEM simulations. The models chosen in this study included Hertz and Mindlin & Deresiewicz theories for the calculation of normal and tangential forces between particles, respectively[38]. The cohesion was included through the simplified Johnson-Kendall-Roberts model[39] which adds an additional normal force contribution as successfully implemented in reference studies[40, 41, 42]. The other non-contact force considered included gravity. The implementation of the above mentioned models as well as their validation within LIGGGHTS was given by Kloss et al.[36]. The impact of fluid presence on the particle motion was ignored in this study, which is a valid assumption for densely packed granular flows involving large particles where body forces such as gravity are

[36] Kloss, C., Goniva, C., Hager, A., Amberger, S., Pirker, S., 2012. Models, algorithms and validation for opensource DEM and CFD-DEM. Prog. Comput. Fluid Dy. An Int. J. 12, 140–152.

[37] Plimpton, S., 1995. Fast parallel algorithms for short-rangemolecular dynamics. J. Comput. Phys. 117, 1–19.

[38] Di Renzo, A., Di Maio, F.P., 2004. Comparison of contact-force models for the simulation of collisions in DEM-based granular flow codes. Chem. Eng. Sci. 59, 525–541.

[39] Johnson, K.L., Kendall, K., Roberts, A.D., 1971. Surface energy and the contact of elastic solids. P. Roy. Soc. Lond. A Mat. 324, 301–313.

[40] Ketterhagen, W.R., 2015. Simulation of powder flow in a lab-scale tablet press feed frame: effects of design and operating parameters on measures of tablet quality. Powder Technol. 275, 361–374.

[41] Mateo-Ortiz, D., Muzzio, F.J., Méndez, R., 2014. Particle size segregation promoted by powder flow in confined space: the die filling process case. Powder Technol. 262, 215–222.

[42] Gopireddy, S.R., Hildebrandt, C., Urbanetz, N.A., 2016. Numerical simulation of powder flow in a pharmaceutical tablet press lab-scale gravity feeder. Powder Technol. 302, 309–327.

several orders of magnitude higher than the hydrodynamic forces[26, 43]. This is true for particles larger than 100 µm, and in case that the particles are lower than 100 µm the effect of fluid presence on the particles can be modeled by coupling the DEM with the conservation of mass, momentum and energy equations of fluid.

The actual bin blender had a volume of 50 L, and the smallest particle size of the granules (active and placebo) was about 75 µm. In this configuration with the actual PSD, the total number of particles in 10 kg of blend is in the order of 3.5 to 5.4 billion. Table 2 shows the number of particles in 1 kg of final blend for the three batches manufactured in this study (see column 2). This is a by far too huge number of particles to simulate with the current computational capacity in a realistic time even for a blending period of 1 minute. To address this challenge, two parameters were changed which include (1) increasing the particle size by multiplication with a constant factor while keeping the distribution shape same as the measured data, and (2) decreasing the dimensions of the geometry while keeping the size ratios equal to the actual equipment. Increasing the particle size from actual values is a common practice in DEM simulations as it is not feasible to simulate true particle size[44]. This increase in particle size results in a decreased number of particles in the system. The extent of particle size increase is generally chosen such that the bulk behavior of material is reproduced while keeping the total computational time under control. It is reported that including higher numbers of particles will have diminishing advantages[45]. In this study, the simulations were performed with particle size increase factors (F_{PS}) of 3, 5, and 7 in order to evaluate the impact of F_{PS} by comparing the sample BU among these three levels. Even with such an increase in particle size, the number of particles in 10 kg of blend is about 10 million (F_{PS}=7) to 200 million (F_{PS}=3), see Table 2. Still it is a huge number of particles considering that the domain in which the blender rotates is about 0.5 x 1.2 x 1.2 m^3. To bridge this gap of unrealistic computational cost, the geometry of the blender was reduced to one-fifth scale (F_G=0.2) uniformly in each dimension. This enabled a fill mass of 80 g (reduction from 10 kg in actual due to decrease in blender dimensions, i.e. 10 kg * 0.2^3) that can be simulated in a reasonable time, as the number of particles in 80 g at F_{PS}=3 is about 1 million to 2 million. The impact of geometry scaling down was studied by performing additional simulations with a geometry reduced to one-tenth in each dimension (results in a fill mass of 10 g) and one-twentieth (results in a fill mass of 1.25 g) by comparing the sample BU among all three. Constant revolutions per minute were applied for all F_G

[43] Ketterhagen, W.R., Am Ende, M.T., Hancock, B.C., 2009. Process Modeling in the Pharmaceutical Industry using the Discrete Element Method. J. Pharm. Sci. 98, 442–470.

[44] Dubey, A., 2017. Powder flow and blending. In: Pandey, P., Bharadwaj, R. (Eds.), Predictive Modeling of Pharmaceutical Unit Operations. Woodhead Publishing, pp. 39–69.

[45] Hassanpour, A., Tan, H., Bayly, A., Gopalkrishnan, P., Ng, B., Ghadiri, M., 2011. Analysis of particle motion in a paddle mixer using Discrete Element Method (DEM). Powder Technol. 206, 189–194.

since all simulation conditions and the actual experiment condition showed a value of Froude number below 0.2, where the degree of mixing is independent of the speed of rotation[46, 47]. Such an increase in particle size and geometry scaling down is valid with a caution, where it is recommended to keep in mind the ratio between blender diameter (D) to mean particle diameter (d), which was found to be critical, and set in the range of 20 to 50[44]. The values of D/d ratio for the minimum and maximum case are about 18 (F_{PS}=7, F_G=0.05) to 167 (F_{PS}=3, F_G=0.2), which are very close to the recommended range for the minimum case and well within the recommended range for the others. DEM simulations were performed not only for the three blends listed in Table 1 but also for a blend having mono-size particles (180 μm in diameter) without cohesion, in order to support the discussion on developing a quantitative sample BU prediction model, see section 2.4. Moreover, blending simulations at different fill amounts were conducted with mono-size particles to capture the wide ranges of blending conditions such as different fill levels. Table 3 summarizes the DEM simulation setups performed in this study together with the particle number in each DEM run. In total, 19 different blending process DEM simulations (7 mono-size particle size cases, 12 poly-size particle cases) were performed in this study. The DEM input parameters to compute the trajectories and velocities of the particles during the blending process are summarized in Table 4. The selected values are well within the reported DEM input parameters[42, 26, 48]. Different fill masses within a feasible fill level range for the blender were evaluated in mono-size particles cases in addition to the target fill mass, which were used to develop a generalized quantitative prediction model.

Table 2 No. of particles in 1 kg of final blends in DEM simulation.

FB No.	No. of particles in 1 kg			
	F_{PS} = 1	F_{PS} = 3	F_{PS} = 5	F_{PS} = 7
1	351,083,189	13,003,081	2,808,666	1,023,566
2	518,777,125	19,213,968	4,150,217	1,512,470
3	540,895,699	20,033,174	4,327,166	1,576,955

[46] Brone, D., Alexander, A., Muzzio, F.J., 1998. Quantitative characterization of mixing of dry powders in V-blenders. AIChE J. 44, 271–278.

[47] Brone, D., Muzzio, F.J., 2000. Enhanced mixing in double-cone blenders. Powder Technol. 15, 215–236.

[48] Kuo, H.P., Knight, P.C., Parker, D.J., Tsuji, Y., Adams, M.J., Seville, J.P.K., 2002. The influence of DEM simulation parameters on the particle behavior in a V-mixer. Chem. Eng. Sci. 57, 3621–3638.

Table 3 Total No. of particles in a blender in each DEM simulation performed in this study. NA: not available

Blend Name	Fill level	F_{PS} = 5	F_{PS} = 7	F_{PS} = 5	F_{PS} = 3	F_{PS} = 5
		F_G = 0.05	F_G = 0.1	F_G = 0.1	F_G = 0.1	F_G = 0.2
Mono disperse blend	25%	2048	6000	16380	75900	131097
Mono disperse blend	37.5%	NA	NA	24650	NA	NA
Mono disperse blend	50%	NA	NA	32889	NA	NA
FB1	25%	3528	10300	28150	130193	224986
FB2	25%	5127	15298	41550	192491	332483
FB3	25%	NA	NA	43273	NA	346654

Table 4 DEM parameters

Parameter	Property of	Mono-disperse particle mixing	Poly-disperse particle mixing
Young's modulus (GPa)	Particle	8.7	8.7
	Wall	210	210
Poisson's ratio (-)	Particle	0.3	0.3
	Wall	0.35	0.35
Coefficient of friction (-)	Particle-particle contact	0.15	0.15
	Particle-wall contact	0.54	0.54
Coefficient of restitution (-)	Particle-particle contact	0.35	0.35
	Particle-wall contact	0.30	0.30
Cohesion energy density (MJ/m^3)	Particle-particle contact	0	1.4
Adhesion energy density (MJ/m^3)	Particle-wall contact	3.0	3.0

The computational geometry as given in Figure 1 at first was filled with the particles similar to the actual blending experiment, i.e., at first little more than 50% (by weight) of total placebo granules were inserted randomly within the blender and they were allowed to settle down due to gravity. Following this, the total amount of active granules was inserted and after settling of these granules the remaining portion of placebo granules was inserted. This was done to achieve a sandwich like structure containing active granules in between the placebo granules, which was similar to the experiment. During the whole filling operation, total kinetic energy of the granules was calculated. When all the particles filling was finished, the particles were given sufficient time so that their total kinetic energy reached close to zero, i.e. in other words all particles were completely settled in the blender. To get a detailed understanding of the blending pattern of these binary poly-disperse particle size mixtures, each particle size was assigned a color. Figure 4 exemplarily shows the FB2 in blender downsized with F_G=0.1 and particles having F_{PS} of 5 to facilitate the understanding of the coloring of particles based on particle size (Figure 4a, red: large size particles, blue: small size particles), and based on material type (Figure 4b) after the sandwich like filling (red: active granules, blue: placebo granules). Following the filling, the lid of the blender, which contains two blades protruding inside the blender, was closed. The lid was placed in such a way that the blades were positioned at 45° to the blender vertical axis. The same procedure was done in simulations as well. After this, the blending was started

at a speed of 6 rpm in anti-clockwise direction. The rotation direction was reversed after every minute of blending.

Figure 4. FB2 at F_G=0.2 and F_{PS}=5 at the state before blending. (a) Particles are colored based on particle size. (b) Particles are colored based on material type.

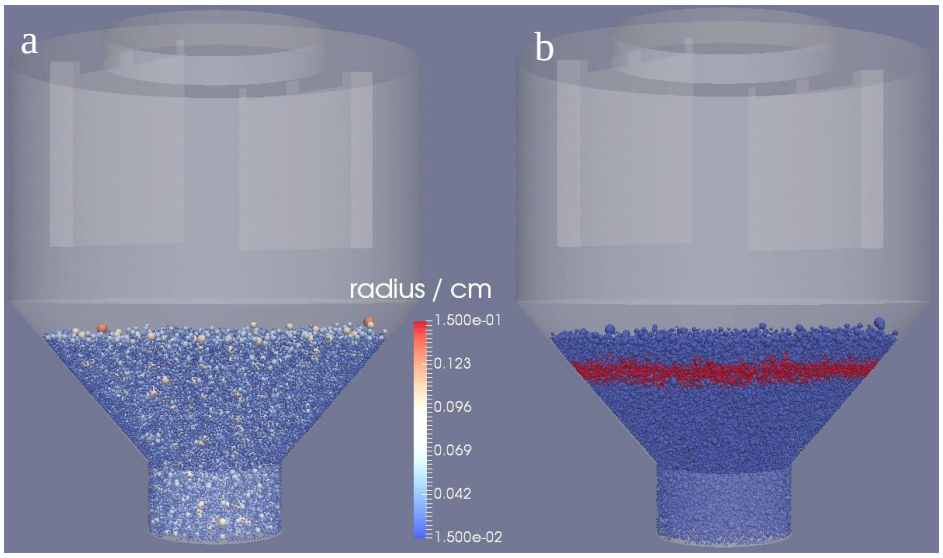

At a given blending time, the powder bed was divided into 10 equivalent mass spaces, which were considered as sampling locations (Figure 5a and 5b). Each of the sampling locations was subdivided into N (N = 4 or 8) equivalent mass spaces as depicted in Figure 5c. The mass contained in the $1/(10N)$ was assumed to be the sample size in DEM simulation. Population BU was calculated using all sample mass spaces existing in the blend. The plateau value of the population BU was calculated by the first-order equation provided below[49].

$$s_t = s_\infty + (s_0 - s_\infty)e^{-kt} \qquad (3)$$

Here s_t denotes the degree of blending (s at time t), s_∞ denotes the plateau value of the population BU as the best possible homogeneity, s_0 is the initial blend uniformity, t is the time, and k is the rate constant for blending, in units of 1/time. A sample BU was also calculated using the samples taken according to a sampling regimen, i.e., 1 sample each from 10 locations (10x1), according to the equation 2. In the case of 10x1 sampling regimen at N = 8, there are 10^8 ways of sample BU values. In this study, a probability density distribution of sample BU was calculated based on all sample BU results. Mean sample BU and the relative standard deviation of the sample BU $RSD_{\text{sample BU}}$ (%) was

[49] Garcia, T.P., Prescott, J.K., 2008. Blending and Blend Uniformity, in book: Pharmaceutical Dosage Forms – Tablets (Vol. 1): Unit Operations and Mechanical Properties, Eds: L.L. Augsburger, S.W. Hoag, informa healthcare, New York, 3rd edition.

calculated based on the probability density distribution. To summarize, each of the 19 DEM simulations were analyzed at two different subdivisions of the sampling locations N (N = 4 or 8). In total 38 s_∞ and sample BU probability density distributions (14 mono-particle size cases, 24 poly-particle size cases) were calculated. A qualitative analysis was also carried out to visualize the blending pattern of these binary mixtures.

Figure 5 Sampling locations in DEM simulation. (a) Top view. (b) Side view. (c) Subdivision of the sampling locations into 8 equivalent spaces (N = 8).

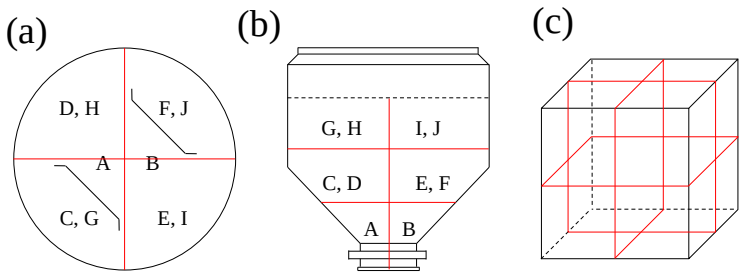

2.4. Quantitative prediction of sample BU

Quantitative prediction was demonstrated based on the predicted s_∞ and sample BU probability density distribution through the equations discussed in the following section. It has been reported that the theoretical variance at the randomly mixed state of a blend (σ_r^2) is calculated by the weight fractions of components and the number of particles in a sample, as shown in equation 4[29].

$$\sigma_r^2 = \frac{p(1-p)}{M} \qquad (4)$$

Here p denotes the weight ratio of the active granules, M denotes the number of particles in the sample. According to the equation 3, the variance of randomly mixed blend becomes an x^{th} part when the number of particles in a sample become x times. Therefore, it is suggested that the sample BU of a blend can be calculated based on the sample BU of the same blend with the same material properties having a different particle number in a sample derived from the differences in F_{PS}, F_G, and N as provided in equation 5.

$$BU_{S1}/BU_{S2} = \left(PN_{S2}/PN_{S1}\right)^{0.5} \qquad (5)$$

Here BU_{S1} and BU_{S2} are the s_∞ of the DEM condition 1 and 2, PN_{S1} and PN_{S2} are the particle numbers in a sample of the DEM condition 1 and 2. Normalized root mean square error (nRMSE), i.e. RMSE divided by the mean predicted s_∞, was used to evaluate the accuracy of the quantitative prediction. For mono-disperse particle size case, (F_{PS}, F_G) = (5, 0.1), N = 8 was considered to be a reference to calculate the nRMSE.

$$\mathrm{nRMSE} = \frac{\sqrt{\frac{\sum_{t=1}^{n}(y_{\mathrm{ref}} - y_{\mathrm{pred}})^2}{n}}}{\overline{y_{\mathrm{pred}}}} \qquad (6)$$

Here y_{ref} and y_{pred} denote the blend uniformity of the reference blend and the predicted values by the other DEM conditions, n denotes the number of predicted values, and $\overline{y_{\mathrm{pred}}}$ denotes the average of the predicted blend uniformity. y_{ref} and y_{pred} in mono-disperse particle size cases are the simulated and predicted s_∞, respectively. y_{ref} of the poly-disperse particle size case denotes the mean value of the three sample BU taken at 10, 15, and 20 min of blending. y_{pred} of the poly disperse particle size case are calculated based on the predicted s_∞ and the analytical error as shown in equation 7.

$$y_{\mathrm{pred,poly}} = \sqrt{s_\infty^2 + s_{\mathrm{a}}^2} \qquad (7)$$

Here s_{a} denotes the analytical error as the standard deviation (0.4%). Though equation 5 can provide good results, however, it does not account for change in total number of particles among different blends. This is because the total number of particles is not included in equation 5 and the number of particles in a sample is independent to the total number of particles in general. Equation 8, which is a variation of equation 5 was developed in this study to achieve a higher prediction accuracy. Total number of particles is a potential critical parameter to the sample BU since it can reflect F_{PS}, F_G, and N.

$$BU_{S1}/BU_{S2} = \left(PN_{S2}/PN_{S1}\right)^a \left(TPN_{S2}/TPN_{S1}\right)^b \qquad (8)$$

Here TPN_{S1} and TPN_{S2} are the total particle numbers in a blender of the DEM condition 1 and 2, a and b are the exponents of PN and TPN, respectively. Exponents a and b were calculated based on an optimization by the generalized reduced gradient (GRG) method, which is one of the nonlinear programming methods[50]. The GRG method derives the approximated gradient of an objective function by moving each decision variable, i.e., exponents a and b. The mono-disperse PSD cases were used as a training set to optimize the exponents a and b. The nRMSE of mono-disperse PSD cases calculated by considering the mean sample BU at (F_{PS}, F_G) = (5, 0.1), N = 8 as a reference with the condition that the objective function was to be minimized. Based on the derived gradient, a better solution was searched iteratively until a local optimal solution was found which satisfies the predetermined constraints. Local optimal solutions were obtained by evaluating 100 randomly selected initial points of exponents a and b to find a global optimal solution.

[50] Lasdon, L.S., Fox, R.L., Ratner, M.W., 1974. Nonlinear optimization using the generalized reduced gradient method. RAIRO—Oper. Res.—Recherche Opérationnelle 8 (3), 73–103.

The prediction accuracy of equation 5 and 8 was evaluated by calculating the nRMSE of the poly-disperse PSD cases, i.e., three FBs. Three FBs are independent of the data used to optimize the exponents *a* and *b* in equation 8, according to the principle of external validation.

Results

3.1. Experimental results: granule properties, sample BU, and sample CU

Physical properties of the three final blends (FBs) were evaluated as shown in Table 1 and Figure 6. FB1 contained the active granules A1 whose particle size was smaller than that of placebo granules P1. FB2 contained active granules A2 and placebo granules P2 that had similar particle size distribution. FB3 contained the active granules A3 whose particle size was larger than the placebo granules P3 in x_{50}. Bulk and tapped densities of the active granules were smaller than those of the placebo granules, while the differences within the same components were negligible. Active granules, placebo granules, and FBs showed LoD of 2.0 – 2.2%, 0.5%, and 0.7 – 1.0%, respectively. All granules were classified as good or flee-flowing powders according to the flow function coefficient, ffc. All granules had ffc values between 8 and 15.5. It was confirmed that the active ingredient content among PSD fractions of the active granules was comparable, as the active ingredient concentration in the PSD fractions ranged from 87.4% to 106.5%. Hence, it was considered acceptable to assume that there is no variation of API content among PSD fractions of the active granules in DEM simulation. The shapes of the active and placebo granules were quite spherical with an aspect ratio of 0.88, which was considered enough to assume that they are spherical in DEM simulation.

The sample BU and the sample CU are summarized in Table 5. The sample BU was determined after 10 min, 15 min and 20 min blending time at which blending is supposed to be completed and no segregation is assumed to occur. The sample BU fluctuated around the average in all FBs in the three time points, caused by incidental differences in sampling (sampling bias). This is a valid consideration for the blending of the free-flowing granules in a diffusion mixer with baffles (Sudah et al., 2002). The sample CU of the three FBs decreased in the order of FB1, FB3, and FB2 similar to the mean sample BU, while the sample CU were smaller than those of sample BU. This could possibly be because a part of the granules was bottled and therefore segregation in the blend was not fully observed in the sample CU. The three FBs having different sample BU and sample CU were manufactured in 10 kg scale.

Figure 6 PSD of three active granules, placebo granules, and final blends. (a) FB1. (b) FB2. (c) FB3.

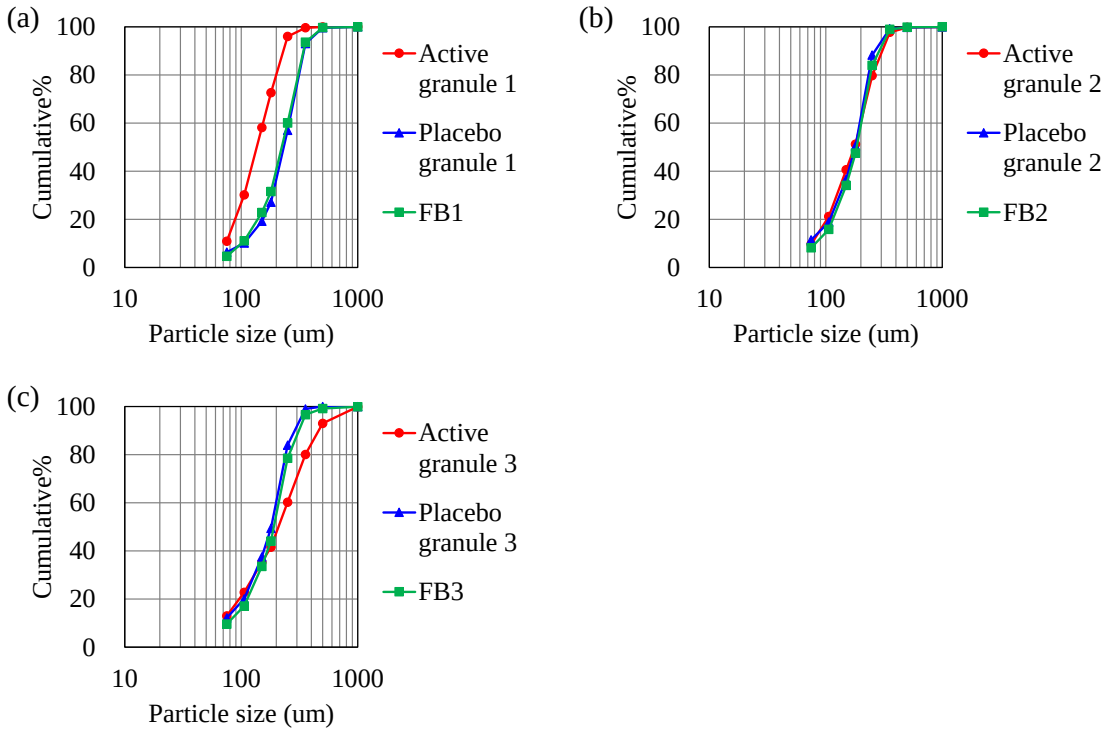

Table 5 Sample BU and sample CU in blending experiments.

Sample	Sample BU *s* (%)				Sample CU *s* (%)
	10 min	15 min	20 min	Mean	
FB1	8.2	3.9	4.7	5.6	4.7
FB2	1.9	2.5	2.0	2.1	1.5
FB3	3.3	2.9	5.8	4.0	2.5

3.2. Mono sized granular blending in DEM simulation

3.2.1 Qualitative analysis of bi-component mono-disperse particles blending

In the DEM simulation of mono-sized granular blending, a blend of active and placebo granules having the same size (= 180 μm in diameter) and the same density without cohesion was considered, which is able to reach complete random blending in theory. To elucidate the temporal development of blending dynamics, qualitative analysis was carried out by coloring the particles as per the material type as mentioned in section 2.3. The initial state of particles after they were filled into the blender is shown in Figure 7 (t = 0 s), which is the 25% fill level blend at F_G=0.2, F_{PS}=5. The red colored particles indicate the active particles whereas the blue colored ones indicate the placebo particles. These were filled in such a way that a sandwich like structure is established: the active particles are in the middle of placebo particles (see Figure 7). The blending state of this mono-disperse particles is shown after 1, 4 and 12 rotations of the blender in Figure 7, which correspond to 10 s, 40 s and 120 s of blending

time. The front view, bottom view, and half cut front view are displayed for these time intervals. The half cut front view helps to understand whether the blending pattern observed with the front view is limited to blender periphery or appears inside the core of the blender as well. The results reveal that the particles are blending dominantly by diffusion. After one complete rotation, the red particles already start to appear everywhere in the blender: top (see front view at 10 s) to bottom (see bottom view at 10 s) of the blender. This phenomenon is the resultant of the blades, which penetrate the powder bed at an angle of 45° to the blender vertical axis. The blades size and position induce convective blending, may be to a certain extent, as they displace the particles by holding and releasing some of the powder while the blender is rotating. The powder bed at 10 s and 40 s are inclined to the left side walls of the blender due to the rotational direction of the blender, i.e., the blender rotates in anti-clockwise direction and changes its direction after every one minute. This is reflected in particle arrangement at 120 s, where the powder bed is oriented to the right side of the blender walls. The blending pattern at 40 s in front view and half cut front view reveal that blending is more or less complete, however, the bottom view shows that there are still spots where the blending is still incomplete. This can be seen, e.g. in the bottom view at the cone-cylinder and in the left side, where still blue color-rich zones appear. Such a detailed visualization enabled by simulation reveals intriguing blending development, and helps e.g. to identify the critical regions of blending thereby optimizing the sampling locations. The blending pattern shown at 120 s (12 rotations of blending), shows that blending is complete, and any further blending may not be necessary.

Figure 7 Temporal blending evolution of bi-component mixture having mono-disperse PSD with 30 g fill amount at F_G=0.2, F_{PS}=5.

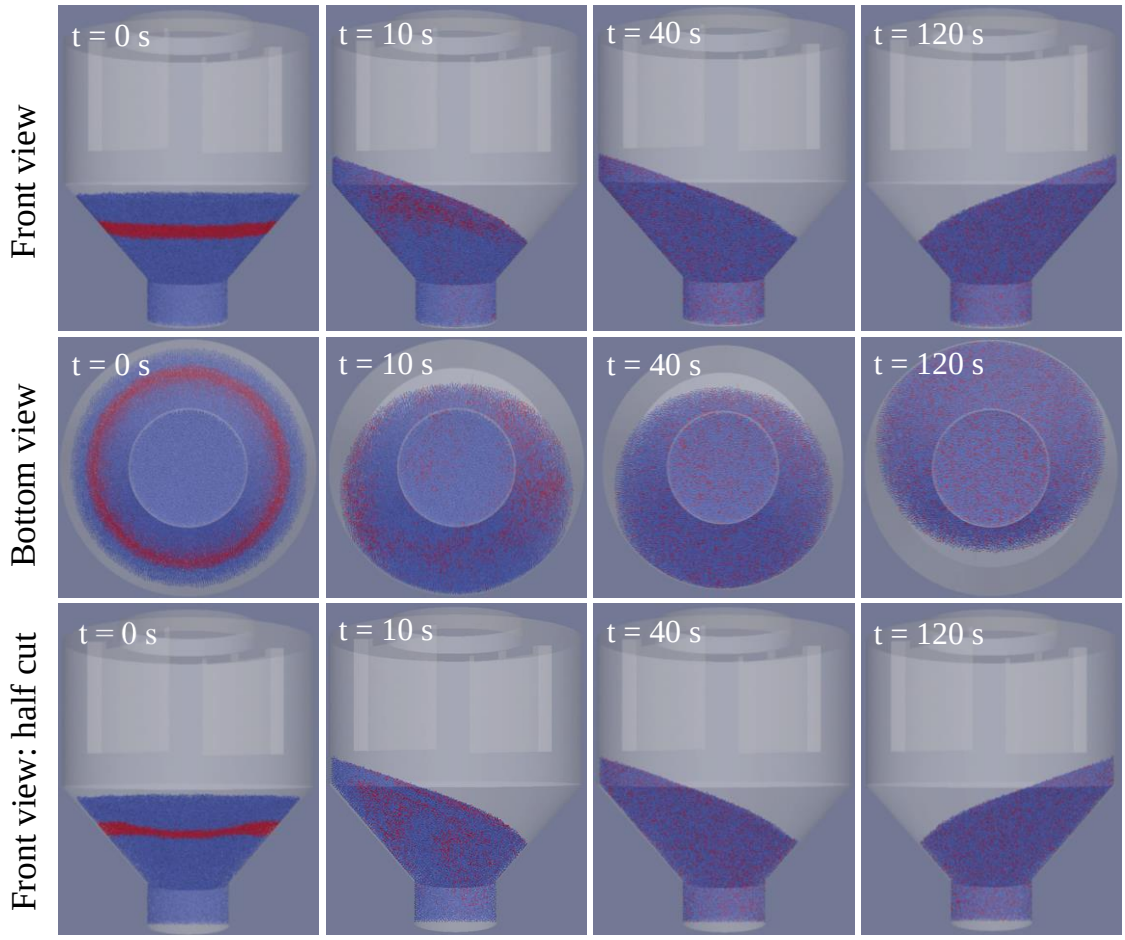

3.2.2 Qualitative evaluation of sample BU in bi-component mono-disperse particles blending

The qualitative observations shown here are in agreement with the time-series population BU results. The population BU of the 14 results; 7 different mono-particle size cases, 2 different number of subdivision in sampling locations for each of the mono-particle size cases, reached a plateau state after 12 rotations of blending. The blending time needed to achieve the plateau state of homogeneity was different reflecting the number of particles in the bin blender as shown in Figure 8 (a) and (b). In the blend at F_G=0.2, F_{PS}=5 where the largest number of particles existed in the bin blender, the population BU reached to the plateau state of homogeneity after 10 to 12 rotations as explained in section 3.2.1. On the other hand, in the blend at F_G=0.05, F_{PS}=5 where the smallest number of particles existed, the blend uniformity reached the plateau state after 1 or 2 rotations. The mean sample BU and the population BU in a given combination of F_G and F_{PS} showed similar values. At the plateau state the probability density distribution of sample BU was normally distributed, which is a reasonable approximation of a binomial distribution for a complete random mixture of a binary blend. The s_∞

calculated by equation 3 using the time series population BU became small as the number of particles in a sample increase as reported in the previous study[29, 30], also shown in Figure 8 (c). The $RSD_{\text{sample BU}}$ at the plateau state of homogeneity, e.g., at 120 sec, was constant regardless of the number of particles in a sample as shown in Figure 8 (d).

Figure 8 DEM results for mono particle size cases. (a) Time-series sample BU and population BU at F_G=0.05, F_{PS}=5. (b) Time-series sample BU and population BU at F_G=0.2, F_{PS}=5. (c) Relationship between No. of particles in a sample and s_∞. (d) Relationship between No. of particles in a sample and $RSD_{\text{sample BU}}$.

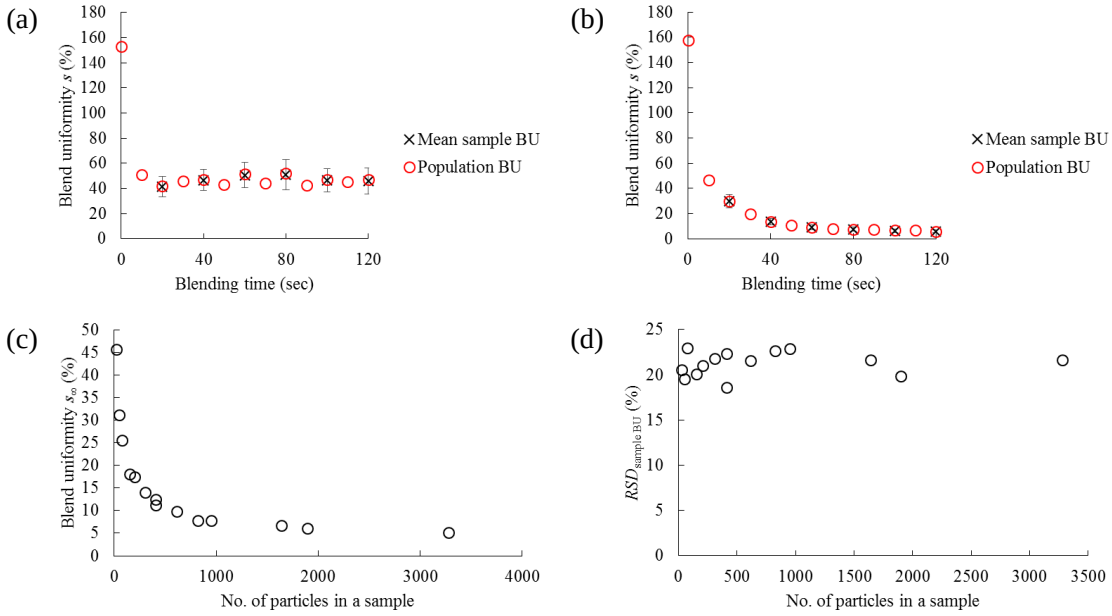

The nRMSE calculated according to equation 5 was 0.093, which implied a prediction error of around 9% of the mean predicted population BU. The nRMSE calculated according to equation 8 was 0.067 and the coefficients in equation 8 determined by the optimization procedure using the training set of mono-size particles cases were: a = 0.554 and b = -0.096. The exponents implied that the sample BU will decrease as the number of particles in a sample increased. At the same time, while the number of particles in a sample has a larger effect on the blend uniformity compared to the total number of particles in the blender, the sample BU will increase when the total number of particles in the blender decreased. Here, assume that the s_∞ of a test blend and a reference blend are $s_{\infty,\,t}$ and $s_{\infty,\,r}$, and $s_{\infty,\,t}$ is predicted based on the $s_{\infty,\,r}$, TPN_r, and TPN_t where TPN_r and TPN_t are the total number of particles in the reference and test blend. In this case, predicted $s_{\infty,\,t}$ using equation 5 is $(TPN_t/TPN_r)^{0.096}$ times smaller than that predicted using equation 8 at the same number of particles in a sample. If TPN_t is 10 times larger than TPN_r, $s_{\infty,\,t}$ predicted according to equation 8 will be 24.7% larger than that predicted

according to equation 5. Therefore it was assumed that the prediction accuracy of equation 5 might be deteriorated when predicting a blend uniformity in an experiment based on the DEM simulation containing a smaller number of particles with the blender geometry downscaling and the particle size upscaling. As it is practically impossible to simulate the blending process of > 1 kg scale by DEM, the sample BU probability density distribution of > 1 kg scale is worth being predicted quantitatively by equation 8 and the DEM results obtained with the downscaled blender geometry F_G and up-scaled particle size F_{PS}. For blender geometry downscaling and particle size upscaling please refer to Chapter 2.3.

3.3 Blending of bi-component poly-disperse PSD

3.3.1 Qualitative analysis of bi-component poly-disperse PSD blending

Similar to the mono-size particles blending pattern, temporal blending evolution of a bi-component mixture having poly-disperse PSD at F_G=0.2, F_{PS}=5 is displayed in Figure 9. The view shown here is from the bottom of the blender. The blending patterns of FB1, FB2 and FB3 are shown in the top, middle and bottom part of this figure, respectively. The PSD of these blends is provided in Table 1 and Figure 6 in section 3.1. The particles are assigned different colors according to their radius; the smallest particles are indicated in blue color and largest particles in red color. Figure 9 shows the initial state of particles after filling the blender (t = 0 s), particles blending pattern at t = 10 s (after 1 rotation), 40 s (after 4 rotations), and 120 s (after 12 rotations). The initial state reveals that particles are homogeneously dispersed across the blender without any segregation (as per the particle size). The individual components are filled in a similar way as done in case of the mono-size particles, however, the active and placebo particles cannot be separately visualized in this figure as the coloring is based on the particle size but not the particle type. The particles' state at 10 s in all FBs shows that the smaller size particles (blue color) are accumulating at the periphery/walls of the blender highlighted by the dotted green ovals, whereas the larger ones stay in the core of the blender. This indicates a segregation based on particle size, and mechanisms of segregation are mainly driven by percolation and trajectory segregation. This can be explained as follows. (1) The smaller particles enter the spaces between the larger particles thereby seep through them (percolation segregation). (2) The larger particles gain higher momentum due to their higher inertia during the blending and fall from the top to the bottom of the container due to gravity along with gained momentum at faster pace (trajectory segregation). Similar segregation was observed at 40 s and 120 s as shown in Figure 9 as the result of these two segregation phenomena. Since these segregation phenomena are caused by particle size differences, the s_∞ is thought to increase as the difference of particle size between active and placebo granules increases.

Figure 9 Temporal blending evolution of bi-component mixture having poly-disperse PSD at F_G=0.2, F_{PS}=5.

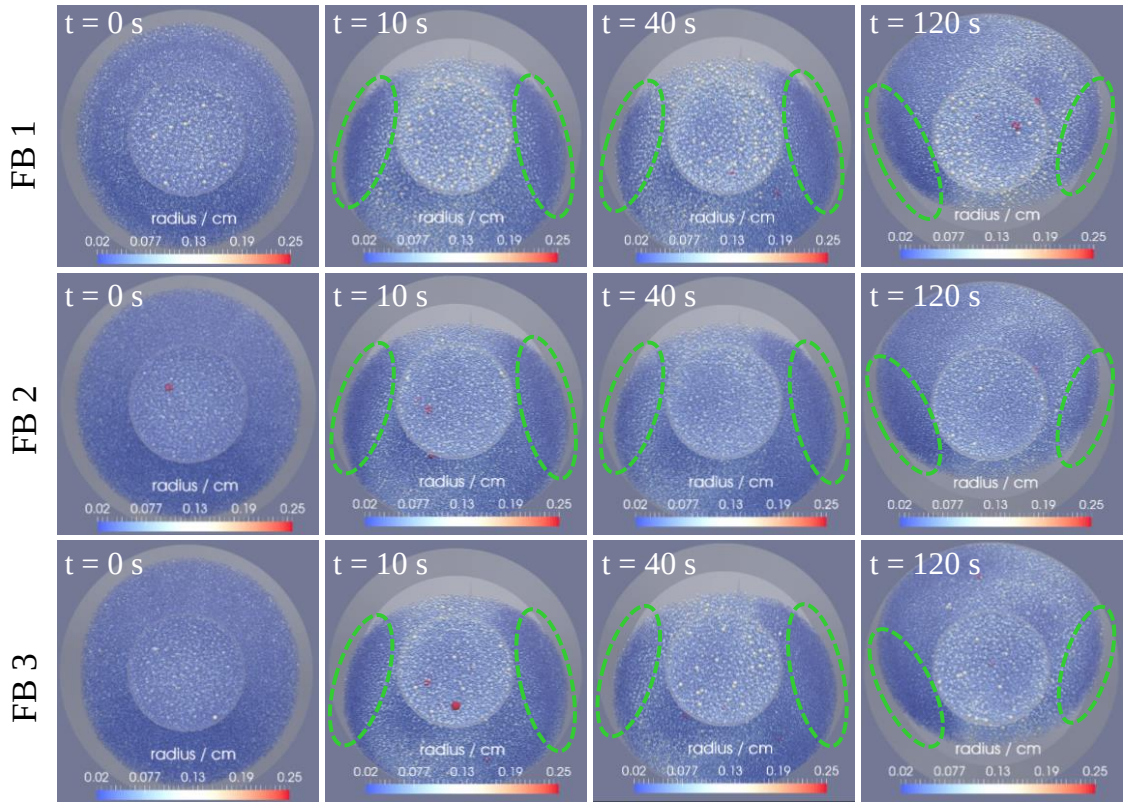

3.3.2 Quantitative evaluation of sample BU in bi-component poly-disperse PSD

The segregation behavior shown in section 3.3.1 was also analyzed quantitatively by collecting samples across the blender. The samples collected at the center of the blender contained less particles than those located at the periphery (data not shown) indicating that the fines are mainly located at the periphery of the blender as observed in Figure 9. Mean sample BU was similar to the population BU in FBs as well as the mono-disperse PSD cases as shown in Figure 10 (a). The time required to reach the plateau state of homogeneity was also correlated to the total number of particles, and the relationship suggested that the blend uniformity after 10 min in 10 kg scale blending experiments are in a plateau state of homogeneity. The time-series population BU did not show the de-mixing after having reached the plateau state of homogeneity, which is common in pharmaceutical formulations unless long blend times or unusual material properties are present[49]. It was confirmed that the s_∞ became small when the number of particles in a sample increases, see Figure 10 (b). On the other hand, when the number of particles in a sample is small, the s_∞ was not clearly correlated to the number of particles in a sample, especially in FB1. This was considered to be because of the prominent segregation in blends containing smaller number of particles in a sample, which was observed as distribution patterns of sample BU. The sample BU distribution patterns depend on the number of

particles in a sample (or in a blender). As shown in Figure 11, the sample BU of FB2 was multimodal or asymmetric unimodal when (F_{PS}, F_G) = (3, 0.1), (5, 0.1), (7, 0.1), and (5, 0.05) where the total number of particles was less than ca. 200,000. Table 6 shows the number % at each particle size fraction in DEM simulation based on the sieve analysis. In poly-disperse PSD DEM simulations particles of 8 different sizes were generated to mimic the cumulative mass % PSD based on the sieve analysis results, assuming that the particles are spherical. As large active particles such as > 500 μm are quite few, the location of large-sized single active particle affected the sample BU significantly if total number of particles in a sample were small. On the other hand, when the total particle number is more than 300,000, such as in case of (F_{PS}, F_G) = (5, 0.2), the sample BU distribution became symmetric unimodal in FB2. The probability density distribution of sample BU at plateau state of homogeneity in blending experiments was considered to be normally distributed considering the gradual changes observed in DEM results similar to the mono-particle size cases. As the s_∞ and the $RSD_{\text{sample BU}}$ at the plateau state of homogeneity depend on the distribution patterns of the sample BU, the s_∞ and the $RSD_{\text{sample BU}}$ calculated at the total particle number of more than 300,000 were considered reliable for quantitative prediction of FB2. Moreover, the required number of particles to achieve a symmetric unimodal sample BU distribution depends on the particle size distribution of the components. When active granules had larger particle size compared to the placebo granules such as in FB3, the probability density distribution of sample BU was not symmetric unimodal even at (F_{PS}, F_G) = (5, 0.2), where ca. 350,000 particles were considered. Similarly, as FB1 contains fewer number of large-sized active particles compared to FB2 and FB3, the required total number of particles to achieve a symmetric unimodal sample BU probability density distribution was smaller than the others. Probability density distribution of sample BU of FB1 was normally distributed in (F_{PS}, F_G) = (3, 0.1) and (5, 0.2). The number of subdivision of sampling locations N also influenced the sample BU probability density distribution. As N affects the number of particles in a sample, it impacts not only the s_∞ and mean sample BU but also the shape of the sample BU probability density distribution. In summary, DEM simulation results in case of (F_{PS}, F_G) = (5, 0.2), N = 8 for FB1 and FB2, (F_{PS}, F_G) = (5, 0.2), N = 4 for FB2, and (F_{PS}, F_G) = (3, 0.1), N = 8 for FB1 showed symmetric unimodal sample BU probability density distribution. As the $RSD_{\text{sample BU}}$ was considered to be constant based on the mono-size cases, it was possible to predict the sample BU probability density distribution quantitatively, based on the s_∞ of these DEM results if the sample BU showed symmetric unimodal distribution. These results demonstrated that the required up-scaling of particle size and downscaling of the blender geometry are different depending on the particle size distribution of the active granules. It was considered that to identify the minimum required total number of particles showing a symmetric unimodal distribution of sample BU probability density distribution, which was required to conduct a quantitative prediction, several DEM simulations varying F_{PS} and F_G need to be performed and the normality of the sample BU distribution needs to be tested. It should be noted that the order of sample

BU probability density distribution range was similar to the experimental results in (F_{PS}, F_G) = (5, 0.2). The sample BU probability density distributions of the FBs were in the order of FB1, FB3, and FB2 from large to small, see Figure 11. Though FB3 requires larger total particle number to achieve a symmetric unimodal distribution than (F_{PS}, F_G) = (5, 0.2), which is needed to predict a sample BU probability density distribution in reality, qualitative comparison between the FBs was successfully demonstrated at least. Quantitative predictions were demonstrated based on the DEM simulation results at (F_{PS}, F_G) = (5, 0.2), N=8 of FB1 and FB2 where the largest number of particles existed in the blender. The sample BU was normally distributed, therefore the s_∞ and the $RSD_{\text{sample BU}}$ should be the most reliable for the quantitative prediction compared to the other DEM simulation results.

Figure 10 DEM results for poly-disperse particle size cases. (a) Time-series mean sample BU and population BU of the FB2 at F_G=0.2, F_{PS}=5. (b) Relationship between No. of particles in a sample and s_∞.

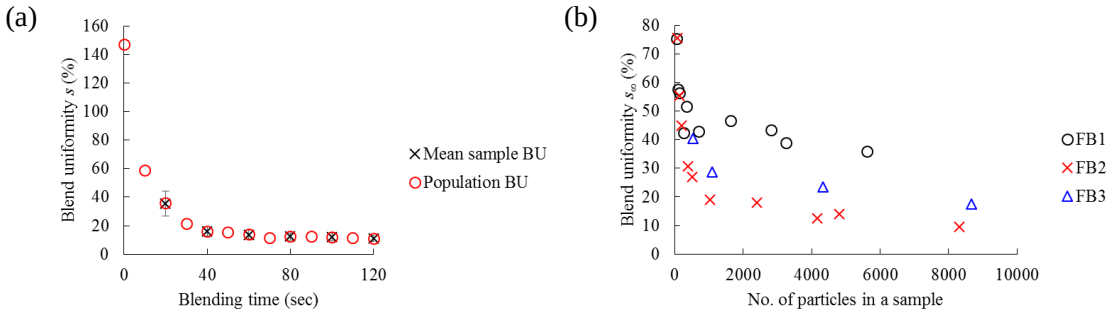

Figure 11 Sample BU results of poly-disperse particle size cases in DEM simulation. (a) FB1, N = 4. (b) FB1, N = 8. (c) FB2, N = 4. (d) FB2, N = 8. (e) FB3, N = 4. (f) FB3, N = 8.

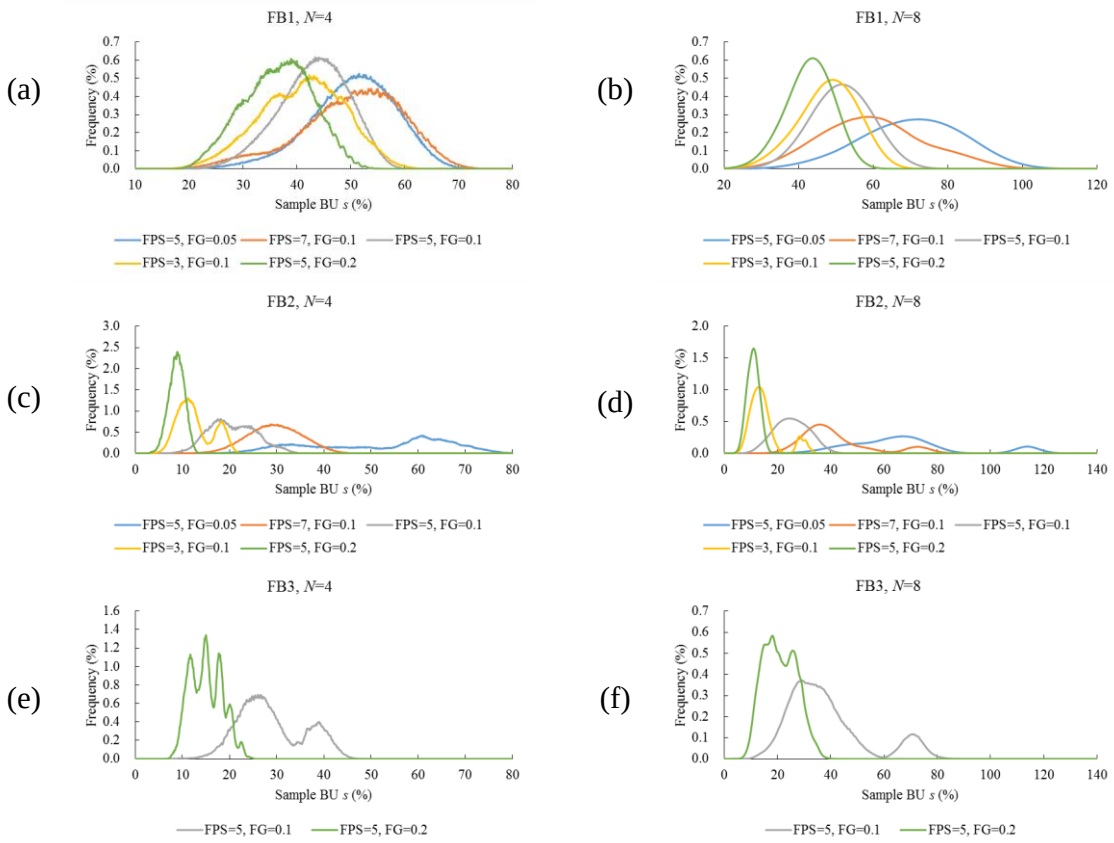

Table 6 Particle size distribution of three active and placebo granules.

Fraction	*Mass% at each particle size fraction in sieve analysis*						*Number% at each particle size fraction in DEM*					
(μm)	A1	A2	A3	P1	P2	P3	A1	A2	A3	P1	P2	P3
1000	0.1	0.3	7.0	0.4	0.2	0.0	$1.1*10^{-4}$	$6.6*10^{-4}$	$1.5*10^{-2}$	$1.5*10^{-3}$	$5.0*10^{-4}$	0.0
500	0.3	2.0	12.9	6.6	0.6	1.0	$5.0*10^{-3}$	$3.8*10^{-2}$	0.2	0.2	$1.0*10^{-2}$	$1.7*10^{-2}$
355	3.6	18.0	19.8	36.1	11.0	15.1	0.1	0.9	1.0	3.2	0.6	0.7
250	23.4	28.5	18.7	29.9	37.8	34.6	2.8	4.3	2.6	7.6	5.5	4.9
180	14.5	10.7	6.2	7.9	13.8	11.9	4.6	4.3	2.3	5.4	5.4	4.5
150	28.0	19.4	12.5	9.1	17.8	17.4	15.3	13.6	8.2	10.7	12.1	11.4
106	19.2	11.5	9.8	3.8	7.4	7.9	29.7	22.8	18.1	12.7	14.2	14.7
75	10.9	9.7	13.0	6.3	11.5	12.2	47.5	54.0	67.6	60.1	62.2	63.8
<75	0.0	0.0	0.0	0.0	0.0	0.0	0.0	0.0	0.0	0.0	0.0	0.0

Quantitative prediction results of sample BU probability density distribution as the mean sample BU calculated by equation 7 and the $RSD_{\text{sample BU}}$ based on equation 5 and equation 8 are provided in Table 7. The predicted results based on equation 5 utilizing the difference in number of particles in a sample showed relatively large prediction errors, as the nRMSE for FB1 and FB2 were 1.345 and 1.122, respectively, which are ca. 15 and 12 times larger than the nRMSE for the mono-size case of 0.093. These results suggested that the number of particles in a sample might not be the only input

parameter to explain the sample BU between the different F_{PS} and F_G in poly-disperse PSD binary mixtures. Since the total number of particles affected the sample BU distribution in DEM simulation, equation 8 was expected to show a better prediction accuracy compared to equation 5. The nRMSE for FB1 and FB2 as the external validation of equation 8 was 0.281 and 0.176, respectively. Although the average of the nRMSEs for FB1 and FB2, 0.228, were smaller than that of the equation 5, it was still larger than the nRMSE for the mono-size case of 0.067, which is the minimum value in the optimization of exponents a and b in equation 8. This larger nRMSE in the external validation could be originated both from the disturbance caused by the sampling operation in experiments and inaccurate mean sample BU in experiments due to the limited number of experimental data (n=3 per FB). As FB1 and FB2 are independent of the determination of the exponents *a* and *b*, these results suggest that the equation 8 has a higher prediction accuracy compared to equation 5 in this study. Though the smallest particle size of the granules was less than 100 μm where the effect of fluid presence on the particles might be not negligible, the sample BU prediction was successfully demonstrated, possibly because the majority of the granules were larger than 100 μm. The predicted sample BU distributions of FB1 and FB2 in the 10 kg scale blending are provided in Figure 12. The probability to pass or fail the sample BU requirement, such as not more than 5.0 SD%, can be easily calculated based on the predicted sample BU probability density distribution. Considering the nature of DEM, the quantitative sample BU probability density distribution of the blend having a given particle size should be able to be predicted at a comparable accuracy by using the DEM simulation and equation 8 if the assumption in DEM simulation, i.e., the impact of fluid presence on the particle motion was negligible, is valid in the given blend. Those in-silico experiments will provide a comprehensive understanding of the relationship between particle size or in a broader sense physical properties and sample BU beyond the verified range, without dispensing any of the materials. This means that the allowable range of physical properties where the target quality is satisfied with desired probability, e.g., > 90% probability to satisfy the sample BU < 5.0% SD, can be identified by performing additional in-silico experiments. Further, as the sample BU probability density distribution predicted by the DEM simulation is reflecting the sampling regimen, it is possible to evaluate the allowable ranges of physical properties taking the effect of sampling regimen in a specific formulation in a specific blender into account. For example, sampling regimen of 5x1, which is defined as taking a sample each from 5 locations, was predicted to have broader sample BU distributions compared to those of 10x1 in FB1 and FB2 at the same sample size, see Figure 12. The probability to satisfy the sample BU < 5.0% SD at the sampling regimen of 5x1 and 10x1 in FB1 were 71.1% and 80.8%, respectively. In summary, the probability to satisfy the desired blend uniformity at given physical properties (e.g., particle size distribution, cohesiveness, etc.) of components can be identified based on the DEM simulations that reflect the effect of sampling regimen in blend uniformity analysis. A reliable, scientifically verified acceptance criteria for the physical properties of components can be

gained based on the visualized edges of failure expressed as the probability to satisfy the desired blend uniformity that are calculated by the comprehensive in-silico experiments utilizing DEM simulation. The hybrid approach of the actual experiments for the verification of the in-silico experiments and complemental in-silico experiments demonstrated in this study will contribute to the higher assurance of blend and content uniformity of drug product, which leads to the higher assurance of safety, efficacy, and efficiency to the patients finally.

Table 7 Predicted mean sample BU *s* and $RSD_{\text{sample BU}}$ of FB1 and FB2 based on the DEM simulation results at F_G=0.2 and F_{PS}=5.

Blend	Mean sample BU *s* (%)			$RSD_{\text{sample BU}}$ (%)[2]
	Experiments[1]	Equation 5	Equation 8	
FB1	5.6	2.4	4.4	16.7
FB2	2.1	1.0	1.8	21.9

1 Mean of the sample BU evaluated at 10 min, 15 min, and 20 min blending in 10 kg scale experiments
2 $RSD_{\text{sample BU}}$ (%) is calculated from DEM simulation

Figure 12 Comparison of the sample BU probability density distribution for poly-disperse particle size blending in (F_{PS}, F_G) = (5, 0.2), N = 8.

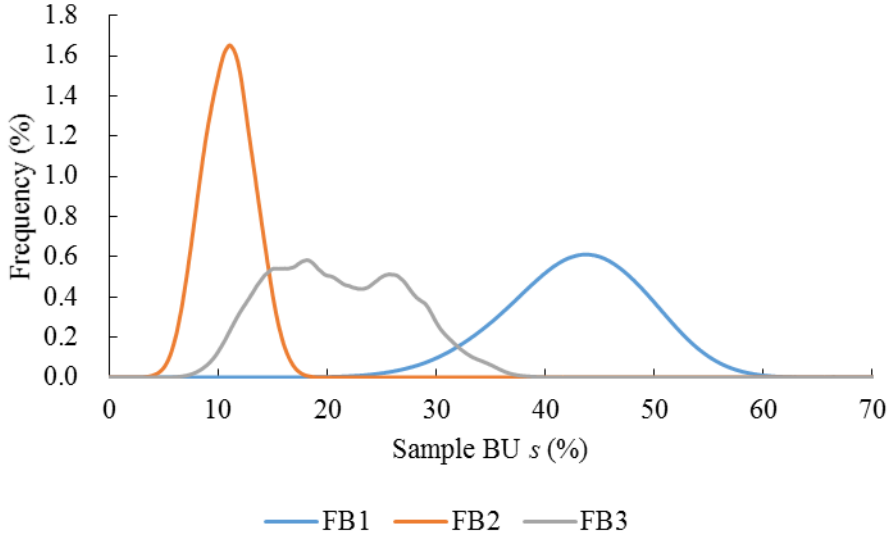

Conclusions

Qualitative and quantitative prediction of sample BU probability density distribution in a binary granular mixture was successfully demonstrated. The segregation due to the differences in physical properties of granules, such as particle size distribution between the active and placebo granules, was observed both visually and numerically using DEM simulation. The quantitative prediction of the sample BU probability density distribution of the three FBs manufactured in 10 kg scale was

successfully demonstrated with keeping the computational time reasonably low, by up-scaling the particle size and downscaling the blender geometry. Prediction accuracy of the s_∞ as the nRMSE was 0.228, indicating a prediction error of around 23%. The nRMSE could be derived both from the disturbance caused by the sampling operation in experiments and inaccurate mean sample BU in experiments due to the limited number of experimental data (n=3 per FB). The total number of particles in the blender and the number of particles in a sample were considered to be critical parameters in predicting the sample BU of a blend in experiments based on DEM results. As the $RSD_{\text{sample BU}}$ was confirmed to be constant regardless of the number of particles in a sample and total number of particles, it was concluded that the sample BU probability density distribution was successfully predicted based on DEM simulations. The hybrid approach combining the limited number of actual experiments for verification purpose and the complemental in-silico experiments towards the blending process development demonstrated in this study showed potential to provide a comprehensive understanding of the blending process efficiently, without dispensing huge amount of materials for exploratory, trial and error experiments. A similar approach could be applicable to not only other types of batch type blenders (V-blenders, double cone blenders, cube blenders, etc) but also continuous manufacturing facilities. This fact also suggests a possibility to evaluate and compare the mixing performance of the blenders based on the expected blend uniformity at the manufacture of a given formulation. Further development in computational capability in near future will accelerate the demonstrated hybrid approach, resulting in a higher assurance level of drug product quality based on the concept of Quality by Design.

Case study 2 - Scientific rationale for sampling regimen and acceptance criteria of blend uniformity based on Monte Carlo simulation

Powder Technology 301 (2016) 336–341

Contents lists available at ScienceDirect

Powder Technology

journal homepage: www.elsevier.com/locate/powtec

Scientific rationale for sampling regimen and acceptance criteria of blend uniformity based on Monte Carlo simulation

Shuichi Tanabe [a,b,*], Takuya Miyano [a], Jin Maeda [a], Hiroshi Nakagawa [a], Tomoyuki Watanabe [a], Hidemi Minami [a], Nora A. Urbanetz [b]

[a] Formulation Technology Research Laboratories, Daiichi Sankyo Co., Ltd., Hiratsuka 2540014, Japan
[b] Pharmaceutical Development, Daiichi Sankyo Europe GmbH, Pfaffenhofen 85276, Germany

Outline

The scientific rationale for setting acceptance limits for the blend uniformity is studied in a blending process. Blend uniformity, defined as the homogeneity of active ingredients in the blend, is one of the intermediate CQAs to assure the CQA of content uniformity in the finished drug product. A challenge in the BUA is that the homogeneity of the whole potential samples not being tested in the bulk blend needs to be assured based on the homogeneity of the actually tested samples. Certainly, the sampling regimen, which is the combination of sampling locations and the number and amount of samples from each sampling location, and the acceptance criteria are the key factors for assuring the homogeneity of the whole bulk blend. However, there is little literature on how to correlate the key factors and the resultant assurance level of bulk blend homogeneity. Herein the aim of this case study is to develop a scientific rationale for the selection of sampling regimen and acceptance criteria, which includes setting of the requirements for the whole potential samples not tested in the bulk blend. The comprehensive blending process control can be established together with the process model developed in case study 1 finally.

Abstract

This study proposes an alternative sampling regimen (number of sampling points, number of samples from each sampling point) and setting of the acceptance criteria for blend uniformity based on a statistical rationale. Currently, the sampling regimen and the acceptance criteria for the blend uniformity test of powder blends are determined according to the withdrawn guidance for industry by the Food and Drug Administration (FDA) and the proposal of the International Society for Pharmaceutical Engineering (ISPE)-sponsored Blend Uniformity and Content Uniformity (BUCU) Group to substitute the withdrawn guidance. However, both approaches lack scientific rationale in their publications. Herein this study addresses the scientific background based on the simulations utilizing the Monte Carlo method, in order to provide a scientific rationale for the sampling regimen and acceptance criteria. False positive probability, defined as the probability of failure to meet the minimum necessary requirement in future samples even when the tested sample satisfies the acceptance criteria in fact were used to evaluate the adequacy of the sampling regimen and acceptance criteria. This study aims at stimulating the discussion about blend uniformity that may ensure a higher quality of pharmaceutical products finally.

Keywords: Blend and content uniformity, Monte Carlo simulation, Statistics

Introduction

The blending process is one of the common critical manufacturing processes to assure the quality of finished products such as uniformity of active ingredients content in the finished dosage units, defined as content uniformity. In general, samples taken from various points of bulk powder blend are evaluated to estimate the homogeneity of the active ingredients in the powder blend; i.e., blend uniformity. The sampling regimen, which is the combination of sampling points and the number of samples from each sampling point, and the acceptance criteria are the key factors in blend uniformity test. This is because usually the quality of the bulk powder is assured based on the test results of the samples. In the pharmaceutical industry, the discussion for the sampling regimen and the acceptance criteria for the blend uniformity test have been raised recently, initiated by the Food and Drug Administration (FDA). In August 2013, the FDA announced the withdrawal of its draft guidance for industry on Powder Blends and Finished Dosage Units — Stratified In-Process Dosage Unit Sampling and Assessment[27]. FDA's major concern was that Sections V and VII of the withdrawn draft guidance, which had been used as a basis for the sampling regimen and the acceptance criteria of blend uniformity test, no longer represented the agency's current thinking. The agency's recommendation to address the concerns is twofold. First, between- and within-location variability in the powder blend is a critical component of finished product quality and therefore should be evaluated. Second, the

procedures and acceptance criteria in USP <905> are not a statistical sampling plan and so the results of the procedures should not be extrapolated to larger populations[28, 35]. Considering these points, a systematic sampling regimen for the blend uniformity test is required taking the between- as well as the within-location variability into account, since the within-location variability; i.e., sampling bias, may bias the between-location variability which reflects the true variability of the active ingredient's content in the bulk powder blend. Regarding the acceptance criteria for the samples, the statistical rationale is desired to assure the homogeneity of the bulk powder blend considering the applied sampling regimen.

In 2014, the Blend Uniformity and Content Uniformity Group (BUCU Group) of the International Society for Pharmaceutical Engineering (ISPE) published two papers to propose the modifications to the withdrawn FDA draft guidance[28, 35]. The statistical rationale for the proposed sampling regimen and the acceptance criteria for the content uniformity test of finished dosage units are provided in the publications and the ASTM E2709-12 and ASTM E2810-11[51, 52]. However, there is little scientific or statistical rationale for the proposal of the sampling regimen and the acceptance criteria of the blend uniformity compared to the content uniformity. In addition, the BUCU Group encouraged other statistical, science and risk-based approaches in their publication. Application of process analytical tools such as in-line monitoring of the blend uniformity throughout the blending process would be one of the alternative modern approaches they had described for example[53, 54]. However, not only PAT offering continuous monitoring of blend uniformity but also traditional endpoint controls with higher quality assurance could be beneficial to reduce research and development cost. The aim of this study is to evaluate the usefulness of the Monte Carlo simulation for the statistical rationale of the alternative sampling regimen and acceptance criteria following the BUCU Group´s call for other statistical, science and risk-based approaches.

---

[51] American Society for Testing and Materials, 2012. Standard Practice for Demonstrating Capability to Comply with an Acceptance Procedure. ASTM E2709-12.

[52] American Society for Testing and Materials, 2011. Standard Practice for Demonstrating Capability to Comply with the Test for Uniformity of Dosage Units. ASTM E2810-11.

[53] El-Hagrasy, A.S., Morris, H.R., D'Amico, F., Lodder, R.A., Drennen III, J.K., 2001. Near-Infrared Spectroscopy and Imaging for the Monitoring of Powder Blend Homogeneity. J. Pharm. Sci., 90, 1298–1307.

[54] Wu, H., Tawakkul, M., White, M., Khan, M., 2009. Quality-by Design (QbD): An integrated multivariate approach for the component quantification in powder blends. Int. J. Pharm., 372, 39–48.

Methods

2.1. Acceptance criteria of population blend uniformity – lower probability bound (LB)

In general, content uniformity of the finished dosage units such as tablets and capsules is affected by the four factors: mean concentration of the active ingredients in the powder blend used, uniformity of the active ingredient amount in the powder blend used, mean weight of unit dosage forms, and the weight variation of unit dosage forms. Segregation of the active ingredients content during the unit dosing process such as tableting and capsule filling will be also a factor affecting content uniformity. Therefore, the acceptance criteria of the blend uniformity should be equal to or lower than the acceptance criteria for the content uniformity of unit dosage forms in order to ensure that the tablets manufactured using the powder blend meet the content uniformity test. In addition, since the blend uniformity test is conducted for the samples taken from the population, i.e., bulk powder blend, the acceptance criteria for the samples should be set considering the estimated probability density distribution of the population. Based on this consideration, the minimum necessary requirement for the population blend uniformity, and the acceptance criteria for the samples taken from the powder blend were set as follows:

The minimum necessary requirement for the population powder blend was set such that it will assure that the future samples taken from the population will meet the USP<905> acceptance criteria with the predefined probability at least (lower probability bound (LB)). This is the same requirement for the population drug product content uniformity provided in ASTM E2810, which is the upper limit of the standard deviation (SD) of the assay with respect to the mean assay value. Note that the assay is defined as a percentage of active ingredients' label claim in powder blend, tablets, and finished dosage units. LB=95% was selected in this study because it is provided in the ASTM E2810 as an example, and commonly used in the regulatory area. At LB=95%, the upper limit of the assay SD, i.e., homogeneity of the active ingredients, at the mean assay value of 100% is 6.0%[55]. Generally, the target assay value in the blending process is 100%, therefore, the minimum necessary requirement for the population assay SD was set to not more than 6.0%.

2.2. Estimation of false positive probability based upon Monte Carlo simulation

To compare the adequacy of the sampling regimen and acceptance criteria of samples to assure the population blend uniformity, false positive probability, defined as the probability of failure to the minimum requirement in future samples even when the tested sample satisfies the acceptance criteria, were calculated. The false positive probabilities of the various sampling regimen and acceptance criteria were calculated based upon probability density distributions. As pointed out by the agency,

[55] Bergum, J.S., Li, H., 2007. Acceptance Limits for the New ICH USP 29 Content-Uniformity Test. Pharm. Tech., 90–100.

two individual variations, between- and within-location variability, should be considered to estimate the probability density distributions, however, it is difficult to establish the mathematical estimation model of the probability density distribution that has two independent variabilities. Alternatively, the distribution was calculated using the Monte Carlo method. Monte Carlo simulation is widely applied in science and engineering with experiments on random numbers[56]. The algorithm used here is a simple sampling method as follows and illustrated in Figure 1.

1. 400 combinations of between-location variability (σx) and within-location variability (σy) were prepared. σx and σy were ranged from 0.5% to 10.0%. The two variations were changed independently in 0.5% steps to cover the entire possible situation.
2. The assay SD of any optional sampling regimen (e.g., 3 samples each from 10 points) were calculated thirty thousand times (sample size $N = 3.0\times10^4$) per each combination of σx and σy to acquire the respective probability density distribution of the assay SD. The sample size N is determined considering the robustness of the estimated probability as described below. Note that these probability densities are based on the assumption of normal distributions by using normal random number generator whose accuracy was confirmed (see Appendix).
3. The probabilities that satisfy the predefined acceptance criteria (e.g., assay SD ≤ 5.0%) (*P1*) and the probabilities that deviate from the minimum necessary requirement for the population (assay SD > 6.0%) (*P2*) for each combination of σx and σy were calculated.
4. The false positive probability that the future sample of the population will deviate from the minimum necessary requirement although the current sample satisfies the predefined acceptance criteria (P3) was calculated. *P3* is calculated by equation 1 as follows:

$$P3 = P1P2/100 \qquad (1)$$

[56] Huang, C.Y., Ku, S.M., 2010. Prediction of drug particle size and content uniformity in low-dose solid dosage forms. Int. J. Pharm. 383, 70–80.

Figure 1 Algorithm of the Monte Carlo simulation in the case of sampling regimen 10×3, acceptance criteria of not more than 5.0% SD

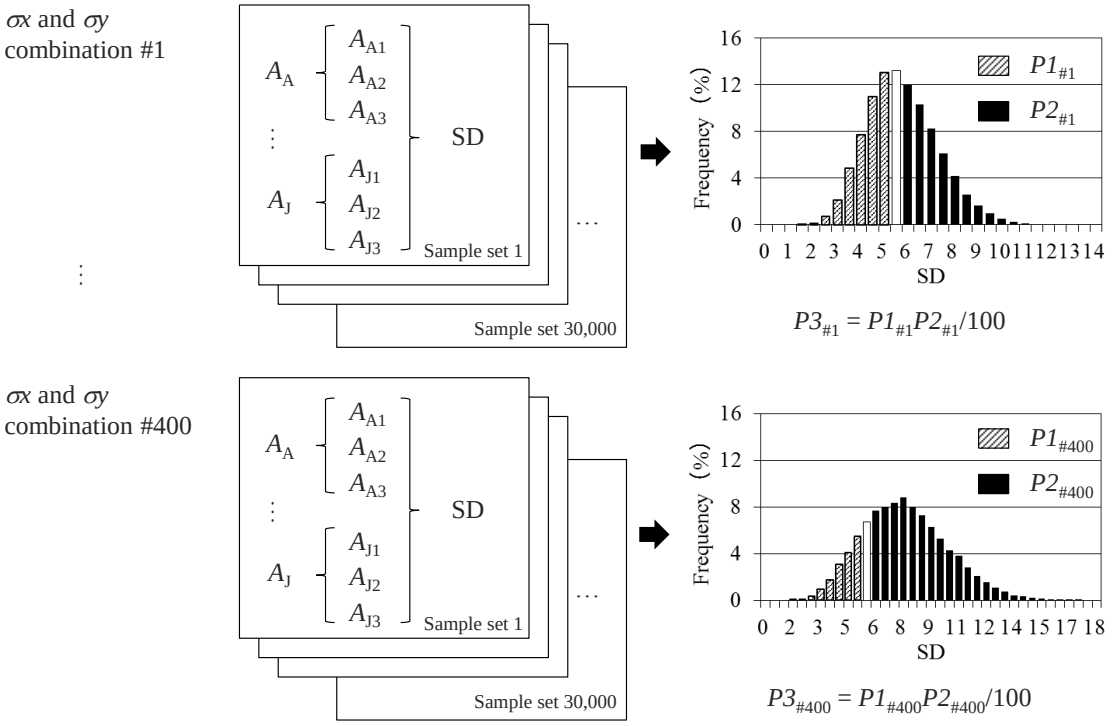

A low P3 means that at the combination of σx and σy, sampling regimen, and acceptance criteria, future samples from the population powder blend whose sample had met the acceptance criteria will satisfy the minimum necessary requirement. Therefore *P3* is comparable to the confidence level (C) in the ASTM E2810.

The sample size N for the Monte Carlo simulation has determined based upon the Chernoff bound;

$$N(\varepsilon,\delta) \geq \frac{\ln(2/\delta)}{2\varepsilon^2} \qquad (2)$$

With the Equation 2, the smallest sample size required to assure that the probability of an estimation error exceeding ε is less than or equal to δ is calculated[57, 58]. For this study, $\varepsilon = \delta = 0.01$ which correspond to a 1% error was selected as a robust estimation, and the smallest required sample size *N*

[57] Chernoff, H., 1952. A measure of asymptotic efficiency for test of hypothesis based on the sum of observations, Ann. Math. Statist. 23, 493–507.

[58] Tempo, R., Bai, E.W., Dabbene, F., 1997. Probabilistic robustness analysis: Explicit bounds for the minimum number of samples. Syst. Control Lett. 30, 237–242.

is 2.6×10^4. In order to be on the safe side, 2.6×10^4 was rounded up to 3.0×10^4.

In this study, the sampling regimen is abbreviated as follows: 10×3 for 3 samples each from well-distributed 10 points in the container blender. The Monte Carlo simulation was conducted for various sampling regimens such as 10×1, 10×2, 10×3, and 6×2, and the predefined acceptance criteria was not more than (NMT) 3.0% SD, 4.0% SD, or 5.0% SD. Figure 2 is an example of the sampling regimen of 10×3. Equation 3 and 4 represent the calculation procedure of the individual assays to acquire the SD of the sample.

$$A_p = M + \sigma x C \qquad (3)$$

$$A_{pq} = A_p + \sigma y C \qquad (4)$$

Where A_p denotes assay of location *p*, M denotes the target assay of the blend (100%), *C* denotes normal random number, and A_{pq} denotes assay of the individual sample from the location *p*. In the case of 10×3 provided in Figure 2, *p* = A, B, C, D, E, F, G, H, I, and J and *q* = 1, 2, and 3. Sample SDs were calculated by using the individual assay value. Note that the simulation conducted in this study is built on the assumption that the samples are taken from the well-distributed sampling points.

Figure 2 Example of sampling regimen 10×3 from container blender. (a) side view (b) top view

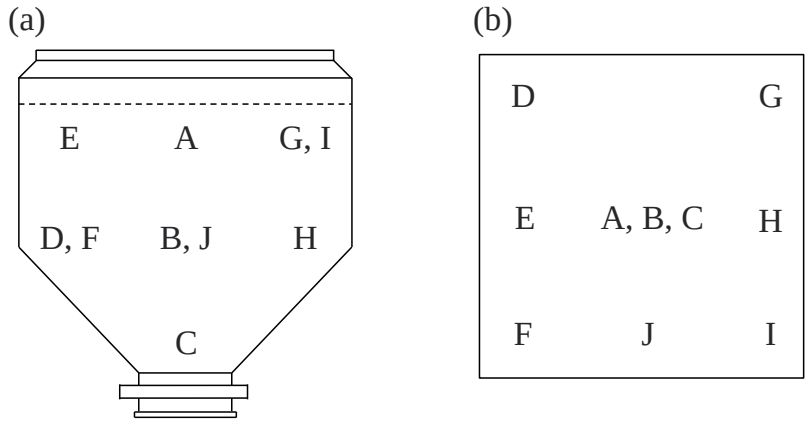

2.3. Comparison of the prediction accuracy of between- and within-location variability

When the assay SD of the powder blend sample is close to the acceptance criteria, it is worth to identify whether σx or σy was the cause to avoid the false positive. In such cases, the accurate prediction of σx and σy would be preferred. In particular, the accurate prediction is desired in the cases where *P3* was expected to be high. This is because the high *P3* means that the probability density distribution of the assay SD is relatively wide, therefore, there is a possibility that the sample blend uniformity may have been estimated lower than the actual one due to the wide distribution even when

the sample satisfies the acceptance criteria near the limit. Herein the accuracy of the predicted between- and within-location variability (*sx* and *sy*) to the σx and σy whose *P3* were predicted to be high was evaluated through variance components analysis (VCA) in the Monte Carlo simulation. The model associated with the prediction of *sx* and *sy* by the VCA is given as:

$$x_{ij} = \mu + a_i + e_{ij} \qquad (5)$$

Where x_{ij} is the observation of the *j*th unit in the *i*th sampling point, μ is the general mean, a_i is the effect of *i*th sampling point, and e_{ij} is the residual error consisting of within-location variation. The *sx* and *sy* were calculated as equation 6 and 7.

$$sx = \sqrt{\frac{ns_{\mathrm{LM}}^2 - sy^2}{n}} \qquad (6)$$

$$sy = \sqrt{\frac{\sum_{l=1}^{n} sy_l^2}{n}} \qquad (7)$$

Where *n* denotes number of samples per each sampling point, s_{LM}^2 denotes variance of the mean assay values of each sampling point, sy_l^2 denotes the variations of the assay values in each sampling point. When ns_{LM}^2 minus sy_l^2 became negative, it was assumed as zero. *sx* and *sy* were calculated thirty thousand times (sample size $N = 3.0\times10^4$) to obtain the probability density distribution based on the sample sets provided by equation 3 and 4. The accuracy of *sx* and *sy* to the σx and σy were compared between the sampling regimens based on the estimated probability density distributions.

Results and Discussion

The simulation results of the sampling regimen 10×1, acceptance criteria of NMT 5.0% SD was thought to be a reference to the others since it had been applied as a standard procedure on the basis of the withdrawn guidance. Figure 3 shows an example of probability density distribution of 10×1, (σx, σy) = (4, 2). When the acceptance criteria for the sample assay SD was set to be NMT 5.0%, then *P1*=74.1%, *P2*=6.2%, and *P3*=4.6%, respectively.

Figure 3 Probability density distribution of the assay SD using the sampling regimen 10×1, (σx, σy) = (4, 2)

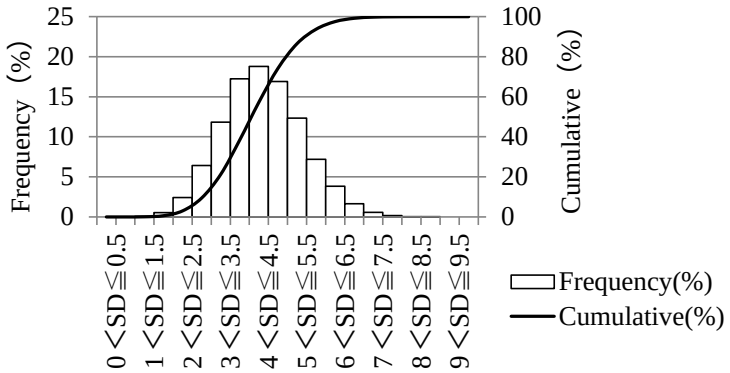

Figure 4 shows the P3 of each combination of σx and σy for the sampling regimen of 10×1 and the acceptance criteria of NMT 5.0% SD. Its horizontal axis is for the between-location variation, and the vertical axis is for the within-location variation. The green colored combination shows 2.5% ≤ *P3* < 5.0%, the blue colored combination shows 5.0% ≤ *P3* < 10.0%, and the red colored combination shows 10.0% ≤ *P3*, respectively. There exist many colored combinations, that is, there are risks to deviate the minimum necessary requirement in the future samples even when the sample under investigation meets the acceptance criteria.

Figure 4 *P3* of the each combination of σx and σy for 10×1, acceptance criteria NMT 5.0% SD

Within location variation (σy) \ Between location variation (σx)	0.5	1.0	1.5	2.0	2.5	3.0	3.5	4.0	4.5	5.0	5.5	6.0	6.5	7.0	7.5	8.0	8.5	9.0	9.5	10.0
0.5	0.0	0.0	0.0	0.0	0.0	0.0	0.2	1.7	5.3	9.4	12.0	12.6	11.0	8.7	6.8	4.8	3.6	2.5	1.9	1.3
1.0	0.0	0.0	0.0	0.0	0.0	0.0	0.3	2.2	5.9	9.7	12.4	12.3	10.8	8.9	6.5	4.7	3.3	2.4	1.7	1.2
1.5	0.0	0.0	0.0	0.0	0.0	0.1	0.7	3.1	7.1	10.9	12.6	12.1	10.2	8.3	6.1	4.4	3.2	2.5	1.5	1.0
2.0	0.0	0.0	0.0	0.0	0.0	0.3	1.5	4.6	8.6	11.7	12.5	11.6	9.9	7.7	5.7	4.1	2.9	2.2	1.6	1.1
2.5	0.0	0.0	0.0	0.0	0.3	1.0	3.1	6.8	10.3	12.4	12.4	11.0	9.0	7.0	5.2	3.9	2.9	2.0	1.5	1.0
3.0	0.0	0.0	0.1	0.3	1.0	2.8	5.8	9.2	11.8	12.5	12.0	10.4	8.4	6.3	4.7	3.4	2.4	1.8	1.3	0.9
3.5	0.2	0.4	0.7	1.6	3.4	5.8	8.8	11.4	12.5	12.5	10.8	9.3	7.3	5.6	4.0	3.1	2.2	1.6	1.1	0.8
4.0	1.7	2.1	3.2	4.7	6.8	9.4	11.4	12.6	12.2	11.3	10.0	7.8	6.3	4.8	3.8	2.4	2.0	1.3	1.0	0.7
4.5	5.1	5.8	7.3	8.4	10.2	11.8	12.6	12.7	11.7	10.2	8.5	6.7	5.1	4.0	3.1	2.3	1.5	1.3	0.8	0.6
5.0	9.3	10.1	10.9	11.8	12.5	12.5	12.4	11.3	10.1	8.9	7.1	5.5	4.2	3.2	2.5	1.9	1.4	1.1	0.7	0.6
5.5	12.2	12.2	12.7	12.6	12.3	11.9	11.1	9.8	8.5	7.0	5.7	4.4	3.5	2.6	2.1	1.6	1.3	0.9	0.7	0.5
6.0	12.3	12.3	12.1	11.7	11.0	10.3	9.2	8.0	6.8	5.6	4.4	3.5	2.9	2.2	1.7	1.2	0.8	0.8	0.5	0.5
6.5	11.0	10.7	10.3	9.9	9.3	8.2	7.2	6.3	5.4	4.5	3.6	2.8	2.2	1.7	1.3	1.0	0.7	0.6	0.4	0.4
7.0	8.8	8.6	8.5	7.6	7.0	6.5	5.7	4.6	4.1	3.2	2.6	2.1	1.8	1.3	1.0	0.8	0.6	0.5	0.3	0.3
7.5	6.9	6.7	5.9	5.9	5.3	4.7	4.1	3.7	3.2	2.6	2.0	1.5	1.2	0.9	0.9	0.6	0.4	0.4	0.3	0.2
8.0	5.0	4.6	4.4	4.1	3.7	3.6	3.0	2.6	2.2	1.8	1.5	1.2	1.0	0.8	0.6	0.5	0.4	0.3	0.2	0.2
8.5	3.6	3.4	3.2	3.1	2.9	2.6	2.3	1.9	1.6	1.5	1.2	0.9	0.9	0.7	0.5	0.4	0.4	0.3	0.2	0.2
9.0	2.5	2.5	2.4	2.1	2.0	1.9	1.6	1.4	1.3	1.0	0.7	0.7	0.5	0.4	0.4	0.4	0.3	0.2	0.2	0.2
9.5	1.8	1.9	1.5	1.6	1.4	1.2	1.1	1.1	0.8	0.7	0.6	0.5	0.4	0.4	0.3	0.3	0.2	0.2	0.2	0.1
10.0	1.3	1.1	1.1	1.0	1.0	0.9	0.8	0.8	0.7	0.6	0.5	0.4	0.3	0.3	0.3	0.2	0.1	0.1	0.1	0.1

To compare the risks for the deviation in the future samples, four different sampling regimens (10×1, 10×2, 10×3, and 6×2) with various acceptance criteria (NMT 3.0% SD, 4.0% SD, and 5.0% SD) were evaluated as shown in Figure 5. The number of the colored combinations decrease as replicates

increase, and they decrease when tighter acceptance criteria are applied. 10×1 with the acceptance criteria of NMT 3.0% SD, 10×3 with the acceptance criteria of NMT 3.0% SD, and 10×3 with the acceptance criteria of NMT 5.0% SD that are the alternative procedures proposed by the BUCU Group, were confirmed to be much more conservative compared to the 10×1 with acceptance criteria of NMT 5.0% SD, the conventional approach according to the withdrawn guidance. The simulation proved that by applying tighter acceptance criteria, one can assure the homogeneity of the bulk powder blend without taking replicate samples from each sampling point, though it is impossible to predict the between- and within-location variability. In addition, using 6×2 with the acceptance criteria of NMT 4.0% SD, lacks red colored regions at all. This means that the false positive probability is not more than 10% regardless of the between-location variation σx and within-location variation σy. Therefore by applying 6×2 with acceptance criteria of NMT 4.0% SD, the population blend uniformity could be assured with C=90%/LB=95%, that would be an equivalent or even more severe quality control without increasing the number of samples significantly compared to the 10×3 with the acceptance criteria of NMT 5.0% SD, the stage 2 blend testing proposed by the BUCU Group. This assurance level is higher than that for the content uniformity test proposed by the BUCU Group, C=50%/LB=95% for process qualification, process verification and routine release testing of drug products. This difference would be appropriate considering the risks of content uniformity failure due to processes such as segregation during tableting.

Figure 5 *P3* of the each combination of σx and σy for various sampling regimen and acceptance criteria (AC). (a) 10×1, AC: NMT 5.0% SD, (b) 10×2, AC: NMT 5.0% SD, (c) 10×3, AC: NMT 5.0% SD, (d) 6×2, AC: NMT 5.0% SD, (e) 10×1, AC: NMT 4.0% SD, (f) 10×2, AC: NMT 4.0% SD, (g) 10×3, AC: NMT 4.0% SD, (h) 6×2, AC: NMT 4.0% SD, (i) 10×1, AC: NMT 3.0% SD, (j) 10×2, AC: NMT 3.0% SD, (k) 10×3, AC: NMT 3.0% SD, (l) 6×2, AC: NMT 3.0% SD

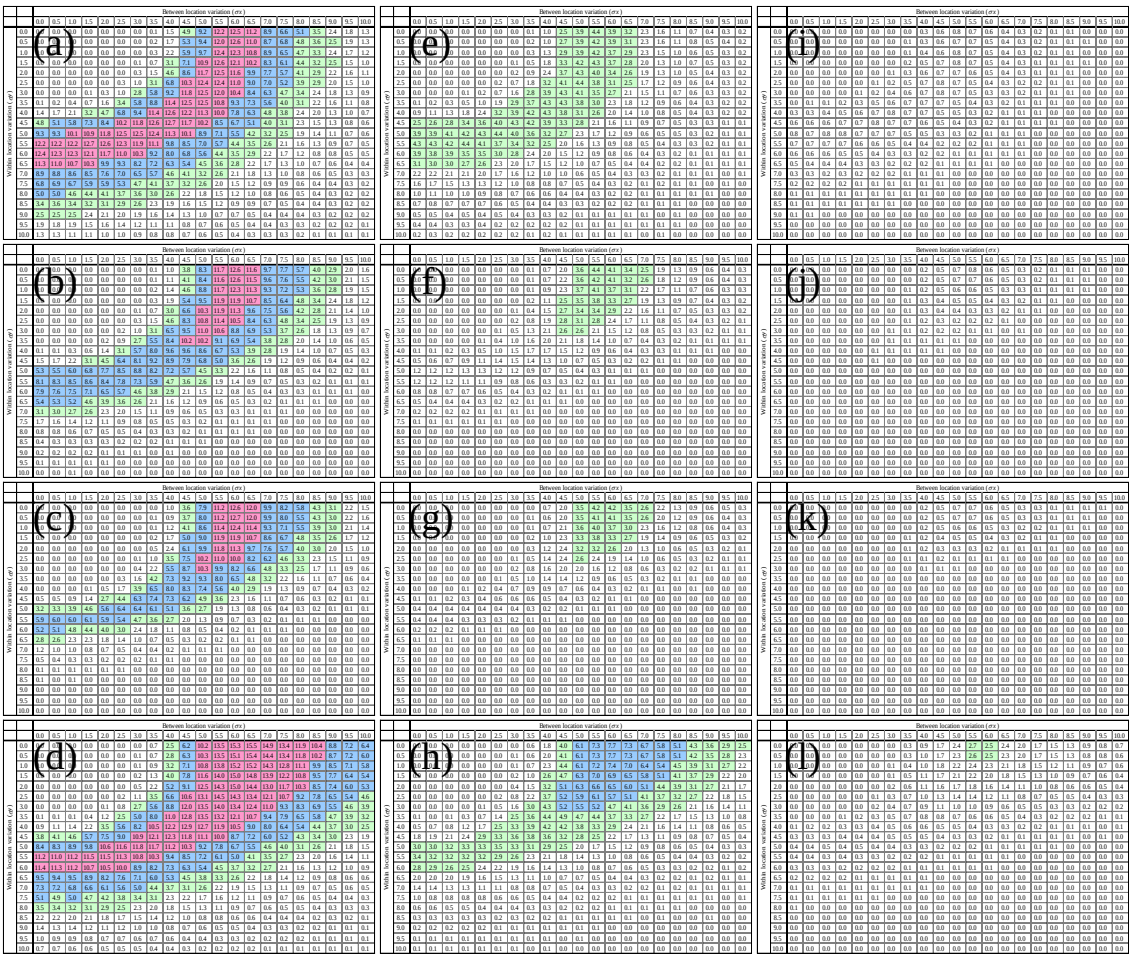

To compare the prediction accuracy of σx and σy between the sampling regimens of 10×3 and 6×2, probability density distributions of *sx* and *sy* at the three combinations of σx and σy: (σx, σy) = (6, 0.5), (5, 3), and (0.5, 5.5) were evaluated. According to Figure 5, (σx, σy) = (6, 0.5) was expected to have the highest P3 due to the high σx in the sampling regimens of 10×3 and 6×2. (σx, σy) = (5, 3) was also predicted to have relatively high P3, and both σx and σy were the cause of the high P3. P3 at (σx, σy) = (0.5, 5.5) was also expected to be high compared to the other combinations, and σy was the cause of the high P3. Figure 6 shows the probability density distributions of *sx* and *sy*. As shown in Figure 6 (a) and (b), in the case of (σx, σy) = (6, 0.5), the predicted range of *sx* was significantly higher than *sy* reflecting the σx and σy. It was confirmed that though it was difficult to predict σx accurately based on *sx* in both sampling regimens, the accurate estimation of σy was considered possible. Furthermore, since the distribution range of *sx* was confirmed much higher than that of *sy*, *sx* will be identified correctly as the cause of the high assay SD in both sampling regimens. In the case of (σx, σy) = (0.5, 5.5) provided in Figure 6 (c) and (d), the distribution range of *sy* was confirmed to be higher than that of *sx* though their distributions overlap. Based on the distributions, it was confirmed that *sy* will be identified correctly as the cause of high assay SD. When both σx and σy were the cause of the high assay SD as is the case of (σx, σy) = (5, 3), it was considered difficult to predict the causes because both, σx and σy, have wide distribution in both sampling regimens as shown in Figure 6 (e) and (f). To summarize, the adequacy of the root cause analysis was confirmed to be comparable between the sampling regimens of 10×3 and 6×2.

Figure 6 Probability density distributions of *sx* and sy. (a) 10×3, (σx, σy) = (6, 0.5), (b) 6×2, (σx, σy) = (6, 0.5), (c) 10×3, (σx, σy) = (0.5, 5.5), (d) 6×2, (σx, σy) = (0.5, 5.5), (e) 10×3, (σx, σy) = (5, 3), (f) 6×2, (σx, σy) = (5, 3)

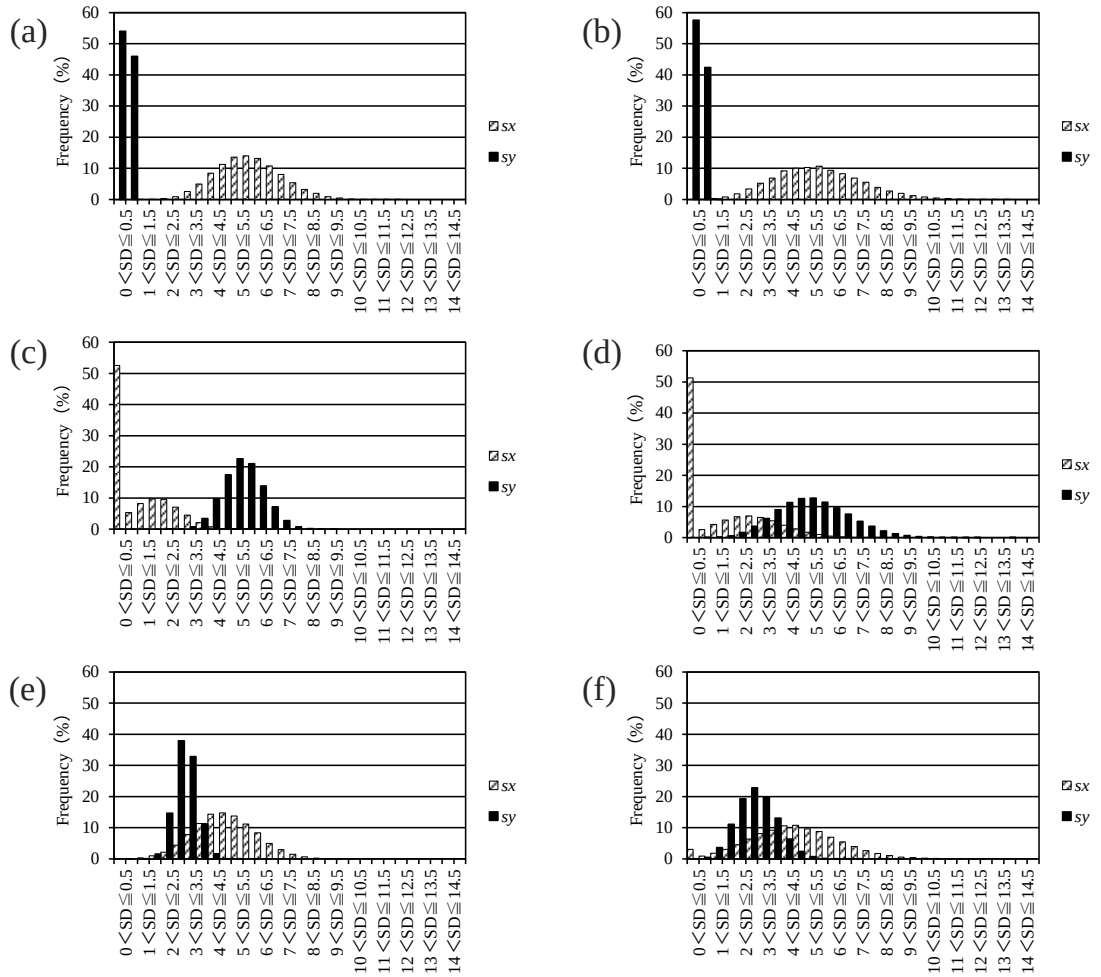

It was expected that once the process and the analytical validation of sampling method will have been accomplished (e.g., sampling bias was validated to be not > 2%), it will be possible to select the appropriate sampling regimen and the acceptance criteria assuring the desired level of *P3* within the range of $\sigma y \leq 2\%$. The uniformity of the powder blend, which affect a critical quality attribute of content uniformity, will be assured on a scientific basis through the applied sampling regimen and acceptance criteria, without fixing the sampling points and the number of samples from each sampling point in a blind way.

In conclusion, Monte Carlo simulation enables to estimate the risks on blend and content uniformity for each sampling regimen and acceptance criteria. Therefore, by utilizing the Monte Carlo simulation, it is possible to provide the scientific rationale for the any sampling regimen and acceptance criteria.

Conclusions

Monte Carlo simulation revealed that the novel sampling regimen and the acceptance criteria proposed by the BUCU Group in ASTM E2709 and ASTM E2810 can assure higher probability of passing the minimum necessary requirement for future samples compared to the conventional procedure based on the withdrawn FDA draft guidance for industry on Powder Blends and Finished Dosage Units — Stratified In-Process Dosage Unit Sampling and Assessment. In addition, the simulation had confirmed that both, the sampling regimen and the acceptance criteria affect the probability of the future samples that will satisfy the minimum necessary requirement. Therefore, it is possible to assure the same probability using other sampling regimens and acceptance criteria as the procedure proposed by the BUCU Group. Furthermore, by combining the VCA for the sample measurement results and the Monte Carlo simulation, the accuracy of *sx* and *sy* to the σx and σy in respective sampling regimens were successfully estimated. It was concluded that by utilizing the Monte Carlo simulation, it is possible to provide the scientific rationale for the any sampling regimen and acceptance criteria.

Appendix

Normality of the random number generated in the Monte Carlo simulation is tested by comparing observed and theoretical distribution of chi-squared value[59]. A sample value of chi-square in the sampling regimens of 10×1 is calculated as follows at the situation in which σy is zero:

$$\chi^2_{MC} = \frac{Vdf}{\sigma^2} \qquad \text{(A1)}$$

Where χ^2_{MC} denotes a sample value of chi-square, *V* denotes unbiased sample variance, *df* denotes degree of freedom (*df* = 9 for 10×1), and χ^2 denotes population variance, which is equal to σx^2. χ^2_{MC} is calculated thirty thousand times to build the cumulative percentage distribution. Theoretically, the distribution of χ^2_{MC} should have a chi-squared distribution with 9 *df* if the samples generated in the Monte Carlo simulation are normally distributed. Since χ^2_{MC} is independent of σx, 2.0% is applied to σx in this test. As shown in Table A1, the difference between χ^2_{MC} and theoretical chi-squared value χ^2 was not more than 0.5% at 1.0%, 2.5%, 50.0%, 97.5%, and 99.0% cumulative points, which suggest that the normality of random number generated in the Monte Carlo simulation is reliable.

[59] Greenwood, P.E. and Nikulin, M.S., 1996. A guide to chi-squared testing. New York: Wiley & Sons, Inc..

Table A1 Observed and theoretical values of chi-square

	1.0%	2.5%	50.0%	97.5%	99.0%
χ^2_{MC}	2.088	2.700	8.343	19.02	21.67
χ^2	2.096	2.688	8.336	19.02	21.66
% difference	0.382	0.446	0.084	0	0.046

Case study 3 - Selection of a round convex tablet shape that mitigates the risk of chipping and capping based on systematic evaluation by utilizing multivariate analysis

European Journal of Pharmaceutical Sciences 120 (2018) 212–221

Contents lists available at ScienceDirect

European Journal of Pharmaceutical Sciences

journal homepage: www.elsevier.com/locate/ejps

Selection of a round convex tablet shape that mitigates the risk of chipping and capping based on systematic evaluation by utilizing multivariate analysis

Shuichi Tanabe[a,b,c,*], Hiroshi Nakagawa[a], Tomoyuki Watanabe[a], Hidemi Minami[a], Shuichi Ando[a], Nora A. Urbanetz[b], Regina Scherließ[c]

[a] Formulation Technology Research Laboratories, Daiichi Sankyo Co., Ltd., 1-12-1 Shinomiya, 2540014 Hiratsuka, Japan
[b] Pharmaceutical Development, Daiichi Sankyo Europe GmbH, Luitpoldstrasse 1, 85276 Pfaffenhofen, Germany
[c] Department of Pharmaceutics and Biopharmaceutics, Kiel University, Grasweg 9a, 24118 Kiel, Germany

Outline

In case study 3, process optimization based on a process model is studied with focus on tablet shape. Unlike a blending process, a tableting process is typically a continuous process, therefore it is possible to perform various process conditions including DoEs with reasonable cost. Chemometric techniques, PLSR for example, is widely applied for industrial process modeling when plenty of data is available. This is because the accuracy and the applicable range of a chemometric model depend on the quality and quantity of the data set used for model development. Further, the PLSR model has an additional advantage as PLSR is one of the linear regression methods that can solve the multicollinearity problem by using latent variables, which are linear combinations of the original input parameters and are independent of each other. The optimization of tablet shape is one example of a multivariate problem that is not understood comprehensively, as the parameters determining the tablet shape, i.e., cup depth and surface radius, are mutually correlated to form a convex cup portion of a tablet. Because of the multicollinearity, similar tablet shape can be built with different combinations of tablet shape parameters, which makes the comprehensive understanding of the relationship between tablet shape and the physical robustness difficult. Herein the aim of this case study is to demonstrate the practical benefits of process modeling and optimization of a multicollinearity problem through the selection of a tablet shape having the desired physical robustness.

Abstract

Selecting a tablet shape that minimizes the risk of chipping and capping during manufacture is important in pharmaceutical industry. Here, the selection was performed based on systematic evaluation for the first time. Abrasion and stress relaxation time were utilized as indices of the occurrences of chipping and capping, respectively. Partial least square regression models that used tablet shape parameters to estimate the tablet's abrasion and stress relaxation time were utilized to develop response surface plots of the effect of the tablet shapes on the occurrence of chipping and capping systematically, and to identify an optimum tablet shape that is expected to have a low occurrence of chipping and capping. A verification study using commercial scale facilities proved that the optimum tablet shape had a lower occurrence of chipping and capping compared to suboptimum examples as speculated by their abrasion and stress relaxation time. The observed mathematical relationship between the tablet shapes and the occurrence of chipping and capping were consistent with the previous studies based on the comparison of limited number of tablet shapes using different formulations. Consequently, it is expected to be applicable to other formulations beyond the evaluated formulation in the present study.

Keywords: Abrasion, Stress relaxation time, Partial least squares regression (PLSR)

Introduction

Tablets are a common pharmaceutical solid dosage form consisting of one or more active ingredients in combination with excipients. In general, tablets are manufactured by compression of a powder blend or granules, and a polymer coating is often applied to the tablets. The tablets are packed in blisters or bottles to be shipped to hospitals or community pharmacies. Physical defects of the tablets are one of the most common problems resulting from the compression process and the following processes of handling, coating, packaging, and shipping, since the physical defects will have a negative impact on critical quality attributes such as assay, content uniformity, and visual appearance.

Figure 1 shows two common types of tablet physical defects. The physical defect provided in Figure 1 (a), generally called chipping, is the loss of a small portion at the edges or the cup surface. Chipping is considered to be due to a low inter-granular binding force that apart from chipping also leads to low tablet hardness and high friability. Figure 1 (b) shows a partial or complete separation of the cup portion of the tablet, generally called capping. It was considered that the elastic recovery of a tablet after compression is one of the primary causes of the physical defects including capping, which is correlated with other reported root causes such as die-wall pressure during decompression, non-uniform density and stress distribution in a tablet. Air entrapment at the compression has also been known as one of the other common root causes of capping, which can be solved by prolonging the

total compression time[60]. Garr and Rubinstein (1991)[61] reported that the occurrence of capping increased as the elastic energy stored at the end of compression, i.e., the residual die-wall pressure, which causes elastic recovery during decompression, became high. The non-uniformity of shear stress and density distributions in a tablet are caused by the elastic recovery, which was considered to be the root cause of chipping and capping during the tableting process and the following processes[62, 63]. The type of the physical defects derived from the tablets' elastic recovery depends on the tablet shape[62]. Akseli (2013)[63] reported that the elastic properties of a tablet measured after the compression also correlated with the capping tendency, whereas Garr and Rubinstein (1991)[61] and Wu (2008)[62] focused on the stress relaxation and elastic recovery during the compression process.

Figure 1 Typical cracks in 8 mm diameter tablets. (a) Chipping. (b) Capping.

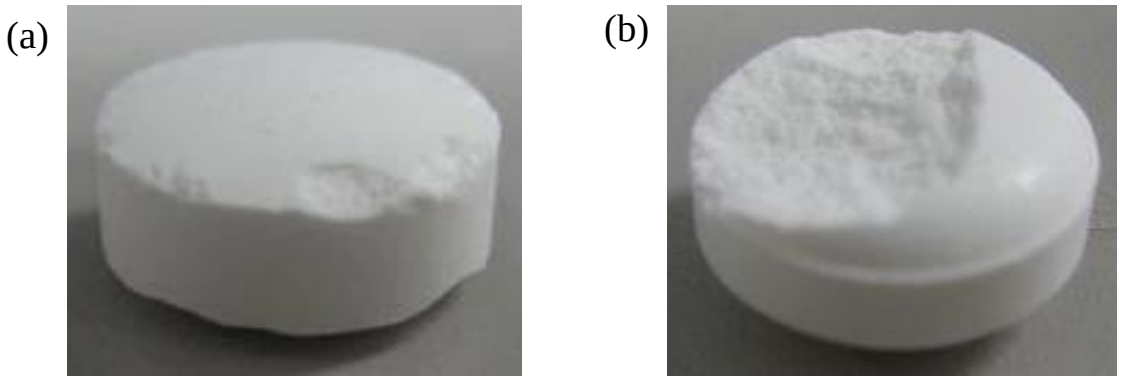

Tablet shape is one of a number of factors affecting the mechanical strength of tablets, even among round tablet shapes. The round tablet is recognized as the most common tablet shape, usually consisting of a cylinder portion with a flat face or convex as shown in Figure 2. In most cases the curvature of the convex cup portion is composed of a single or double radius. Figure 3 shows the definitions of the parameters that constitute a single or double radius cup portion. *R1*, *R2*, cup depth

[60] Tanino, T., Aoki, Y., Furuya, Y., Koji, S., Takeda, T., Mizuta, T., 1995. Occurrence of capping due to insufficient air escape during tablet compression and a method to prevent it. Chem. Pharm. Bull. 43, 1772–1779.

[61] Garr, J.S.M. and Rubinstein, M.H., 1991. An investigation into capping of paracetamol at increasing speed of compression. Int. J. Pharm. 72, 117–122.

[62] Wu, C.Y., Hancock, B.C., Mills, A., Bentham, A.C., Best, S.M., Elliott, J.A., 2008. Numerical and experimental investigation of capping mechanisms during pharmaceutical tablet compaction. Powder Technol. 181, 121–129.

[63] Akseli, I., Ladyzhynsky, N., Katz, J., He, X., 2013. Development of predictive tools to assess capping tendency of tablet formulations. Powder Technol. 236, 139–148.

(*C*), diameter (*DIA*), land, α, and β define the cup portion. The value obtained by dividing *C* by *DIA* can be used to classify a convex tablet into categories such as a shallow convex (*C*/*DIA* = ca. 0.07), standard convex (*C*/*DIA* = ca. 0.10), deep convex (*C*/*DIA* = ca. 0.13), and extra deep convex (*C*/*DIA* = ca. 0.19). Chowhan et al. (1992)[64] reported that the friability of extra deep convex tablets was lower than that of standard and deep convex tablets. Wu et al. (2008)[62] reported that single radius standard convex tablets had a higher occurrence of capping compared to single radius shallow convex and flat-faced cylindrical tablets, whereas the single radius shallow convex and flat-faced cylindrical tablets had a higher occurrence of chipping. The type of the physical defects correlated with the tilt angle of intensive shear stress band at the edge of cup portion during decompression estimated by X-ray tomography and finite element (FE) modeling in the same study. The tilt angle of the intensive shear stress band against compression direction was larger in the single radius standard convex tablet compared with the single radius shallow convex tablet and flat-faced cylindrical tablets. The larger tilt angle of the intensive shear stress band was considered to facilitate the separation of the cup portion in the single radius standard convex tablet. On the other hand, the low tilt angle of the intensive shear stress band against compression direction lead to the loss of a small portion at the edge of the cup portion in the single radius shallow convex tablet and flat-faced cylindrical tablets[62]. Laity et al. (2010)[65] reported that flat-faced cylindrical tablets had a higher occurrence of chipping compared to that of the single radius extra deep convex tablets. The results by small-angle X-ray scattering (SAXS) measurement and FE modeling showed that the flat-faced cylindrical tablets had a low density part at the bottom corners but the single radius extra deep convex tablets appeared to present well compacted regions over most of their surfaces. Furukawa et al. (2015)[66] reported that when comparing the single radius shallow convex tablet and the double radius deep convex tablets, the occurrences of capping were higher in the double radius deep convex tablets compared to the single radius shallow convex tablets due to the difference in plastic strain distribution during compression. These studies proved that the tablet shape affects the occurrence of chipping and capping. However, in these reference studies the mechanical strength of limited numbers of tablet shapes were evaluated by using different formulations. Due to the lack of a systematic evaluation of tablet mechanical strength versus shape to gain a comprehensive understanding of the chipping and capping behavior, by employing such a

---

[64] Chowhan, Z.T., Amaro, A.A., Ong, J.T.H., 1992. Punch geometry and formulation consideration in reducing tablet friability and their effect on in vitro dissolution. J. Pharm. Sci. 81, 290–294.

[65] Laity, P.R., Han, L., Elliott, J., Cameron, R.E., 2010. Variation in compaction behaviour for tablets of different size and shape, revealed by small-angle x-ray scattering. J. Pharm. Sci. 99, 4380–4389.

[66] Furukawa, R., Chen, Y., Horiguchi, A., Takagaki, K., Nishi, J., Konishi, A., Shirakawa, Y., Sugimoto, M., Narisawa, S., 2015. Numerical evaluation of the capping tendency of microcrystalline cellulose tablets during a diametrical compression test. Int. J. Pharm. 493, 182–191.

systematic approach the proposal of a tablet shape that has a lower occurrence of both chipping and capping has not yet occurred. Thus, the approach to the selection of a round tablet shape by pharmaceutical companies has been generally performed for all compounds having different physical and chemical properties through trial-and-error procedures to minimize the chipping and capping. Herein, the aim of this study is to understand the effect of a round tablet shape on the mechanical strength systematically and to select a round tablet shape that has a lower occurrence of chipping and capping compared to other round tablet shapes based on this systematic understanding.

A round convex tablet shape was the focus of the systematic evaluation in this study since it is the most common tablet shape in use today. Target values of *DIA*, tablet weight (*W*), and apparent tablet density (*D*) are usually fixed according to formulation and the desired quality attributes such as dissolution. Therefore, the effects of *R1*/*DIA*, *R2*/*DIA*, and *C*/*DIA* on the occurrence of chipping and capping at the target values of land, *W*, and *D* were evaluated. The ideal combinations of *R1*/*DIA*, *R2*/*DIA*, and *C*/*DIA* in terms of the mechanical strength of the tablet were identified based on this evaluation. Abrasion (*A*) and stress relaxation time (*RT*) were utilized as indices of physical defects, i.e., chipping and capping. Tablets that have few abrasions are expected to show a lower occurrence of chipping[67]. Tablets that have a short stress relaxation time are expected to show fewer occurrences of both chipping and capping[61, 62]. This is because the short stress relaxation time of a tablet implies that the tablet stores low elastic energy at the end of compression due to the immediate relaxation, which results in its low die-wall pressure and low elastic recovery during decompression compared with the other tablets having the same formulation. The low elastic recovery correlates with less variation of the shear stress in a tablet, which had been reported to be the root cause of chipping and capping[62].

[67] Osei-Yeboah F., Sun C.C., 2015. Validation and applications of an expedited tablet friability method. Int. J. Pharm. 484, 146–155.

Figure 2 Round tablet shapes. (a) Top view. (b) Side view of a flat-faced cylindrical tablet. (c) Side view of a convex tablet.

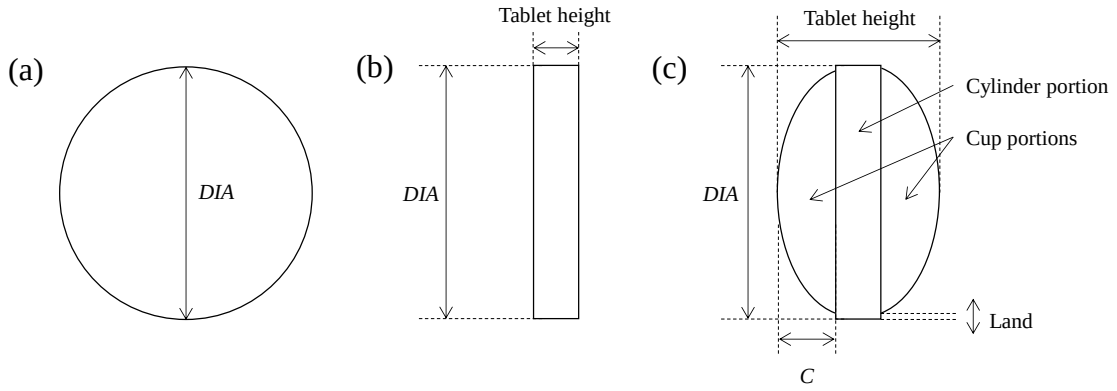

Figure 3 Definitions of the parameters that constitute a single or double radius cup portion. (a) Single radius convex cup portion. (b) Double radius convex cup portion.

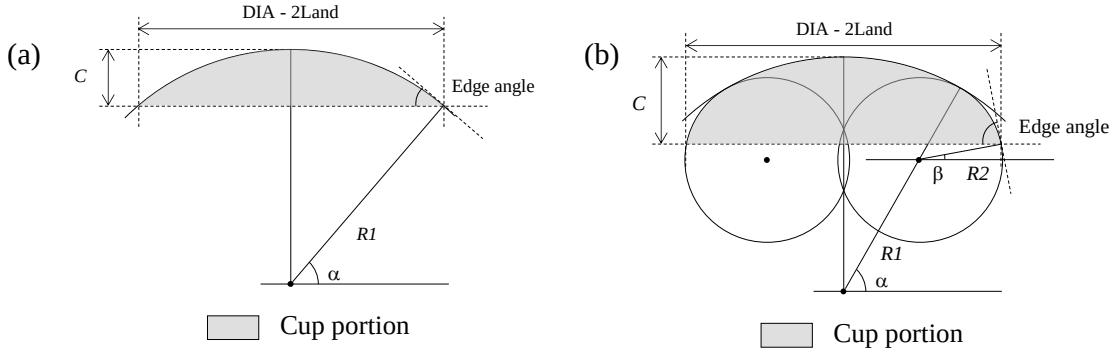

Materials and Methods

Tablets used in this study were immediate release tablets mainly composed of active ingredient and mannitol. Fluid bed granulation followed by screening was performed to prepare the granules. Then the granules were blended with magnesium stearate to be compacted. All tablets were proportionally similar, which means that the granule formulation was the same. In general, the round convex tablets manufactured by a rotary tableting machine had two equal convex portions at the top and bottom, and a cylinder portion in between. The parameters provided in Figure 3 are dependent upon each other to satisfy a smooth convex cup portion as shown in Equations 1 and 2.

$$C = R1(1-\sin\alpha) + R2(\sin\alpha - \sin\beta) \quad (1)$$

$$\frac{DIA}{2} - Land = R1\cos\alpha + R2(\cos\beta - \cos\alpha) \quad (2)$$

Where $R1 \geq R2$, $\alpha \geq \beta$, $DIA/2 \geq$ Land. Angles of α and β are determined dependently when *R1*, *R2*, *C*, *DIA*, and Land are determined. Per definition, in the case of a single radius convex tablet, *R2* is equal

to *R1* and β is equal to α. The edge angle, which is the tangent angle at the edge of the cup portion, is the complementary angle of β. The cylinder diameter is equal to *DIA*.

Tablet height is correlated to *W* and *D*. In general, the length of land is determined to provide punches for compression with a sufficient pressure resistance. Therefore, usually it is constant with any combinations of *R1*, *R2*, *C*, and *DIA*.

The use of normalized values of *R1*, *R2*, and *C* by *DIA* for defining the optimum tablet shape is considered reasonable, since the tablet shape defined by *R1*/*DIA*, *R2*/*DIA*, and *C*/*DIA* can summarize the optimum tablet shape in various *DIA* in a simple form. To evaluate the effects of *R1*/*DIA*, *R2*/*DIA*, and *C*/*DIA* on the abrasion and the stress relaxation time systematically, partial least squares regression (PLSR) models that use *R1*/*DIA*, *R2*/*DIA*, and *C*/*DIA* to estimate tablets' abrasion and stress relaxation times were developed. PLSR is one of the linear regression methods that can solve the multicollinearity problem by using latent variables[68, 69]. The main advantage of the PLSR is that it can generate latent variables, which are independent from each other, and cope with mutually correlated input variables[24], e.g., *R1*/*DIA*, *R2*/*DIA*, and *C*/*DIA*. *W*, *D*, and the three granule properties bulk specific volume (SV_B), tapped specific volume (SV_T), and mean volume diameter (*MVD*) were also used as input parameters in the PLSR models to take into account their effects on abrasion and stress relaxation time. The ideal combination of *R1*/*DIA*, *R2*/*DIA*, and *C*/*DIA* was determined based on the predicted abrasion and stress relaxation time of the various combinations that were practically available and within the confidence limits of the PLSR models.

The identified optimum round tablet shape according to the PLSR models and the suboptimum examples, called a verification set in this study, were manufactured and handled in commercial scale facilities in order to mimic real conditions for verifying its mechanical strength. Abrasion and stress relaxation times were evaluated to confirm their consistency with the predicted values by the PLSR models. The number of defective tablets observed after the manufacture was evaluated and taken as an indicator for the mechanical strength of the evaluated samples.

2.1. Calibration set and test set

The distribution of calibration set and test set for the PLSR model development was shown in Figure 4. Tabulated data of the calibration set and the test set were provided as supplementary information. *R1*, *R2*, *C*, *DIA*, and land were assumed equal to the dimensions of the punches and dies used. *DIA* and *W* were strongly correlated according to principle as provided in Figure 4 (d). *D* and *W* showed

[68] Wold, H, 1974. Causal flows with latent variables: Partings of the ways in the light of NIPALS modelling. Eur. Econ. Rev. 5, 67–86.

[69] Geladi, P., Kowalski, B.R., 1986. Partial least squares regressions: a tutorial. Anal. Chim. Acta. 185, 1–17.

moderate correlation in the data set as shown in Figure 4 (e). Land, defined in Figure 2 (c), of all punches used in this study is 0.1 mm. The calibration set contains 100 combinations using 40 different punches, various *W*, and *D* including a wide range of tablet shapes of single and double radius convex tablets that have been generally manufactured in the pharmaceutical industry. Thirteen different punches were used to prepare the test set containing thirteen combinations, which by principle was independent of the calibration set. Tableting of the calibration set and the test set were carried out using a rotary tableting machine VIRGO (Kikusui Seisakusho Ltd., Kyoto, JP) equipped with a gravity feeder. Turntable rotation speed was 30 rpm which corresponds to the dwell time of ca. 0.03 sec. The ratio of the pre-compression force to the main compression force was 30% in the calibration set and test set manufacture. Figure 5 shows four typical round tablet shapes that were included in the calibration set. Figures 5 (a) and (b) show single radius and double radius shallow convex tablets, respectively. Figures 5 (c) and (d) show single radius and double radius deep convex tablets, respectively. The four typical tablet shapes provided in Figure 5 are highlighted by dotted circles in Figures 4 (a), (b), and (c).

Figure 4 Tablet shape distributions in calibration set and test set. (a) Three-dimensional distribution of *R1*/*DIA*, *R2*/*DIA*, and *C*/*DIA*. (b) *R1*/*DIA* - *R2*/*DIA*. (c) *R1*/*DIA* - C/*DIA*.

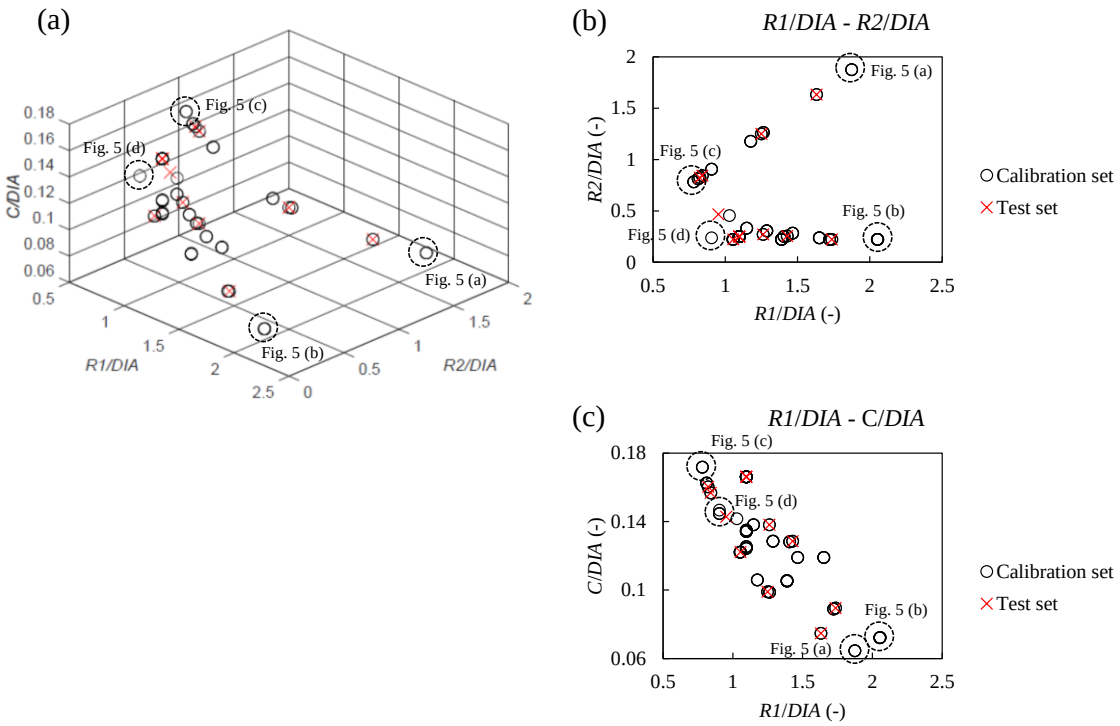

Figure 4 Tablet shape distributions in calibration set and test set (continued). (d) *DIA - W.* (e) *D - W.*

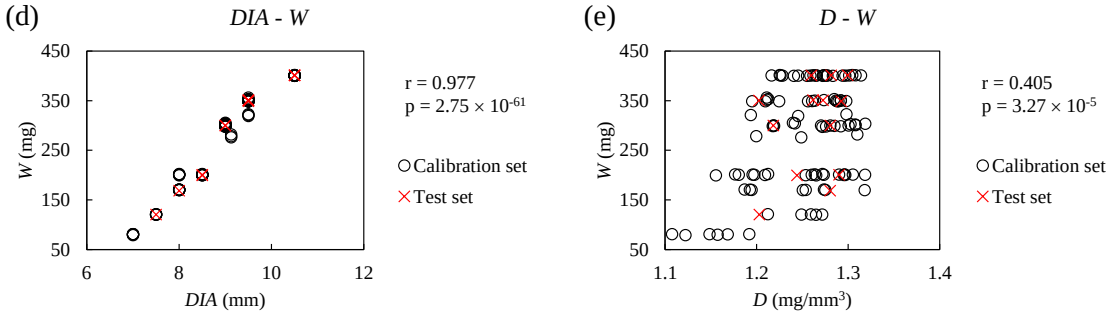

Figure 5 Four typical tablet shapes. (a) Single radius shallow convex tablet. *R1*/*DIA* = 1.875, *C*/*DIA* = 0.065. (b) Double radius shallow convex tablet. *R1*/*DIA* = 2.056, *R2*/*DIA* = 0.222, *C*/*DIA* = 0.072. (c) Single radius deep convex tablet. *R1*/*DIA* = 0.782, *C*/*DIA* = 0.172. (d) Double radius deep convex tablet. *R1*/*DIA* = 0.905, *R2*/*DIA* = 0.238, *C*/*DIA* = 0.147.

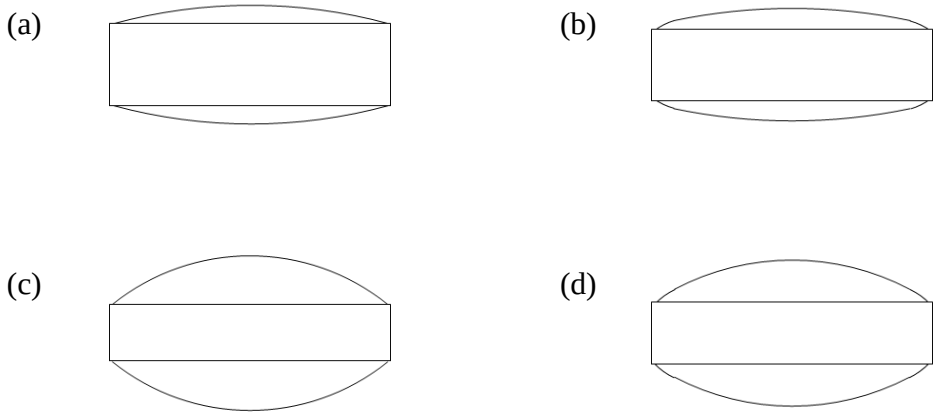

2.2. Abrasion test

An abrasion test was conducted to evaluate the tablets' friability using the abrasion tester SZ-03 (Rinkan Kogyo Co., Ltd., Kanagawa, JP) proposed by Webster and van Abbé (1955)[70], shown in Figure 6. In this tester, 10 weighed tablets are loaded into the upper side of borosilicate glass cylinder equipped with a sieve at the center, and the cylinder moves upwards and downwards at 250 rpm for 2 minutes. This analysis provides the friability of samples at a more severe frictional condition than the friability test provided in USP/EP/JP, which helped us to identify the most robust round tablet shape. Abrasion was calculated by Equation 3.

[70] Webster, A.R. and van Abbé N.J., 1955. A test for the mechanical strength of compressed tablets. J. Pharm. Pharmacol. 7, 882–891.

$$A = \frac{100(W_I - W_F)}{W_I} \qquad (3)$$

Where A denotes abrasion (%), W_I denotes initial mean tablet weight, W_F denotes mean tablet weight after abrasion. An average value of n=2 tests was reported in this study.

Figure 6 Abrasion tester. (a) Appearance of the tester. (b) Cylinder geometry. (c) Geometry and schematic image of movement.

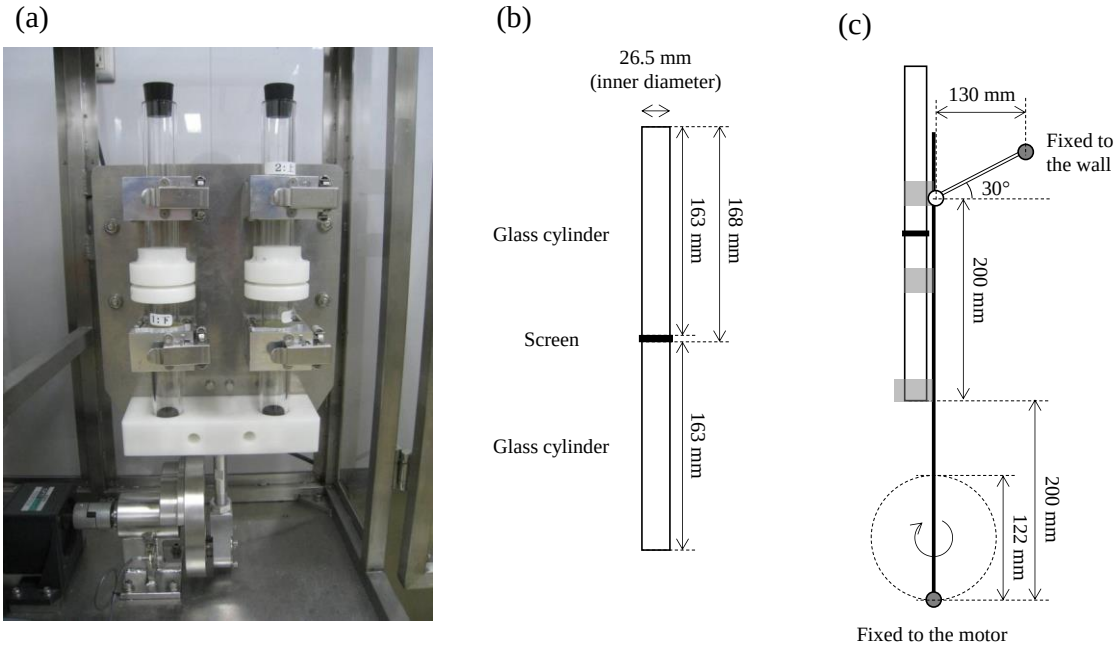

2.3. Stress relaxation time measurement

Stress relaxation time was measured using the texture analyzer TA-XT2i (Eko Instruments Co., Ltd., Tokyo, JP) working with a 5 kg load cell. The schematic image of stress relaxation time measurement was provided in Figure 7. Tablets were placed on a flat surface and their tops pressed from above at 0.05 mm/s until the force reached to 9.81 N which is equal to 1 kg. At the position of 9.81 N force, the probe stopped at the 9.81 N force position and the decay of the force was recorded, i.e., the stress relaxation profile, for 10 seconds. Here the stress relaxation was assumed to obey the Maxwell model, consisting of a Hookean spring and a Newtonian dashpot in series[71]. Using the stress relaxation profile, the stress relaxation time was calculated by Equation 4.

[71] Christensen, R.M., 1971. Theory of viscoelasticity. Academic Press, New York.

$$RT = -\frac{t}{\log \frac{F_t}{F_0}} \quad (4)$$

Where *RT* denotes stress relaxation time, *t* denotes delay time (10 s for this study), F_0 denotes the force at the beginning (9.81 N), F_t denotes the force at 10 s. An average value of n=5 tests was reported in this study.

Figure 7 Schematic image of stress relaxation time measurement

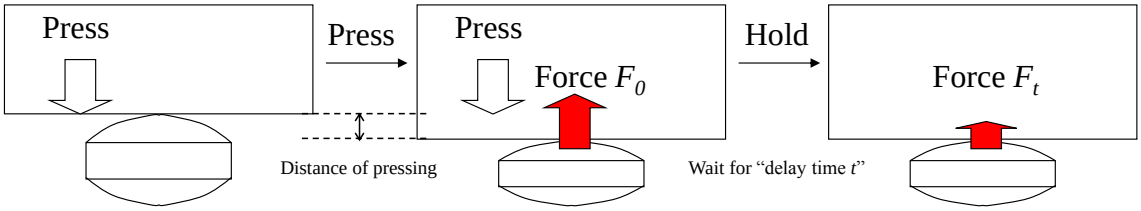

2.4. Bulk and tapped specific volume measurement

The bulk and tapped specific volume of lubricated granules were measured in duplicate according to the standards provided in Japanese Pharmacopoeia 17th edition, 3.01 Determination of bulk and tapped densities, Method 1: Measurement in a graduated cylinder. Tapping apparatus SZ-02 (Rinkan Kogyo Co., Ltd., Kanagawa, JP) was used for this analysis.

2.5. Mean volume diameter measurement of the granules

The mean volume diameter was measured according to the standards provided in Japanese Pharmacopoeia 17th edition, 3.04 Particle size determination, Method 2: Analytical sieving method. The measurement was performed by using Robot Sifter RPS-105 (Seishin Enterprise Co., Ltd., Tokyo, JP). Eight test sieves of 1000 μm, 500 μm, 355 μm, 250 μm, 180 μm, 150 μm, 106 μm and 75 μm openings and a sieve diameter of 75 mm are used.

2.6. Tablet weight and apparent tablet density measurement

The values of tablet weight and height of 20 tablets were measured using the automated tablet tester WHT 3ME (Pharma Test Apparatebau AG, Hainburg, GER) and mean values were calculated. Apparent tablet density was calculated by Equation 5.

$$D = W/(2CV + (DIA/2)^2 \pi (H - 2C)) \quad (5)$$

Where *D* denotes apparent tablet density (mg/mm^3), *W* denotes tablet weight (mg), *CV* denotes cup volume of a tablet (mm^3), *DIA* denotes tablet diameter (mm), π denotes circular constant, *H* denotes tablet height (mm), *C* denotes cup depth of a tablet (mm).

2.7. Partial Least Squares Regressions

SV_B, SV_T, *MVD*, *R1*/*DIA*, *R2*/*DIA*, *C*/*DIA*, *D*, and *W* are the input variables in the PLSR models that predict abrasion and stress relaxation time. The input variables and output variables of abrasion as well as stress relaxation time were centered by subtracting mean values and scaled by dividing by the sample standard deviation, which is a so-called auto-scaling. Base-10 log transformation was applied to abrasion before the auto-scaling to correct for heteroscedasticity, and to convert distributions into more symmetric curves[72]. SIMCA 13.0.3 (Umetrics, Umeå, SWE) was used to build the PLSR models. The number of latent variables was determined on the basis of the root-mean-square error of cross validation (RMSECV) of the leave-one-out cross validation. External validation using the test set provided in Figure 4 and in supplementary information was performed to test the prediction accuracy of the PLSR models.

2.8. Identification of optimum round tablet shape based on the PLSR models

The optimum round tablet shape was defined as the combination of *R1*/*DIA*, *R2*/*DIA*, and *C*/*DIA* that showed least abrasion and the shortest stress relaxation time of all combinations. The coefficients of the *R1*/*DIA*, *R2*/*DIA*, and *C*/*DIA* were used to identify their contributions to the output parameters[23]. The optimum combination was identified based on the predicted abrasion and stress relaxation times of the tablet shapes that were well distributed within the reliable ranges of the PLSR models, defined as the prediction set. The reliability of the predicted abrasion and stress relaxation times by the PLSR models was assured by the Hotelling's T^2 calculated with Equation 6 and the sum of squared residuals Q calculated with Equation 7 (squared prediction error, SPE)[23, 24, 73, 74].

$$T^2 = \sum_{i=1}^{K} \frac{t_i^2}{s_{t_i}^2} \qquad (6)$$

$$Q = \sum_{p=1}^{P} (x_p - \hat{x}_p)^2 \qquad (7)$$

---

[72] van den Berg, R.A., Hoefsloot, H.C.J., Westerhuis, J.A., Smilde, A.K, van der Werf, M.J., 2006. Centering, scaling, and transformations: improving the biological information content of metabolomics data. BMC Genomics 7, 142.

[73] Jackson, J. E., Mudholkar, G. S., 1979. Control Procedures for Residuals Associated With Principal Component Analysis. Technometrics. 21, 3,341–349.

[74] Kamohara, H., Takinami, A., Takeda, M., Kano, M., Hasebe, S., Hashimoto, I., 2004. Product Quality Estimation and Operating Condition Monitoring for Industrial Ethylene Fractionator. J Chem. Eng. Japan. 37, 3, 422–428.

Here, K is the number of adopted latent variables, t_i is the score of the ith latent variable, $s_{t_i}^2$ is its variance, P is the number of input variables, and x_p and $\hat{x}_p$ are experimental and reconstructed values of the pth input variable. Muteki et al. (2011)[23] reported that the two distance criteria, T^2 and Q, could test the validity of the PLSR model under new input variables. In the present work, the abrasion and stress relaxation time values were predicted with the constraint of 99% confidence intervals for both T^2 and Q.

2.9. Verification of the mechanical strength of tablets against physical defects

The tablets of the verification set were transferred using the material handling facility illustrated in Figure 8. The number of physically defected tablets was counted by visual inspection after the transferring in order to verify the assumption that the differences of abrasion and stress relaxation time caused by the differences in tablet shapes reflect the occurrences of physical defects. Tablets that had a physical defect bigger than ca. 1 mm^2 were considered as the defected tablets. Note that the comparison of the number of physically defected tablets was performed between the samples that had the same tablet weight and were manufactured by using the same tableting machine.

Figure 8 Material handling facility used in the verification study

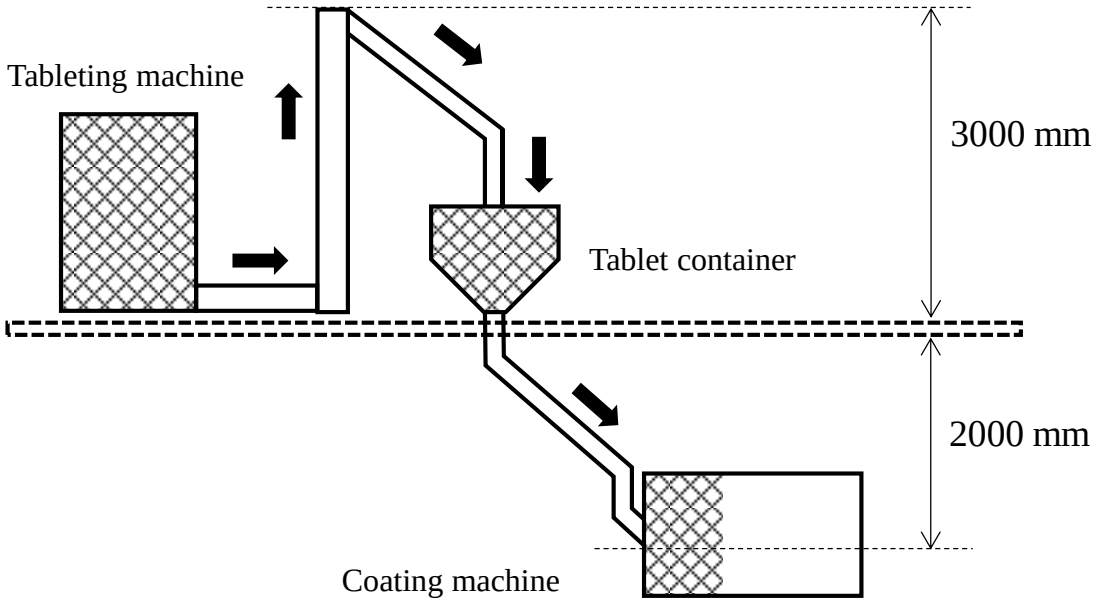

Results

3.1. Relationship between tablet shape and the mechanical strength

Three latent variables were adopted for the PLSR models predicting abrasion and stress relaxation time. Figure 9 and Table 1 show the prediction performances of the PLSR models such as correlation coefficients, slopes, intercepts, RMSECV, and external validation results expressed as the root-mean-

square errors of prediction (RMSEPs). The prediction of abrasion of fragile tables exhibiting abrasion is > 2% is less accurate, possibly due to the relatively large analytical errors of the destructive testing of fragile tablets. Table 2 shows the coefficients of input variables of the two PLSR models. The absolute values of the coefficients of *R2*/*DIA* and *C*/*DIA* for abrasion were greater than that of *R1*/*DIA*, which suggests that the variations of *R2*/*DIA* and *C*/*DIA* have a greater influence on abrasion than that of *R1*/*DIA*. On the other hand, the absolute value of the coefficient of *R1*/*DIA* for stress relaxation time was greater than those of *R2*/*DIA* and *C*/*DIA*.

Figure 9 Prediction performances of the PLSR models for (a) abrasion and (b) stress relaxation time. Solid and dotted lines are the regression line and the 95% upper and lower confidence intervals of prediction, respectively. Dashed line shows y = x.

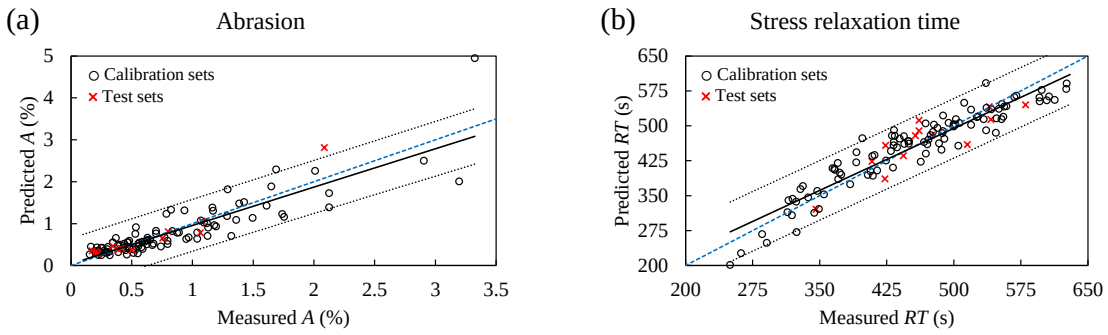

Table 1 Prediction performances of the PLSR models

Parameters	PLSR model for *A*	PLSR model for *RT*
Correlation coefficient	0.880	0.942
Slope	0.913	0.886
Intercept	0.046 %	51.6 s
RMSECV	0.345 %	32.6 s
RMSEP	0.232 %	30.9 s

Table 2 Coefficients of input variables of the PLSR models

Input variable	Abrasion	Stress relaxation time
	Coefficients	Coefficients
SV_B	0.01951	-0.11259
SV_T	-0.00530	-0.08816
MVD	-0.13389	-0.01048
R1/*DIA*	0.07435	0.19862
R2/*DIA*	0.31845	0.07791
C/*DIA*	-0.35884	-0.06953
D	-0.60307	0.60154
W	-0.28901	0.25441

Figures 10 (a) and (b) show the response surfaces of abrasion for six tablet shape groups of a prediction set differentiated by three levels of *C*/*DIA* (0.08, 0.12, and 0.16), and three levels of *R2*/*DIA* (0.2, 0.8, and 1.4). Figures 10 (c) and (d) show the response surfaces of stress relaxation times for the same tablet shape groups. For the prediction of abrasion and stress relaxation times, constant input variables of granule properties, apparent tablet density, and tablet weight were used to evaluate the effect of tablet shape parameters; SV_B = 2.7 mL/g, SV_T = 2.2 mL/g, *MVD* = 135 um, *D* = 1.28 mg/mm^3, and *W* = 400 mg. It was assumed that the granule properties does not affect the magnitude relations of the abrasion and stress relaxation time among the tablet shapes, whereas the granule properties do affect the numerical values of the abrasion and stress relaxation time. Therefore, to maximize the predictable ranges of *R1*/*DIA*, *R2*/*DIA*, and *C*/*DIA* according to the T^2 and *Q*, the granule properties applied were the average values of the calibration set. The values of *D* and *W* used were the target values in the verification study. Figure 10 clearly shows the practical effect of the variation in *R1*/*DIA*, *R2*/*DIA*, and *C*/*DIA* on abrasion and stress relaxation time within the applicable ranges according to the constraints of Equation 1, Equation 2, and the PLSR models. As expected by the coefficients of PLSR models, abrasion and stress relaxation times were reduced when *R1*/*DIA* and *R2*/*DIA* decreased and *C*/*DIA* increased. These results indicated that the single radius shallow convex tablet (e.g., Figure 5 (a)) was the worst tablet shape in terms of the occurrence of chipping and capping compared to the other tablet shapes. The estimated best tablet shape was the double radius deep or extra deep convex tablet (e.g., Figure 5 (d)). The worst and the best tablet shapes in the prediction set are provided in Table 3. Samples P1 and P2 showed the lowest abrasion and stress relaxation time, respectively. Samples P3 and P4 showed the highest abrasion and stress relaxation time, respectively. As expected by the response surface plots, the tablet shapes that minimize and maximize the abrasion were similar to the tablet shapes that minimize and maximize stress relaxation time as well as their predicted abrasion and stress relaxation time. The differences of abrasion and stress relaxation time in the best (sample P1) and the worst (sample P3) tablet shapes were considered significant, since the differences were 1.144% and 126.4 s, respectively, which were more than four times greater than the RMSEPs (0.232% and 30.9 s). In summary, the PLSR models proved that both abrasion and stress relaxation times could be reduced significantly by optimizing the tablet shape.

Figure 10 Response surfaces of abrasion and stress relaxation time. (a) Response surfaces of abrasion with *C*/*DIA* = 0.08, 0.12, and 0.16. (b) Response surfaces of abrasion with *R2*/*DIA* = 0.2, 0.8, 1.4. (c) Response surfaces of stress relaxation time with *C*/*DIA* = 0.08, 0.12, and 0.16. (d) Response surfaces of stress relaxation time with *R2*/*DIA* = 0.2, 0.8, 1.4.

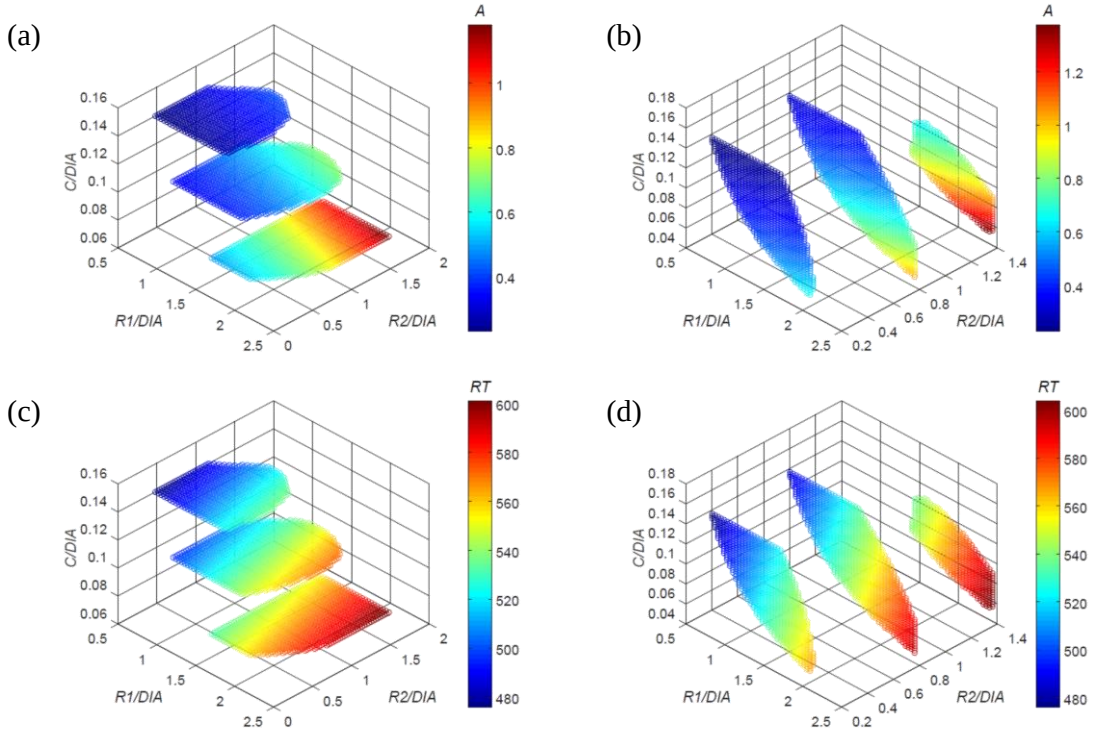

Table 3 Best and worst tablet shapes in prediction set

No.	*R1/DIA*	*R2/DIA*	*C/DIA*	A_{pred}	RT_{pred}
	-	-	-	%	s
P1	0.838	0.200	0.164	0.230	476.0
P2	0.838	0.143	0.160	0.231	475.9
P3	2.400	1.400	0.052	1.374	602.4
P4	2.438	1.400	0.055	1.355	603.9

3.2. Verification results using material handling facilities at commercial scale

The assumption that the differences of abrasion and stress relaxation time caused by differences in tablet shapes reflects the occurrence of physical defects was verified by using the four tablet shapes provided in Table 4, which is defined as the verification set. The verification set contained two DIA: 8.5 mm for samples V1 and V2 and 10.5 mm for samples V3 and V4. Samples V1 and V2 were manufactured by using a rotary tablet press AQU3 10362L2J II (Kikusui Seisakusho Ltd., Kyoto, JP). Samples V3 and V4 were manufactured by using a rotary tablet press VIRGO (Kikusui Seisakusho Ltd., Kyoto, JP). Pre-compression force ratio of 30% to the main compression force was applied in

the verification set manufacture. Turntable rotation speed was 30 rpm. The resultant dwell time in the AQU3 10362L2J II and VIRGO was 0.015 sec and 0.03 sec, respectively. The objective of the verification study using the two DIA tablets was to check that the optimal tablet shape defined by *R1*/*DIA*, *R2*/*DIA*, and *C*/*DIA* is effective in different *DIA*s when the granule properties, tablet weight, and tablet density are equivalent. Samples V1 and V3 were single radius and double radius deep convex tablets, respectively, that were located close to the optimal tablet shape of the prediction set. Sample V2 was a so called single radius standard convex tablet, which had a larger *R1*/*DIA*, *R2*/*DIA*, and smaller *C*/*DIA* than sample V1. Sample V4 was a double radius standard convex tablet, which had a larger *R1*/*DIA* and smaller *R2*/*DIA* and *C*/*DIA* than sample V3.

Table 4 Verification set consisting of 4 samples

No.	SV_B mL/g	SV_T mL/g	*MPS* μm	*DIA* mm	*R1*/*DIA* -	*R2*/*DIA* -	*C*/*DIA* -	*D* mg/mm^3	*W* mg	*A* %	*RT* s	A_{pred} %	RT_{pred} s
V1	2.79	2.26	174.1	8.5	0.824	0.824	0.160	1.270	200.3	0.4	285.4	0.486	441.1
V2	2.71	2.29	179.3	8.5	1.176	1.176	0.106	1.250	201.5	1.2	471.6	0.964	476.9
V3	2.53	2.13	149.8	10.5	0.952	0.467	0.143	1.274	401.0	0.4	324.3	0.320	490.8
V4	2.53	2.13	149.8	10.5	1.651	0.238	0.119	1.269	400.5	0.2	435.4	0.388	529.6

The correlation between the measured and the predicted abrasion and stress relaxation times was similar, as shown in Table 4. However, the verification set was outside of the confidence limits of the PLSR models, mainly due to the granule properties derived from the different granulation condition, meaning that the calculated numerical values are not accurate for prediction. Note that the granule properties, apparent tablet density, and tablet weight used for the prediction were as follows; SV_B = 2.7 mL/g, SV_T = 2.2 mL/g, *MVD* = 135 um, *D* = 1.28 mg/mm^3, and *W* = 200 mg (V1 and V2) and 400 mg (V3 and V4). Sample V2 showed an increased abrasion and stress relaxation time compared to sample V1. Abrasion of sample V4 was reduced compared to sample V3, but they were considered comparable since the difference was small and most likely within the range of the error of the analytical technique. On the other hand, the difference of stress relaxation time was significant between sample V3 and sample V4. In summary, it was confirmed that the verification set contained the tablet shapes closest to the optimum shape and suboptimum examples that had higher abrasion and/or stress relaxation times.

Table 5 shows the results of the verification study. Sample V1 showed only 19 cracked tablets among the 200,000 tablets, whereas the sample V2 showed 811 cracked tablets at the same scale. The type of physical defects, i.e., chipping and capping, was not evaluated because in the practical manufacture both defects are not acceptable and in most cases it is difficult to distinguish between the two. For the comparison of sample V3 and sample V4, sample V3 showed 3 cracked tablets, whereas the sample V4 showed 10 cracked tablets among 7,500 tablets. The difference of the number of cracked tablets was smaller than that when comparing the samples V1 and V2. This could be because

the sample V4 showed sufficiently low abrasion compared to the sample V1, though the stress relaxation time was relatively long. In summary, it was proven that by selecting the appropriate tablet shape without changing formulation, including tablet weight, apparent tablet density, and the granule properties, it is possible to prevent tablets from cracking during manufacture. Abrasion and stress relaxation time were demonstrated as effective indicators for estimating the mechanical strength of tablets against physical defects in their manufacture.

Table 5 Results of the verification study

No.	*Number of cracked tablets*	*Number of sample tested*	*% of cracked tablets*
V1	19	200,000	0.010
V2	811	200,000	0.406
V3	3	7,500	0.040
V4	10	7,500	0.133

Discussion

The overall relationship between the tablet shapes and the mechanical strength could be identified in this study. Comparing results with previous studies the consistency of this relationship can be confirmed. In detail, as mentioned earlier Chowhan et al. (1992)[64] reported that the friability of extra deep convex tablets was lower than that of standard and deep convex tablets. Laity et al. (2010)[65] reported that flat-faced cylindrical tablets showed higher occurrences of chipping than single radius extra deep convex tablets. As provided in Figure 10, our analysis showed that instances of abrasion become fewer as *R1*/*DIA* and *R2*/*DIA* decrease and *C*/*DIA* increases, which leads to fewer occurrences of chipping. Since the flat-faced cylindrical tablets can be assumed to have an *R1*/*DIA* approaching infinity and a *C*/*DIA* approaching zero, these observations were consistent with the results of Chowhan and Laity. Furukawa et al. (2015)[66] reported that double radius deep convex tablets (*R1*/*DIA* = 1.38, *R2*/*DIA* = 0.47, *C*/*DIA* = 0.13) showed a higher occurrence of capping compared to single radius shallow convex tablets (*R*/*DIA* = 1.50, *C*/*DIA* = 0.08) during a diametrical compression test. Abrasion of the single radius shallow convex tablet evaluated in Furukawa's study was significantly higher than that of the double radius deep convex tablet, whereas the stress relaxation time of the single radius shallow convex tablet was equal to or greater than that of the double radius deep convex tablet according to the PLSR models, as shown in Table 6. The granule properties used in Furukawa's study were assumed to be equal to the formulation used in this study for predicting the abrasion and the stress relaxation time, on the estimation of the difference in abrasion and stress relaxation time derived from the tablet shapes used in Furukawa's study. It was considered that due to the high instance of abrasion of the single radius shallow convex tablet, the single radius shallow convex tablet showed a chipping tendency rather than a capping tendency, although the stress relaxation times of the single radius shallow convex tablets were similar to those of the double radius deep convex tablets. The

double radius deep convex tablets showed a capping tendency in the hardness test rather than a chipping tendency because of the low instance of abrasion and relatively high stress relaxation time. At the same time, the tilt angle of the intensive shear stress band at the edge of the cup portion may be different reflecting the differences in tablet shape as reported by Wu et al. (2008)[62]. The difference of the tilt angle of the intensive shear stress band determined the type of the physical defects derived from the stored elastic energy during decompression. They reported that a single radius standard convex tablet has a higher occurrence of capping compared to single radius shallow convex and flat-faced cylindrical tablets, whereas the single radius shallow convex and flat-faced cylindrical tablets have a higher occurrence of chipping. According to Figure 10, the single radius shallow convex and the flat-faced tablets were expected to have more increased abrasion and stress relaxation times than the single radius standard convex tablets. However, possibly due to the insufficient mechanical strength to withstand chipping rather than capping, which derived from the abrasion, the stress relaxation time, and the tile angle of the intensive shear stress band, the single radius shallow convex and flat-faced tablets showed chipping. These facts imply that the type of physical defects depend on the tablet shape, abrasion, and stress relaxation time. Though the thresholds of the tablet shape, abrasion, and stress relaxation time determining the type of the physical defects due to the friability and elastic properties were not evaluated in this study, it was confirmed in this study (as well as in the reference studies) that chipping and capping can be reduced by modifying tablet shapes. In summary, the results obtained in the present study using the formulation mainly composed of active ingredient and mannitol were consistent with the reference studies performed using each of the different formulations. The formulations used in the reference studies were as follows. Chowhan (1992)[64] used a formulation composed of active ingredient, microcrystalline cellulose, lactose, starch, citric acid, povidone, methylcellulose, stearic acid, and magnesium stearate. Laity (2010)[65] and Furukawa (2015)[66] used a formulation composed of microcrystalline cellulose. Wu (2008)[62] used a formulation composed of lactose. Therefore, the observed effects of the tablet shapes on the occurrences of chipping and capping are considered reasonable, and will be applicable to not only the evaluated formulation in the present study, but to other formulations as well. To the best of the author's knowledge, the response surface plots of the effect of tablet shapes defined by *R1*/*DIA*, *R2*/*DIA*, and *C*/*DIA* on the occurrence of chipping and capping were developed for the first time. The verification study and the comparison with the previous studies suggested that the response surface plots are applicable to the selection of a single and double radius convex tablet shape, which has high mechanical strength, in various formulations containing several active ingredients and excipients having different physical and chemical properties.

Table 6 Predicted abrading and stress relaxation time of the tablet shapes used in Furukawa's report

Shape	*DIA*	*R1*	*R2*	*C*	*D*	*W*	*R1/DIA*	*R2/DIA*	*C/DIA*	A_{pred}	RT_{pred}
-	mm	mm	mm	mm	mg/mm^3	mg	-	-	-	%	s
Double radius convex	8.0	11	3.75	1.02	1.30	200	1.38	0.47	0.13	0.5	494.7
Single radius convex	8.0	12	12	0.65	1.30	200	1.50	1.50	0.08	1.2	528.1

As a matter of fact, the maximum allowable compression force of punches decreases as edge angle increases, which takes place when *R1*/*DIA* and *R2*/*DIA* decrease and *C*/*DIA* increases. The potential risk of tablet weight non-uniformity is also increased when *C*/*DIA* increases. The required fill depth in a tableting process to achieve the target weight increased when the *C*/*DIA* increased. Usually, the potential risk of incomplete die filling will increase as the required fill depth increases, which leads to tablet weight non-uniformity. Nevertheless, this identified relationship between the tablet shape and the mechanical strength is beneficial to the pharmaceutical industry, since this information could support the appropriate selection of a tablet shape for any given formulation, providing a lower risk of physical defects in tablets. Understanding the systematic relationship between tablet shapes and their mechanical strength against physical defects on the basis of abrasion and stress relaxation time can save significant resources, API, and reduce the formulation and process development time. It is expected that further root cause analysis of the chipping and capping employing not only the microscopic analysis based on SAXS and FE modeling, but also macroscopic analysis, such as the simulation of mechanical stress during material handling in manufacturing using a discrete element method, could serve to validate the observations in this study.

Conclusions

PLSR models successfully revealed the systematic relationship between tablet shape and the mechanical strength of tablets, i.e., abrasion and stress relaxation time. The PLSR models indicated that tablet abrasion and stress relaxation time significantly changed by varying *R1*/*DIA*, *R2*/*DIA*, and *C*/*DIA*. A verification study using commercial scale facilities proved that the optimum tablet shape of double radius deep or extra deep convex tablets have a lower occurrence of physical defects compared to the suboptimum examples as speculated by their abrasion and stress relaxation times. The observed effects of tablet shapes on the occurrences of chipping and capping were consistent with a general understanding according to previous studies based on microscopic analysis, such as SAXS, FE modeling, etc. Consequently, the identified optimum tablet shape was considered reasonable, and the response surface plots of the effect of tablet shapes defined by *R1*/*DIA*, *R2*/*DIA*, and *C*/*DIA* on the occurrence of chipping and capping will be applicable to other formulations beyond the successfully evaluated formulation in this study.

Case study 4 - Setting the process parameters for the coating process in order to assure tablet appearance based on multivariate analysis of prior data

International Journal of Pharmaceutics 511 (2016) 341–350

Contents lists available at ScienceDirect

International Journal of Pharmaceutics

journal homepage: www.elsevier.com/locate/ijpharm

Setting the process parameters for the coating process in order to assure tablet appearance based on multivariate analysis of prior data

Shuichi Tanabe[a,b,*], Hiroshi Nakagawa[a], Tomoyuki Watanabe[a], Hidemi Minami[a], Manabu Kano[c], Nora A. Urbanetz[b]

[a] Formulation Technology Research Laboratories, Daiichi Sankyo Co., Ltd., Hiratsuka 254-0014, Japan
[b] Pharmaceutical Development, Daiichi Sankyo Europe GmbH, Pfaffenhofen 85274, Germany
[c] Department of Systems Science, Kyoto University, Kyoto 606-8501, Japan

Outline

In case study 4, process modeling and optimization based on the PLSR model are studied in a batch coating process. As the coating process is a typical batch process and the final process in tablet manufacture, preparing a sufficient number of experimental results for DoE or for PLSR modeling is unrealistic. As the coating process is a thermodynamic process where the spray drying of coating suspension at the surface of tablet cores occurs, a traditional semi-empirical thermodynamic model is available to predict the moisture content and exhaust air temperature as the indicators of the process and the resultant tablet quality. However, to obtain a high prediction accuracy by the semi-empirical thermodynamic model a couple of preliminary experiments are needed anyway. On the other hand, if the coating equipment has been used previously in the manufacture of other products, the existing data set might be able to be used to develop a product-independent process model if the multicollinearity problem in the existing data were avoided. Therefore, the PLSR modeling of a coating process is demonstrated to show the prediction accuracy compared to the conventional semi-empirical thermodynamic model. The optimization of the coating process to improve the tablet appearance was performed as an example of practical application of the PLSR model in process development.

Abstract

Designing efficient, robust process parameters in drug product manufacturing is important to assure a drug's critical quality attributes. In this research, an efficient, novel procedure for a coating process parameter setting was developed, which establishes a prediction model for setting suitable input process parameters by utilizing prior manufacturing knowledge for partial least squares regression (PLSR). In the proposed procedure, target values or ranges of the output parameters are first determined, including tablet moisture content, spray mist condition, and mechanical stress on tablets. Following the preparation of predictive models relating input process parameters to corresponding output parameters, optimal input process parameters are determined using these models so that the output parameters hold within the target ranges. In predicting the exhaust air temperature output parameter, which reflects the tablets' moisture content, PLSR was employed based on prior measured data (such as batch records of other products rather than design of experiments), leading to minimal new experiments. The PLSR model was revealed to be more accurate at predicting the exhaust air temperature than a conventional semi-empirical thermodynamic model. A commercial scale verification demonstrated that the proposed process parameter setting procedure enabled assurance of the quality of tablet appearance without any trial-and-error experiments.

Keywords: Tablet film coating, Process parameter optimization, Scale-up, Multivariate analysis, Partial least squares regression (PLSR)

Introduction

The utilization of a tablet film coating process is recognized as one of the common unit operations in the pharmaceutical industry. In general, the film coating on pharmaceutical solid dosage forms aims at providing distinguishability, functionality, and elegance[8, 75]. Suitable process conditions that assure a desired product quality often depend on manufacturing scale, equipment used, and formulation, and thus process parameter settings have generally been researched at each scale in most current equipment and drug product formulations. Considering the concept of quality by design (QbD), a systematic approach defined in ICH Q8 should be applied for determining manufacturing process parameter settings to assure the desired product quality[3]. An enhanced approach for determining the functional relationships between process parameters and critical quality attributes (CQAs), such as tablet functionality and appearance, has been developed to realize more robust processes and higher assurances of the CQAs[6, 8]. Teckoe et al. (2013)[7] developed a design space through design of

[75] Knop, K., Kleinebudde, P., 2013. PAT-tools for process control in pharmaceutical film coating applications. Int. J. Pharm. 457, 527–536.

experiments (DoE) to visualize acceptable ranges of process parameters that can assure two CQAs, i.e., tablet appearance and disintegration time, within an acceptable process time. DoE is a typical approach for developing a reliable process model with minimal and well-organized experiments. As resources are limited and as the coating process is typically the final process of a tablet's manufacturing, it has been considered practically difficult to conduct many commercial scale experimental studies, even with the benefit of sophisticated DoEs to reduce the amount of experimentation and its impact on pharmaceutical companies. A significant workload reduction could be attained if prior knowledge (such as existing product batch records) is fully utilized for product-independent process modeling and optimization. The product-independent process models for assuring the CQA of tablet appearance require standardized product-independent output parameters. Macroscopic and microscopic moisture content, spray mist condition, and mechanical stress on tablets are the typical product-independent output parameters that affect tablet appearance[25], and the desired appearance can be attained by setting these four output parameters within their respective optimal ranges[76].

Regarding macroscopic and microscopic moisture content, exhaust air temperature T_{EA} and local moisture M_{LM}, defined as the maximum amount of water received in a single rotation, have been reported as macroscopic and microscopic indices, respectively, to derive desirable process parameters with less trial-and-error experiments[13, 76, 77]. Few models for the mist condition have been reported, i.e., size and distribution of mist droplets in the spray area, because this mist condition can be easily evaluated through an actual experiment without coating. Mechanical stress, which is the last parameter in the four output parameters affecting coating appearance, is difficult to measure directly; therefore, some computational simulation models for predicting the mechanical stress on tablets have been developed based on a discrete element method[78, 79]. However, from a viewpoint of practicality, it would not always be suitable for predicting the optimal coating parameter because of the huge workload involved in generating the simulation and the difficulty in validating the predicted mechanical stress on tablets. In this report, hence we focused on optimizing the former two parameters of macroscopic and microscopic moisture content by using prediction models, and the latter two of

---

[76] Pandey, P., Turton, R., Joshi, N., Hammerman, E., Ergun, J., 2006. Scale-up of a Pan-Coating Process. AAPS Pharm. Sci. Tech. 7, Article 102.

[77] Prpich, A., am Ende, M. T., Katzschner, T., Lubczyk, V., Weyhers, H., Bernhard, G., 2010. Drug product modeling predictions for scale-up of tablet film coating—A quality by design approach. Comput. Chem. Eng. 34, 1092–1097.

[78] Hancock, B. C., Mojica, N., St.John-Green, K., Elliott, J. A., Bharadwaj, R., 2010. An investigation into the kinetic (sliding) friction of some tablets and capsules. Int. J. Pharm. 384, 39–45.

[79] Kodam, M., Curtis, J., Hancock, B., Wassgren, C., 2012. Discrete element method modeling of bi-convex pharmaceutical tablets: Contact detection algorithms and validation. Chem. Eng. Sci. 69, 587–601.

mist condition and mechanical stress were determined based on the results of previous experience.

There is a traditional chemical engineering calculation used to justify the relationship between moisture content and temperature, however, the conventional model for predicting exhaust air temperature T_{EA} exhibits a challenge in its prediction accuracy. T_{EA} has been predicted by semi-empirical thermodynamic models[12, 13, 77]. In such semi-empirical thermodynamic models, the intrinsic heat loss for a given coater, which is required to predict T_{EA}, is determined based on a set of experimental data. However, it is difficult to identify the representative tablet surface temperature, which is needed to estimate the intrinsic heat loss based on the mass heat balance. Although exhaust air temperature is utilized as tablet surface temperature in some thermodynamic models, it is not identical to the tablet surface temperature within common coating equipment equipped with a non-circulation type drying system. This is due to a very short contact time between the inlet air and tablets. Since this deviation in the intrinsic heat loss leads to deteriorating prediction accuracy in the semi-empirical thermodynamic model, there is a need for building a precise prediction model for the exhaust air temperature.

Based on the above background, the issue that should be solved in setting these process parameters is to develop a more precise model that predicts the exhaust air temperature without a DoE study, leading to a reduced workload compared with sophisticated systematic experiments. In this work, a practical process parameter setting based on prior knowledge is performed at a commercial scale. In the proposed process parameter setting method, the output parameters of exhaust air temperature as an index of macroscopic moisture content, local moisture as an index of microscopic moisture content, mist condition, and mechanical stress on tablets were taken into account to assure the CQA of tablet appearance. As part of the proposed process parameter setting, a novel exhaust air temperature prediction model based upon multivariate analysis was developed and its prediction accuracy was compared with the conventional thermodynamic model. Since the prediction accuracy might deteriorate due to multicollinearity of process parameters when various manufacturing results are used instead of DoE results, partial least squares regression (PLSR) is used to construct the exhaust air temperature prediction model. PLSR is one of the linear regression methods that can solve the multicollinearity problem by using latent variables[14, 15]. Among the other output parameters, the local moisture MLM was calculated through a physical formula. No models were developed to predict the mist condition and mechanical stress on tablets in this work.

Materials and Methods

2.1. Materials

Eleven formulations (formulation A to K) were used in this study. All of these formulations were immediate release tablets with various shapes. The tablet coater used in this work was the AQUA COATER® AQC-17AF from Freund corporation, which is a typical drum coating apparatus. Both

input and output manufacturing data in the formulations A to J were derived from the corresponding batch records obtained over the past several years from the target coating machine.

2.2. Exhaust air temperature prediction

2.2.1. Conventional mass heat balance model

In the steady state of an aqueous coating process, the following mass heat balance equation applies:

$$Q = Q_E + Q_H + Q_L \qquad (1)$$

where Q is the difference in heat quantity between inlet and exhaust air, Q_E is latent heat of vaporization of water in the coating suspension, Q_H is sensible heat used to warm the water in the coating suspension to the tablet surface temperature, and Q_L is intrinsic heat loss of the coating equipment. In constant-pressure drying, the change of heat quantity is equal to the enthalpy change ($Q = \Delta H$) since changes in potential energy are negligible. On the basis of the mass heat balance equation (1), a semi-empirical thermodynamic model for predicting the exhaust air temperature was developed by am Ende and Berchielli (2005)[13]. In this model, tablet surface temperature is assumed equal to the exhaust air temperature, and the latent heat of water vaporization is fixed at 540 cal/g regardless of the tablet surface temperature. The intrinsic heat loss Q_L is calculated by equation (2), and it is described with the product of heat loss factor f_{HL} and difference in the temperature between exhaust air T_{EA} and operating room T_R[12, 13, 80].

$$Q_L = Q - (Q_E + Q_H) = f_{HL}(T_{EA} - T_R) \qquad (2)$$

where f_{HL} is defined as intrinsic heat efficiency that depends on the mechanical characteristics of the coating equipment, such as surface area; f_{HL} is not affected by manufacturing conditions. When the semi-empirical thermodynamic model was used in this study as the reference, the f_{HL} for a given coater was determined based on a set of experimental data provided in Table 1 as performed by Prpich (2010)[77]. The f_{HL} was varied as a fitting parameter to minimize the residual sum of squares (RSS) between the measured and the predicted exhaust air temperatures. The calculated f_{HL} which minimized the RSS was used to predict the exhaust air temperature for the given coater based on the Q, Q_E, and Q_H at the given process parameters. Q, Q_E, and Q_H are calculated through:

$$Q = M_{IA} C_{P,A} (T_{IA} - T_{EA}) \qquad (3)$$

$$Q_E = M_W H_{V,W} \qquad (4)$$

[80] Dewettinck, K., Visscher, A. D., Deroo, L., Huyghebaert, A., 1999. Modeling the steady-state thermodynamic operation point of top-spray fluidized bed processing. J. Food Eng. 39, 131–143.

$$Q_{\mathrm{H}} = M_{\mathrm{W}} C_{\mathrm{P,W}} (T_{\mathrm{EA}} - T_{\mathrm{C}}) \qquad (5)$$

and the exhaust air temperature T_{EA} is calculated by substituting equations (2), (3), (4), and (5) into equation (1).

$$M_{\mathrm{IA}} C_{\mathrm{P,A}} (T_{\mathrm{IA}} - T_{\mathrm{EA}}) = M_{\mathrm{W}} H_{\mathrm{V,W}} + M_{\mathrm{W}} C_{\mathrm{P,W}} (T_{\mathrm{EA}} - T_{\mathrm{C}}) + f_{\mathrm{HL}} (T_{\mathrm{EA}} - T_{\mathrm{R}}) \qquad (6)$$

$$T_{\mathrm{EA}} = \frac{M_{\mathrm{IA}} C_{\mathrm{P,A}} T_{\mathrm{IA}} + M_{\mathrm{W}} C_{\mathrm{P,W}} T_{\mathrm{C}} - M_{\mathrm{W}} H_{\mathrm{V,W}} + f_{\mathrm{HL}} T_{\mathrm{R}}}{M_{\mathrm{IA}} C_{\mathrm{P,A}} + M_{\mathrm{W}} C_{\mathrm{P,W}} + f_{\mathrm{HL}}} \qquad (7)$$

where $C_{\mathrm{P,A}}$ denotes specific heat of air (0.238 cal/g °C), $C_{\mathrm{P,W}}$ denotes specific heat of water (1 cal/g °C), $H_{\mathrm{v,w}}$ denotes latent heat of water vaporization (540 cal/g), M_{w} denotes spray rate of water (g/min), T_{EA} denotes exhaust air temperature (°C), and T_{IA} denotes inlet air temperature (°C). In this study, coating suspension temperature T_{C} (°C) was defined as being identical to room temperature T_{R} (°C) because the coating suspension was stored overnight in an air-conditioned operating room. Inlet air volume M_{IA} (g/min) was calculated from inlet air volume F_{IA} (m^3/min).

$$M_{\mathrm{IA}} = F_{\mathrm{IA}} \rho \qquad (8)$$

$$\rho = \frac{\mathrm{PM}}{\mathrm{R}(273.15 + T_{\mathrm{IA}})} \qquad (9)$$

where ρ (g/m^3) is air density in the coating pan at ambient pressure when the air follows ideal gas law, P denotes pressure of atmosphere (1.01325×10^5 Pa), M denotes mean molecular weight of ideal gas (28.8 g/mol), R denotes gas constant (8.31451 Pa m^3/mol K), and T_{IA} (°C) denotes inlet air temperature.

2.2.2. Partial least squares regression (PLSR)

The PLSR model was developed using the calibration set shown in Table 1. The process parameters that potentially affect the exhaust air temperature were used as input variables of the PLSR model to predict the exhaust air temperature. The employed eight input variables were inlet air temperature T_{IA} (°C), dew point temperature T_{D} (°C), room temperature TR (°C), absolute humidity of inlet air H_{IA} (g water/kg DA), inlet air volume F_{IA} (m^3/min), spray rate of water M_{W} (g/min), drum rotational speed D (rpm), and charge amount W_{T} (kg). The following preprocessing was applied in this study:

$$x_i^{\mathrm{P}} = \frac{x_i}{\sqrt{\frac{1}{N}\sum_{i=1}^{N} x_i^2}} \qquad (10)$$

where x_i and x_i^{P} are the ith experimental value and its preprocessed value, and N is the number of

samples in the calibration set. SIMCA® (Umetrics) was used to build the PLSR model. The number of latent variables was determined on the basis of the root-mean-square error of cross validation (RMSECV) of the leave-one-out cross validation.

Table 1 Calibration set consisting of 50 samples

No.	Formu-lation	T_D	H_{IA}	T_R	T_{IA}	F_{IA}	D	M_W	W_T	T_{EA}
		°C	g water/kg DA	°C	°C	m^3/min	rpm	g/min	kg	°C
1	A	20.9	9.488	22.8	70	40	2.0	268.7	162.92	48.6
2	A	20.8	9.252	22.8	70	40	3.0	275.9	162.92	48.9
3	A	21.0	9.360	22.8	70	40	6.0	386.6	162.92	45.1
4	A	24.9	7.797	22.6	70	40	6.0	384.8	187.52	44.4
5	A	26.2	4.686	22.0	70	40	6.0	384.4	190.14	44.7
6	A	25.0	6.457	22.5	70	40	2.0	275.3	191.49	47.5
7	A	25.3	6.802	22.5	70	40	3.0	275.8	191.49	47.4
8	B	25.3	4.925	22.5	70	40	3.0	320.3	186.12	46.4
9	B	24.5	6.054	22.5	70	40	2.0	329.5	190.26	45.3
10	B	25.5	6.404	22.5	70	40	6.0	384.3	190.26	44.3
11	B	26.6	9.331	22.0	70	40	2.0	321.1	191.95	46.4
12	C	23.9	10.403	22.1	72	50	4.0	437.2	332.24	47.4
13	C	24.1	10.741	22.1	72	50	7.0	492.6	332.24	46.7
14	C	23.5	10.381	22.2	75	50	3.0	325.3	306.30	51.7
15	C	24.2	11.022	22.2	72	50	5.0	489.4	306.30	46.6
16	C	24.0	10.680	22.2	72	50	7.0	491.8	306.30	47.0
17	D	23.3	10.264	22.8	72	50	4.0	424.7	337.37	48.0
18	D	23.7	10.500	22.8	72	50	7.0	492.9	337.37	46.8
19	D	23.5	10.593	22.2	73	50	4.0	438.2	299.15	48.5
20	D	23.7	10.714	22.2	73	50	8.0	492.4	299.15	47.4
21	D	26.1	3.374	22.1	75	50	3.0	341.6	340.87	50.1
22	D	26.0	3.354	22.1	72	50	4.0	401.6	340.87	48.5
23	D	26.4	3.650	22.1	72	50	7.0	452.6	340.87	47.6
24	E	23.0	10.296	22.0	70	50	2.5	434.5	325.23	45.5
25	E	23.3	10.473	22.0	70	50	4.0	434.1	325.23	46.6
26	E	23.8	10.560	22.0	68	50	2.0	439.9	307.65	44.0
27	E	23.8	10.560	22.0	70	50	5.0	492.9	307.65	44.5
28	E	25.8	8.352	22.4	78	50	2.5	440.7	343.21	50.1
29	E	25.8	8.564	22.4	80	50	4.0	439.9	343.21	53.3
30	E	24.0	9.016	22.4	85	60	2.5	331.4	326.32	61.7
31	E	24.1	9.071	22.4	85	60	4.0	331.1	326.32	63.9
32	E	23.7	9.228	22.6	80	60	2.5	322.9	339.06	56.4
33	E	23.9	9.151	22.6	80	60	4.0	330.5	339.06	58.6
34	E	24.6	9.350	22.3	80	55	2.5	329.4	341.34	55.6
35	E	24.6	9.152	22.3	80	55	4.0	330.9	341.34	57.5
36	E	24.4	9.237	22.2	80	50	2.5	330.2	341.74	54.1
37	E	24.4	9.237	22.2	80	50	4.0	329.6	341.74	55.8
38	F	24.2	9.512	22.1	63	50	4.0	417.0	497.63	41.9
39	F	23.1	7.995	22.6	63	50	4.0	410.2	497.47	42.0
40	G	24.1	9.071	22.1	63	50	5.0	415.9	482.38	42.5
41	G	24.0	2.790	22.4	63	50	5.0	414.7	482.98	42.4
42	G	23.9	3.330	22.4	63	50	5.0	414.2	482.98	42.1
43	H	25.4	2.830	22.7	70	50	6.0	486.9	385.23	44.8
44	H	25.3	9.381	22.6	70	50	3.0	436.2	347.66	45.8
45	H	23.9	5.202	22.6	70	50	4.0	435.9	360.29	46.0
46	I	23.1	9.526	22.7	70	50	4.0	437.3	370.17	45.8
47	I	25.9	8.489	23.0	70	50	3.0	434.9	375.39	46.2
48	I	25.1	8.349	23.0	70	50	6.0	488.4	375.39	44.9
49	J	23.8	10.775	22.2	73	50	3.0	429.9	307.35	48.4
50	J	23.7	10.714	22.2	72	50	2.0	494.9	307.35	46.2

2.2.3. Comparison of thermodynamic model and PLSR model

The prediction accuracies of the semi-empirical thermodynamic and the PLSR models were compared by calculating the root-mean-square error of prediction (RMSEP) in external validation using the test set provided in Table 2. The test set is independent of the batches in the calibration set, according to principle, with a different formulation (formulation K) or the same formulations

(formulations A to J) but different manufacturing batches.

Table 2 Test set consisting of 22 samples

No.	Formu-lation	T_D	H_{IA}	T_R	T_{IA}	F_{IA}	D	M_W	W_T	T_{EA}
		°C	g water/kg DA	°C	°C	m^3/min	rpm	g/min	kg	°C
1	A	23.8	5.819	22.6	70	40	2.0	275.6	187.52	47.3
2	B	25.4	6.604	22.5	70	40	3.0	327.6	190.26	45.9
3	B	25.8	9.407	22.0	70	40	6.0	374.1	191.95	44.8
4	C	23.5	8.931	22.3	72	50	7.0	487.7	338.98	46.4
5	E	25.6	7.418	22.5	79	50	2.5	437.4	339.10	50.6
6	E	25.8	7.718	22.5	80	50	4.0	438.0	339.10	53.3
7	E	23.5	9.301	22.0	80	50	2.5	329.4	337.09	52.1
8	E	23.8	9.284	22.0	80	50	4.0	328.7	337.09	53.7
9	E	24.5	9.293	22.0	80	50	2.5	329.1	337.56	54.2
10	E	24.7	9.207	22.0	80	50	4.0	330.8	337.56	55.8
11	F	24.5	9.293	22.4	63	50	4.0	416.9	497.85	42.1
12	F	22.9	8.254	22.0	63	50	4.0	409.3	497.45	42.3
13	G	24.5	2.875	22.4	63	50	5.0	418.9	482.96	42.0
14	H	25.7	2.638	22.7	70	50	3.0	441.7	385.23	45.7
15	H	25.6	10.733	22.6	70	50	4.0	437.3	347.66	46.0
16	H	24.3	5.764	22.6	70	50	6.0	489.6	360.29	44.7
17	I	23.4	9.480	22.7	70	50	3.0	435.5	370.17	45.7
18	I	23.3	9.636	22.7	70	50	6.0	487.3	370.17	44.7
19	I	25.7	8.635	23.0	70	50	4.0	436.7	375.39	46.3
20	K	23.4	10.323	22.4	73	50	2.0	398.6	286.22	49.4
21	K	23.5	10.381	22.4	73	50	3.0	398.7	286.22	49.9
22	K	23.7	10.500	22.4	73	50	6.0	465.7	286.22	48.4

2.3. Coating process parameter optimization

2.3.1. Proposed process parameter setting procedure

The proposed process parameter setting procedure aims to assure the desired appearance by corresponding output parameters being within the optimal range. This procedure was applied to formulation K, which is not included in the calibration set. As a first step, a cause and effect diagram of a typical non-functional film coating process was developed to summarize the relationship among the CQAs of tablet appearance, process time, output parameters, and input process parameters. As a second step, the target values of the input process parameters were set by optimization calculation based on the product-independent process models that predict exhaust air temperature, local moisture, and process time, whose details will be described in the next section. In the optimization calculation, the acceptable range of the process parameters potentially affecting the mist condition and the mechanical stress on tablets based on the cause and effect diagram were set as one of the constraints, keeping the output parameters within the appropriate range. Finally, an actual coating experiment was conducted with the specified process parameters at a commercial scale to verify the level of refinement evidenced by the process parameter setting procedure.

2.3.2 Models and constraints

As described in section 2.3.1, three models that predict exhaust air temperature, local moisture, and

process time were used in the proposed method. The exhaust air temperature was predicted by the PLSR model. To avoid extrapolation and consequently prevent unexpected errors in the prediction by the PLSR model, Kamohara et al. (2004)[74] proposed a PLSR-based framework, in which a PLSR model was integrated with an online monitoring system based on the concept of multivariate statistical process control (MSPC). MSPC has been widely used as practical technique for fault detection; Hotelling's *T2* and the sum of squared residuals *Q* (squared prediction error, SPE) have been used as monitored indices based on principal component analysis (PCA) [24, 73].

$$T^2 = \sum_{i=1}^{K} \frac{t_i^2}{s_{t_i}^2} \qquad (11)$$

$$Q = \sum_{p=1}^{P} (x_p - \hat{x}_p)^2 \qquad (12)$$

Here, K is the number of adopted principal components, t_i is the score of the ith principal component, $s_{t_i}^2$ is its variance, P is the number of input variables, and x_p and $\hat{x}_p$ are experimental and reconstructed values of the pth input variable. Muteki et al. (2011)[23] reported that the two distance criteria, T^2 and Q, could test the validity of the PLSR model under new input variables. In the present work, therefore, process parameter optimization was conducted with the constraint of 99% confidence intervals for both T^2 and Q.

$$T^2_{\text{predict}} \leq T^2_{99\%} \qquad (13)$$

$$Q_{\text{predict}} \leq Q_{99\%} \qquad (14)$$

A model which calculates the local moisture M_{LM}, defined as the maximum amount of water received in a single rotation, is provided as follows:

$$M_{\text{LM}} = \frac{M_{\text{W}} L_{\text{SA}}}{V_{\text{T}} S_{\text{SA}}} \qquad (15)$$

where M_{W} denotes spray rate of water (g/min), L_{SA} is distance that the spray tracks in the direction of the tablet flow (m), V_{T} is tablet velocity (m/min), and S_{SA} is spray area (m^2).

Process time was selected as an additional constraint, since it is necessary to keep the manufacturing efficiency at a certain level in commercial manufacturing. It is calculated from the amount of coating suspension W_{S} and the spray rate of suspension M_{S}:

$$\text{Process time} = \frac{W_{\text{S}}}{M_{\text{S}}} \qquad (16)$$

The necessary amount of coating suspension in one batch coating depends on the charged uncoated tablet amount, and loss of the suspension during processing. The loss of the suspension sprayed was assumed to be constant in the optimization.

The input process parameters were optimized based on the three models that predict exhaust air temperature, local moisture, and process time, by the generalized reduced gradient (GRG) method, which is one of the nonlinear programming methods[50]. The GRG method derives the approximated gradient of an objective function by moving each decision variable, i.e., process parameter. In this study, the combined index of T^2 and Q was selected as the objective function to be minimized to validate the predicted exhaust air temperature based on the PLSR model[81, 82, 83]. Based on the derived gradient, a better solution is searched iteratively until a local optimal solution is found within the predetermined constraints. Local optimal solutions are obtained by evaluating 100 randomly selected initial points of decision variables to find a global optimal solution.

In the optimization, reducing process time and consequently increasing efficiency was also considered. The manufacturing condition was designed to have three coating steps, in which drum rotation speed was increased step-by-step. In summary, the objective function $F(x)$ to be minimized was defined as the combined index of T^2 and Q in three coating steps:

$$F(x) = \lambda\left(\frac{T_{1st}^2}{T_{99\%}^2} + \frac{T_{2nd}^2}{T_{99\%}^2} + \frac{T_{3rd}^2}{T_{99\%}^2}\right) + (1-\lambda)\left(\frac{Q_{1st}}{Q_{99\%}} + \frac{Q_{2nd}}{Q_{99\%}} + \frac{Q_{3rd}}{Q_{99\%}}\right) \quad (17)$$

where λ denotes a weighing factor between 0 and 1. Because of the complimentary nature of T^2 and Q, λ was fixed to 0.5 to have the same weight in this study[83].

Results and Discussion

3.1. Comparison of semi-empirical thermodynamic model and PLSR model

Six latent variables were adopted into the PLSR model that predict exhaust air temperature on the basis of RMSECV. Figure 1 shows the external validation results; the RMSEP of the PLSR model was 0.80°C while that of the semi-empirical thermodynamic model was 1.76°C. It was confirmed that the PLSR model was more accurate than the semi-empirical thermodynamic model.

---

[81] Raich, A., Çinar, A., 1996. Statistical Process Monitoring and Disturbance Diagnosis in Multivariable Continuous Processes. AIChE J., 42, 995–1009.

[82] Kano, M., Fujiwara, K., 2013. Virtual Sensing Technology in Process Industries: Trends and Challenges Revealed by Recent Industrial Applications. J. Chem. Eng. Japan., 46, 1–17.

[83] Qin, S.J., 2012. Survey on data-driven industrial process monitoring and diagnosis. Annu. Rev. Control 36, 220–234.

Figure 1 External validation results of (a) semi-empirical thermodynamic model and (b) PLSR model. The prediction performance was evaluated on the basis of root-mean-square error of prediction (RMSEP) and correlation coefficient (r) between measured and predicted values of exhaust air temperature T_{EA}.

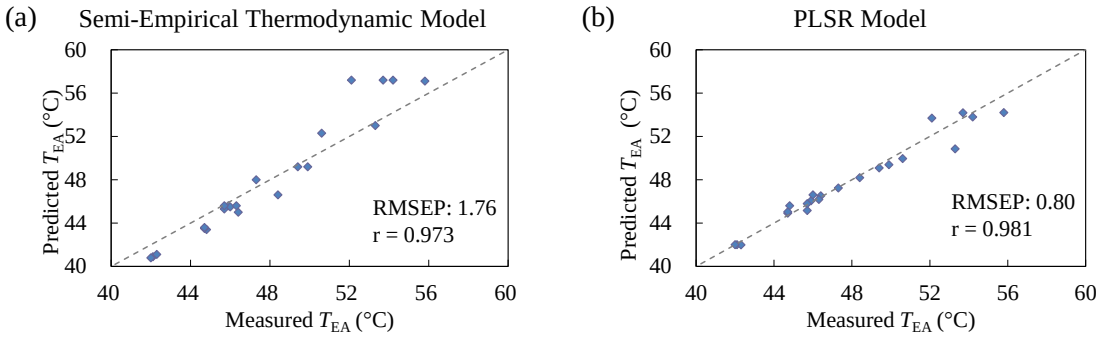

The reason for the lower prediction accuracy of the semi-empirical thermodynamic model can be explained as follows. In the semi-empirical thermodynamic model, the heat loss factor f_{HL} should be constant regardless of the operating condition[13], [77]. As shown in Figure 2, however, the individual f_{HL} were positively correlated to the T_{EA}. The individual f_{HL} were determined with equation (7) based on each of the experimental data provided in Table 1 and Table 2. The dependence of the exhaust air temperature on the difference in temperature between the tablet surface and the exhaust air was considered as the cause of this positive correlation. In general, tablet surface temperature is lower than the exhaust air temperature because of the evaporative cooling at the tablet surface. The difference in temperature between the tablet surface and the exhaust air is larger when the evaporation rate at the tablet surface is higher, which is typically the case with higher tablet moisture content. Therefore, Figure 2 (a) implies that the difference in temperature between the tablet surface and the exhaust air is larger in the lower exhaust air temperature, where the latent heat Q_H is overestimated by the semi-empirical thermodynamic model according to equation (5). Considering this correlation, the semi-empirical thermodynamic model, which assumes the tablet surface temperature is equal to the exhaust air temperature, can predict the exhaust air temperature precisely only when the difference in temperature between the tablet surface and the exhaust air of the batch to be predicted is just equal to the batch used to determine the f_{HL} of a given coater. In addition, the semi-empirical thermodynamic model does not take account of charge amount and drum rotational speed, both of which will affect intrinsic heat loss Q_L. It has been reported that the drying efficiency depends on the charged uncoated tablet amount and the bulk density in coating equipment[84]. As shown in Figure 2 (b), the individual

[84] Himmelblau, D. M., 1982. Basic principles and calculations in chemical engineering 4th edition. Prentice-Hall, Inc., Englewood Cliffs, N. J..

f_{HL} were negatively correlated to D, which implies that the drying efficiency is higher when the drum rotational speed is higher. Though the charged uncoated tablet amount was expected to correlate with the individual f_{HL}, there is no clear correlation that can be observed in the experimental data provided in Table 1 and Table 2. This might be explained by the fact that the effect of the charged uncoated tablet amount on the individual f_{HL} was smaller than that of the other factors such as T_{EA} and D. The above information indicates that in order to improve the prediction accuracy in the semi-empirical thermodynamic model, the f_{HL} needs to be calculated based on the set of experimental data, accounting not only for the difference in temperature between the tablet surface and the exhaust air, but also the drum rotational speed, and the charged uncoated tablet amount and should be similar to the expected condition, since the semi-empirical thermodynamic model does not consider the effects of these variations. If the prediction accuracy of the semi-empirical thermodynamic model shall be improved, multiple experiments in actual commercial scales will have to be conducted to confirm its accuracy.

Figure 2 (a) Relationship between T_{EA} and f_{HL} in the calibration set and the test set (n=72). (b) Relationship between D and f_{HL} in the calibration set and the test set (n=72).

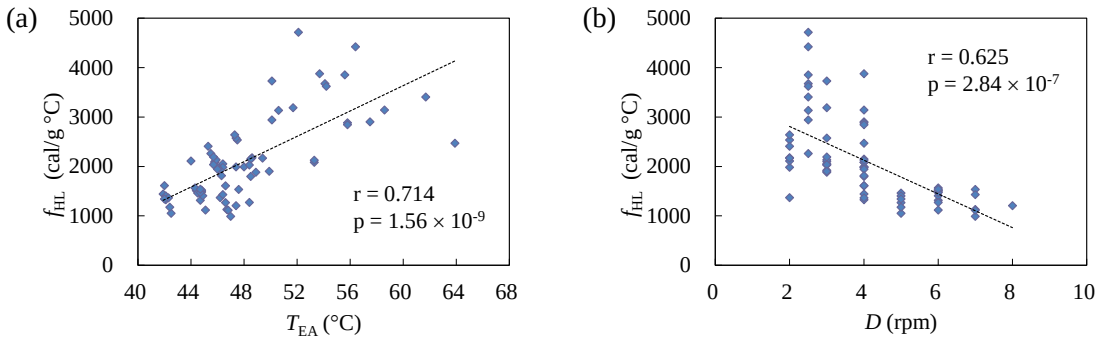

Previous batch records including other drug products' manufacturing should be used effectively to improve prediction accuracy of the exhaust air temperature. The PLSR can easily derive a more accurate model to predict T_{EA} by taking into account the input variables which are not considered in the semi-empirical thermodynamic model without additional experiments, if sufficient data are available. Table 3 shows the coefficients of each input variable of the PLSR model. The order of magnitude of the coefficients and the positive/negative effects of each input variable were matched to the empirical knowledge derived from the manufacturing data. Therefore, the PLSR model can test the robustness of the derived optimal coating process parameters for confirming the exhaust air temperature, if some of the process parameters have a certain range of variation. It was concluded that the PLSR model is more appropriate for the proposed process parameter optimization. The developed PLSR model is provided in equation (18).

$$T_{EA} = s^{y} \sum_{l=1}^{8} c_l \, x_l \big/ s_l^{x} \qquad (18)$$

where s^{y} and s_l^{x} denote the preprocessing factors of the exhaust air temperature and the *l*th input variables of the PLSR model summarized in Table 3, which are calculated from the calibration set according to equation 10, c_l denotes the coefficient of the *l*th input variable as provided in Table 3, x_l denotes the input variables of the PLSR models before preprocessing.

Table 3 Coefficients and preprocessing factors of PLSR model

Input variable		Coefficients	Preprocessing factor
Inlet air temperature	T_{IA}	0.6488	24.29479
Dew point temperature	T_{D}	0.0480	8.679321
Room temperature	T_{R}	0.0567	22.38176
Absolute humidity of inlet air	H_{IA}	0.0119	72.34584
Inlet air volume	F_{IA}	0.5556	49.10193
Spray rate of water	M_{W}	-0.2634	4.378356
Drum rotational speed	D	0.0265	404.0727
Charge amount	W_{T}	-0.0887	327.8024
Exhaust air temperature	T_{EA}	-	48.49255

3.2. Coating process parameter optimization

3.2.1. Typical issue in the conventional process parameter setting procedure

Prior to applying the proposed parameter setting method, a conventional parameter setting was applied to compare the quality of tablet appearance. In the conventional process parameter setting, the equivalent process parameters used in the comparable drug products based on the experts' experiences were applied. Figure 3 shows the tablets having poor appearance, which were found upon visual inspection of a batch manufactured based on the conventional process parameter setting procedure. Cracks and color variation were not observed, but blistering, i.e., filling of deboss, was found in most of the tablets. In general, blistering is caused by entrapment of gas in or under the film due to overheating during spraying. In addition, a small number of twinning tablets were also observed. Since this poor tablet appearance is unacceptable, this process parameter setting procedure requires further trial-and-error experiments to achieve a good quality of tablet appearance.

Figure 3 Appearance of film coated tablets: (a) appearance of the deboss in the conventional process parameter setting procedure (b) twinning observed in the conventional process parameter setting procedure (c) appearance of deboss in the proposed process parameter setting procedure

(a)  (b)  (c) 

3.2.2. Proposed process parameter setting

Risk assessment of a typical non-functional coating process was conducted to set the process parameters systematically. Table 4 shows the cause and effect diagram of a typical non-functional film coating process, which summarizes the relationship among the CQA of tablet appearance, process time, output parameters, and process parameters. Elements 1, i.e., the CQA of tablet appearance and process time, are the quality to be assured or a constraint of the process. Elements 2, i.e., the critical material attributes (CMAs) to assure the CQA of tablet appearance, are controlled properly; namely, it is necessary to make uniform films to prevent defects related to films such as blistering, bridging, or twinning, and to prevent physical defects of tablets such as cracks and abrasion. Elements 3 to assure the above CMAs, i.e., output parameters, vary depending on the variation of the input process parameters. Thus, Elements 1 can be finally assured by adopting the optimal combination of process parameters, i.e., the optimal coating conditions, so that all of Elements 3 (and Elements 2) will be kept within the optimal range.

Table 4 Cause and effect diagram of a typical non-functional film coating process

Elements 1	Elements 2	Elements 3 (output parameters)	Related process parameters
Tablet appearance (CQA)	Uniformity of films	Mist condition	Spray rate of water
			Spray air pressure
			Gun setting
			Gun species
			Water concentration in coating suspension
			Species of solid component in coating suspension
		Local moisture	Spray rate of water
			Drum rotational speed
			Charge amount
			Gun setting
			Gun species
	Elegance of the tablet surface	Mist condition	Spray rate of water
			Spray air pressure
			Gun setting
			Gun species
			Water concentration in coating suspension
			Species of solid component in coating suspension
		Exhaust air temperature	Inlet air temperature
			Dew point temperature
			Room temperature
			Absolute humidity of inlet air
			Inlet air volume
			Spray rate of water
			Drum rotational speed
			Charge amount
		Mechanical stress on tablets	Drum rotational speed
			Charge amount
Process time			Spray rate of water
			Spray air pressure
			Gun setting
			Amount of coating suspension sprayed

The optimal range of the exhaust air temperature and local moisture in formulation K were determined on the basis of the results of the eighteen batches of formulations A and B, because the formulations A, B, and K were manufactured using the same coating suspension. The exhaust air temperature T_{EA} that resulted in a good quality of tablet appearance of formulations A and B was determined as ranging from 44.2°C to 48.3°C. The T_{EA} in formulations A and B was designed to be gradually lowered in three steps from the initial spraying to the endpoint by changing process parameters to achieve a good quality of tablet appearance and shorten process time. Therefore, the target values of T_{EA} in the first, second, and third step were determined as 47.5°C, 47.0°C, and 45.5°C, respectively, to satisfy the acceptable range of T_{EA}, which was identified in the manufacture of formulations A and B, taking the maximum prediction error of 0.8°C in validation into account. The local moisture M_{LM}, calculated by equation (15), of the batches of formulations A and B with a good quality of tablet appearance was not more than 11 g/m^2 (data not shown). Typically, the risks of sticking and/or picking are increased when the M_{LM} is higher, since the cohesive and adhesive forces between tablet-tablet interfaces are higher when the moisture content is higher. The target range of M_{LM}, which was determined to be not more than 11 g/m^2, was judged as suitable to prevent such a failure in appearance. The acceptable range of the process time, the final output parameter represented by equation (16), was set to be not more than 280 min based on the previous manufacturing experiences.

To assure the remaining other two output parameters, i.e., mist condition and mechanical stress on tablets, acceptable ranges of the related process parameters were set based on experiments or previous manufacturing experience. Those relationships between the (input) process and output parameters are summarized as a part of Table 5. Regarding the mist condition, the upper limit for the spray rate at constant spray air pressure was determined through an actual experiment without coating, since the coating suspension, gun species, and gun setting in the manufacture of formulation K is the same as that in the formulations A and B. It was confirmed that the upper limit of M_W should be 494.9 g/min, which is the highest value in the calibration set, to keep the mist conditions such as size and distribution of mist droplets in the spray area acceptable. With respect to the mechanical stress on tablets, drum rotational speed and charged amount were judged to be factors which affect the mechanical stress on tablets. Since the robustness of the formulation K tablet core was comparable to formulations A and B, these process parameters were determined to be the same as formulations A and B.

Table 5 Relationships between process parameters and elements 3 (output parameters)

Process parameters	Output parameters				
	Exhaust air temp.	Local moisture	Mist condition	Mechanical stress on tablets	Process time
Inlet air temp.	Y	-	-	-	-
Dew point temp.	Y	-	-	-	-
Room temp.	Y	-	-	-	-
Absolute humidity of inlet air	Y	-	-	-	-
Inlet air volume	Y	-	-	-	-
Spray rate of water	Y	Y	Y	-	Y
Drum rotational speed	Y	Y	-	Y	-
Charge amount	Y	Y	-	Y	-
Spray air pressure	-	-	Y	-	Y
Gun setting	-	Y	Y	-	Y
Gun species	-	Y	Y	-	-
Water concentration in coating suspension	-	-	Y	-	-
Species of solid component in coating suspension	-	-	Y	-	-
Amount of coating suspension sprayed	-	-	-	-	Y

Y: The process parameter affects the output parameter
-: The process parameter doesn't affect the output parameter

In addition to the above target values and the acceptable ranges, some limits were set as constraints for optimizing the process parameters also provided in Table 5. To predict the potentially affecting environmental factors (weather, season, etc.) of the representative exhaust air temperature, the mean values of the dew point temperature, the room temperature, and the absolute humidity of inlet air in the calibration set were utilized in the optimization because they vary within a small range according to the weather and season. To keep a stable operation, the inlet air volume was set as constant at the three steps. The evaluation ranges of the process parameters to be optimized by the GRG method, i.e., inlet air temperature, inlet air volume, and spray rate of water, were set to be equal to those in the calibration set to optimize them efficiently. To summarize, inlet air temperature, inlet air volume, and spray rate of water were optimized by calculation to satisfy both the target values of the output parameters and the constraints as described in Table 6.

Table 6 Summary of process parameters optimization

Process parameters	1st step	2nd step	3rd step
T_{IA} (°C)	X	X	X
T_D (°C)	24.3	24.3	24.3
T_R (°C)	22.4	22.4	22.4
H_{IA} (g water/kg DA)	8.329	8.329	8.329
F_{IA} (m^3/min)	X	X	X
M_W (g/min)	X	X	X
D (rpm)	2	3	6
W_T (kg)	290	290	290
Constraints and targets	1st step	2nd step	3rd step
T_{EA} (°C)	47.5	47.0	45.5
M_{LM} (g/m^2)	Not more than 11		
Process time (min)	Not more than 280		
T_{IA} (°C)	Between 63 to 85		
M_W (g/min)	Between 268.7 to 494.9		
F_{IA} (m^3/min)	Between 40 to 60, constant during step 1 to step 3		
Hotelling's T^2	Not more than 21.67		
Q (*SPE*)	Not more than 0.0119		
(x)	Minimize, calculated according to equation (17)		

X: Calculated to satisfy constraints

The process parameters determined by the proposed procedure are provided in Table 7. To verify the robustness of the derived optimal coating process parameters, the influence of the normal variation in the process parameters on the exhaust air temperature was investigated. Among the process parameters, WT was expected to have a variation of within 280 kg to 300 kg due to the yields of the previous processes. When the normal variation ranges of T_D, T_R, and H_{IA} were assumed as the ranges of Table 1 and Table 2, the probability that the values of T_D, T_R, and H_{IA} lie outside of the interval $MV \pm \sqrt{2}SD$ did not exceed 0.5 according to the Chebyshev's inequality[85]. Herein, by considering the ranges of T_D, T_R, and H_{IA} as the possible variable ranges, the lowest and the highest exhaust air temperature within the possible variable ranges were predicted. Table 8 shows the predicted lowest and highest exhaust air temperatures in each coating step based on the PLSR model. Note that 1-H in Table 8 means the highest $T_{EA,\,pred}$ and 1-L meant the lowest T_{EA}, pred within the evaluated ranges of W_T, T_D, T_R, and H_{IA} in spray step 1. The Q of 1-H ($T_{EA,\,pred}$ = 48.1°C) exceeded the 99% confidence interval, which means that the predicted exhaust air temperature might be inaccurate. Therefore instead of the 1-H, one additional process condition (1-H') was evaluated in which H_{IA} was decreased to satisfy the 99% confidence interval of T^2 and Q. This was because H_{IA} showed the lowest impact on exhaust air temperature according to Table 3 and therefore the T_{EA}, pred at the 1-H' is close to the $T_{EA,\,pred}$ of 1-H. The exhaust air temperature was confirmed to be within the acceptable range of 44.2°C to 48.3°C when the W_T, T_D, T_R, and H_{IA} changed within the ranges. Note that the other process parameters

[85] Abramowitz, M., Stegun, I. A., 1972. . Handbook of Mathematical Functions: with Formulas, Graphs, and Mathematical Tables. New York: Dover.

were expected to remain constant. The results indicate that the exhaust air temperature at the optimized coating process parameters is expected to be sufficiently robust against expected process parameters' variations.

Table 7 Comparison of coating process parameters of formulation K

Coating conditions	Conventional method			Proposed method			Calibration set	
Coating steps	1	2	3	1	2	3	max	min
T_{IA} (°C)	73	73	73	67	70.5	71.5	85	63
T_D (°C)	23.4	23.5	23.7	24.3	24.3	24.3	26.6	20.8
T_R (°C)	22.4	22.4	22.4	22.4	22.4	22.4	23	22
H_{IA} (g water/kg DA)	10.323	10.381	10.500	8.329	8.329	8.329	11.022	2.790
F_{IA} (m^3/min)	50	50	50	48	48	48	60	40
M_W (g/min)	398.6	398.7	465.7	328.1	401.0	492.2	494.9	268.7
D (rpm)	2	3	6	2	3	6	8	2
W_T (kg)	286.22	286.22	286.22	290	290	290	497.63	162.92
$T_{EA, pred}$ (°C)	49.1	49.4	48.2	47.5	47.0	45.5	63.9	41.9
Hotelling's T^2	3.264	1.322	4.131	3.806	1.256	4.044	21.67[1)]	-
Q (*SPE*)	0.5369	0.4472	0.2441	0.0048	0.0004	0.0001	0.0119[1)]	-
M_{LM} (g/m^2)	14	11	9	11	11	10	-	-
Process time (min)	269 in total			278 in total			-	-

1: 99% confidence interval

Table 8 Robustness of optimized coating process parameters

Coating steps	T_D (°C)	T_R (°C)	H_{IA} (g water/ kg DA)	W_T (kg)	$T_{EA, pred}$ (°C)	Hotelling's T^2	Q (*SPE*)
1-H	26.0	22.8	11.682	280	48.1	9.197	0.0134[1)]
1-H'	26.0	22.8	10.405	280	48.0	6.952	0.0119
1-L	22.6	22.0	4.927	300	47.0	6.366	0.0062
2-H	26.0	22.8	11.682	280	47.6	3.973	0.0014
2-L	22.6	22.0	4.927	300	46.5	6.516	0.0053
3-H	26.0	22.8	11.682	280	46.0	6.253	0.0002
3-L	22.6	22.0	4.927	300	44.9	9.809	0.0061

1: Exceeded to the 99% confidence interval (0.0119)

Figure 3 (c) shows the appearances of coated tablets manufactured at the specified process parameters based on the proposed procedure. Total inspection proved that there was no bridging or twinning. T_{EA} was ranged from 44.8°C to 47.2°C; it was within the preset acceptable range of 44.2°C to 48.3°C. These results demonstrated that the proposed process parameter setting method can assure the desired quality of tablet appearance by controlling the output parameters systematically.

Conclusions

In the present work, a novel efficient process parameter setting procedure was successfully performed to assure the quality of tablet appearance in the film coating process, and an efficient process parameter setting of a particular formulation was realized without trial-and-error experiments and DoE. In the proposed process parameter setting procedure, the target values or ranges of output parameters, including the exhaust air temperature, the local moisture content of tablets, the mist

condition, and the mechanical stress on tablets, were derived, and then appropriate process parameters predicted by the models were identified by using the PLSR model for exhaust air temperature and the formulae for local moisture. The PLSR model to predict exhaust air temperature was developed by using existing batch records, and it achieved a higher prediction accuracy than the conventional semi-empirical thermodynamic model. In the commercial-scale experiment, the output parameters were successfully controlled within the appropriate ranges in the acceptable process time by setting appropriate target values of process parameters through the proposed process parameter setting procedure based on the cause and effect diagram. The results have demonstrated that the proposed process parameter setting procedure can contribute to the efficient scale-up of a tablet film coating process. As a matter of fact, the proposed process parameter setting procedure based on a PLSR model cannot be applied to coating equipment other than the one used for model establishment and the predictable range of the process conditions depends on the data used for the model development. However, the proposed approach is applicable and efficient because it does not require any preliminary experiments such as DoE when sufficient manufacturing batch records are available. Therefore, it can be concluded that the required workload and the cost for process parameter setting will be significantly decreased by applying the proposed approach. The whole approach demonstrated in this work is expected to stimulate PLSR based process development and optimization of a wide range of unit operations, including coating procedures with functional coatings, fluid bed granulation, and spray drying.

Acknowledgement

The authors would like to thank Powrex Co., Ltd. for practical advice.

Overall discussion

The approaches demonstrated in this thesis facilitate understanding of the process performance over a range of material attributes and process parameters with reasonable cost and will contribute to increase the assurance level of the drug product quality with a scientific rationale based on process modeling and the utilization for process control beyond the processes performed in the case studies. The advantages and limitations of the demonstrated process modeling approaches in the four case studies are discussed in the following section.

The computer-aided process modeling utilizing DEM coupled with statistical analysis as shown in case studies 1 and 2 was demonstrated to contribute in developing a process model cost-effectively. Even though up-scaling of particle size and/or down-scaling of geometry of equipment were needed when simulating systems such as > 1 kg due to the current computational capacity, a quantitative prediction of the output parameters was successfully demonstrated by taking the effect of those changes on the process outputs into account. With process simulation resources required in process development can be reduced by reducing the number of experiments needed for both setting the design space and NOR, which in turn accelerates process development. Process modeling by DEM is applicable to any process where particulate matter (particles, granules, or tablets) is involved in manufacturing processes such as transport, storage, blending, granulation, tableting, and coating[43]. However, most of the preliminary DEM based process modeling approaches were limited to capture qualitative trends[86, 87, 88] or quantitative analysis of large particles (> 1 mm in diameter) in experiments[89, 90] due to the inherent computational intensity. Nevertheless, quantitative prediction of the homogeneity will be possible by taking the scale effect based on the comparison of several DEM simulations at different geometry reduction levels and different particle size expansion levels into account and coupling with statistical analysis as demonstrated in case studies 1 and 2. The quantitative

[86] Boerner, M., Bueck, A., Tsotsas, E., 2017. DEM-CFD investigation of particle residence time distribution in top-spray fluidized bed granulation. Chem. Eng. Sci. 161, 187–197.

[87] Nakamura, H., Fujii, H., Watano, S., 2013. Scale-up of high shear mixer-granulator based on discrete element analysis. Powder Technol. 236, 149–156.

[88] Hildebrandt, C., Gopireddy, S.R., Scherlieβ R., Urbanetz, N.A., 2018. Simulation of particle size segregation in a pharmaceutical tablet press lab-scale gravity feeder. Adv. Powder Technol. 29, 765–780.

[89] Fries, L., Antonyuk, S., Heinrich, S., Palzer, S., 2011. DEM-CFD modeling of a fluidized bed spray granulator. Chem. Eng. Sci. 66, 2340–2355.

[90] Ramirez-Aragon, C., Alba-Elias, F., Gonzalez-Marcos, A., Ordieres-Mere, J., 2018. Segregation in the tank of a rotary tablet press machine using experimental and discrete element methods. Powder Technol. 328, 452–469.

in-silico simulation can provide clear correlations between input and output parameters, which are not biased by sampling errors and accidental fluctuations of the process that are the common disturbances in experiments. Those reliable in-silico experimental data at different process conditions will guarantee a better understanding and control of the process based upon accurate responses of the output parameters at given input parameters.

Further on, in case study 1 it was seen that there is a limitation of the level of particle size expansion and geometry reduction to conduct quantitative prediction at a reasonable computational time. As the number of particles in a system decreases by enlarging particle size and shrinking the geometry compared to reality, the effect of single particle performance increases, and above a certain level, the outputs of the DEM simulation do not any more reflect reality. In case study 1 a quantitative prediction of the blend uniformity was impossible when the active component whose homogeneity is to be tested exhibits large particle size distribution for example ranging from < 75 μm to > 500 μm in diameter. Even when considering approximately 350,000 particles at the active to placebo granule ratio of 15:85, there are only 15 particles corresponding to the original active granule particle size fraction of > 500 μm. In that case due to the huge contribution of single large-sized particle the probability density distribution of the blend uniformity calculated by DEM was not symmetric unimodal. As the symmetricity is the precondition of quantitative prediction based on the mean and RSD of the probability density distribution of blend uniformity, quantitative prediction of blend uniformity was not applicable. This issue can be resolved by changing the level of particle size expansion and geometry reduction more close to reality. However, it may diminish the benefit of in-silico simulation as it will require a long computational time. It should be noted that the simulation at the largest particle number run containing ca. 350,000 particles in case study 1 took more than 2 months to simulate 2 minutes blending. Long simulation time might be practically unacceptable considering the process development timeframe and hence experiments might be given preference over the simulation even when considering the cost benefit. In addition, since the existence of fluid/gas is neglected in case study 1, precise prediction of the homogeneity in a strict sense is still no possible with DEM alone, but would need a coupled approach of DEM and Computational Fluid Dynamics (CFD), which is a numerical method solving mass, momentum, and energy of fluids. This applies even more for processes where particles are significantly affected by the presence of a fluid/gas such as pneumatic conveying and die filling with suction pressure during tableting. Further, other critical output parameters in a particulate system such as hardness and porosity of the materials manufactured through compression of particles, e.g., dry granulation, tableting, and encapsulation, and particle size distribution after size reduction process, e.g., screening and milling, are out of evaluation scope in this thesis. It is expected to be captured by DEM simulation quantitatively in the next step.

The reliability and applicability of a process modeling approach based on alternative statistical analysis, i.e., PLSR, to a process where multicollinearity is involved was successfully demonstrated

in case studies 3 and 4. Optimizing tablet shape with respect to the tablets' physical resistance in the subsequent material handling is a typical multivariate problem as discussed in case study 3. A comprehensive visualization of the effect of tablet shape parameters on the physical robustness of the tablet and the tablet shape optimization based on the process model, which was impossible to address by DoE based approach, was demonstrated for the first time. As the response surface of the tablet shape parameters on the tablets' physical robustness were in good agreement with the verification study performed in case study 3 and previous studies where only very limited number of table shapes were compared, accuracy of the process model was shown. As demonstrated in case study 3 the advantage of the PLSR based process modeling is that it can provide a robust process model including a huge variety of input parameters and wide ranges of each input parameter even when multicollinearity is involved. While the resources required to prepare experimental data to build such a model was considered to be a common drawback of both DoE and PLSR based approaches, a solution to this drawback in PLSR modeling was demonstrated in case study 4. In case study 4 the optimization of the process conditions to control the exhaust air temperature was shown. The coating process is a typical batch process where multicollinearity is involved, therefore usually the experimental data performed at a commercial scale are required for PLSR modeling. To reduce the workload significantly the existing product batch records of other drug products were fully utilized for product-independent process modeling and optimization. Through the verification study, it was confirmed that the product-independent PLSR model was more accurate than the conventional semi-empirical thermodynamic model. An optimization of the process conditions to improve tablet appearance was successfully demonstrated with a minimal number of experiments.

However, the limitation in PLSR based process modeling when it comes to nonlinear relationships became apparent in this thesis. In case study 3 the abrasion was confirmed to be nonlinearly related to the tablet shapes and/or properties; the abrasion increased exponentially as the tablet becomes fragile. Though the negative effect of nonlinearity on prediction accuracy was reduced by base-10 log transformation in case study 3, that kind of transformation might be not always effective in increasing the prediction accuracy. Treating nonlinear PLSR as an extension of conventional PLSR has been proposed recently[91], however, its practicability and reliability have not been demonstrated yet and it is not implemented in commercial software. Further research is required to develop a statistical process modeling approach that can cope with both multicollinearity and nonlinearity and to utilize it for process development and control specifically for setting a design space and NOR to assure robust commercial manufacture.

[91] Rosipal, R., Yamanishi, Y., 2011. "Nonlinear partial least squares: An overview" in Chemoinformatics and Advanced Machine Learning Perspectives: Complex Computational Methods and Collaborative Techniques, IGI Global, pp. 169–189.

Outlook

To further facilitate a reliable and cost-effective process modeling in pharmaceutical dosage form development, quantitative prediction based on combined numerical approaches and an extended DEM technique as discussed below are considered as a next step as it can be applicable to a broader range of processes. CFD is a numerical method where the components are assumed to be a continuum and mass, momentum, and energy balances are solved numerically. CFD-DEM coupling is considered to be an appropriate solution to simulate processes where fluids and particulate matter is involved at the same time like fluid bed granulation/drying and pneumatic transportation[86, 89] where for example airflow affects the movement of discrete particles. The Finite Element Method (FEM), which is a different numerical approach where components are treated as a continuous material and the materials' elastic or elasto-plastic deformations are solved numerically, is suitable to describe a compression of densely packed particles such as in roller compaction and tableting processes[92, 93, 94]. Recently a research on DEM-FEM coupling to develop a dynamic process model in the roller compaction process has been reported where particles fed by the screw feeding are compressed to form ribbons[95]. There is another approach towards the elasto-plastic deformation by calculating an adhesive contact model based on DEM[96, 97]. In case study 1 only elastic collision is considered, however, by incorporating the plastic deformation based on the proposed theory, a compaction process and a size reduction process such as in roller compaction and subsequent screening can be numerically addressed. Although those numerical methods have a potential to contribute to process modeling, these approaches are limited to qualitative analysis or quantitative analysis of a laboratory scale process currently, due to the immense computational time required to simulate large-scale processes and the difficulties in verifying the

[92] Cunningham, J.C., Winstead, D., Zavaliangos, A., 2010. Understanding variation in roller compaction through finite element-based process modeling. Comput. Chem. Eng. 34, 1058–1071.

[93] Diarra, H., Mazel, V., Boillon, A., Rehault, L., Busignies, V., Bureau, S., Tchoreloff, P., 2012. Finite element method (FEM) modeling of the powder compaction of cosmetic products: comparison between simulated and experimental results. Powder Technol. 224, 233–240.

[94] Korok, A., Peciar, M., Fekete, R., 2014. Numerical investigation into the influence of the punch shape on the mechanical behavior of pharmaceutical powders during compaction. Particuology, 116–131.

[95] Mazor, A., Orefice, L., Michrafy, A., de Ryck, A., Khinast, J.G., 2017. A combined DEM & FEM approach for modelling roll compaction process. Powder Technol. Article in Press.

[96] Thornton, C., Ning, A, 1998. A theoretical mode1 for the stick/bounce behaviour of adhesive, elastic-plastic spheres. Powder Technol. 99, 154–162.

[97] Pasha, M., Dogbe, S., Hare, C., Hassanpour, A., Ghadiri, M., 2014. A linear model of elasto-plastic and adhesive contact deformation. Granular Matter 16, 151–162.

simulation outputs. However, once the quantitative process modeling based on the numerical approaches can be developed with feasible computational time, a better process understanding which leads to a higher quality assurance level and process robustness against uncontrollable variations such as raw material properties, seasonal effect, etc., will be gained for the processes beyond the blending process demonstrated in this thesis at reasonable cost. Such process modeling innovation will help protecting the environment by reducing the energies and resources required for the QbD approach.

On the other hand, even if the computer-aided process simulation is successfully applied, the computational time required for quantitative DEM simulation should still not be neglected. In such case, statistical process modeling based on a limited number of in-silico experimental results can streamline process development and the utilization for process control similar to the process modeling activities based on actual experiments as demonstrated in case studies 3 and 4. As mentioned in the overall discussion, the PLSR modeling utilized in this thesis is not able to cope with nonlinearity. This drawback needs to be addressed, as nonlinearity and multicollinearity may be involved at the same time in industrial processes[98]. Several nonlinear regression analyses are available and would have a potential to be utilized in process modeling and control[91]. Locally weighted PLSR (LW-PLSR) is one of the nonlinear regression methods based on PLSR[99]. In LW-PLSR, the similarity of a given input parameter condition (as a vector of input parameters) to the individual data in the calibration set is calculated based on a weighted Euclidean distance in the model, and the data having high similarity receive a larger weight in developing the localized prediction model to predict a given input parameter condition. The prediction accuracy of LW-PLSR was demonstrated to be higher than the conventional PLSR if the test set is well within the calibration set[99, 100], therefore it is potentially beneficial for process optimization within a given experimental data set. Meanwhile, in contrast to PLSR, up to now LW-PLSR does not have a clear criterion or a method how to avoid extrapolation, therefore the predicted result might be not reliable. To provide a comprehensive understanding of the process based on a model, a method to evaluate the extrapolation need to be developed for LW-PLSR. Gaussian process regression (GPR) is a different alternative nonlinear regression analysis, which also has a

---

[98] Hsu, S-H., Reklaitis, G.V., Venkatasubramanian, V., 2010. Modeling and Control of Roller Compaction for Pharmaceutical Manufacturing. Part I: Process Dynamics and Control Framework. J. Pharm. Innov. 5, 14–23.

[99] Kim, S., Kano, M., Nakagawa, H., Hasebe, S., 2011. Estimation of active pharmaceutical ingredients content using locally weighted partial least squares and statistical wavelength selection. Int. J. Pharm. 421, 269–274.

[100] Nakagawa, H., Tajima, T., Kano, M., Kim, S., Hasebe, S., Suzuki, T., Nakagami, H., 2012. Evaluation of infrared-reflection absorption spectroscopy measurement and locally weighted partial least-squares for rapid analysis of residual drug substances in cleaning processes. Anal. Chem. 84, 3820–3826.

potential to be used for a comprehensive understanding of a process[101, 102]. As GPR is a probabilistic model, it can predict the reliability of predicted response as error bars on the given input parameters. Hence, the GPR based process modeling has a potential to provide a comprehensive understanding of the processes where multicollinearity and nonlinearity are involved. However, it is not commonly used in the pharmaceutical industry. Further evaluation to apply nonlinear regression analysis for the process development is expected to facilitate the efficient and cost-effective process development.

[101] Rasmussen, C.E., Williams, C.K.I., 2006. Gaussian processes for machine learning. The MIT press, Cambridge, MA.

[102] Yuan, J., Wang, K., Yu, T., Fang, M., 2008. Reliable multi-objective optimization of high-speed WEDM process based on Gaussian process regression. Int. J. Mach. Tools Manuf. 48, 47–60.

Appendix

Abstract

To assure the drug products' quality in the mass-production for commercial distribution, process understanding and control based on a process model is a common and important process development activity in the pharmaceutical industry. The most common of many approaches to build a process model is the Design of Experiments (DoE) approach as recommended by the International Conference on Harmonisation of Technical Requirements for Registration of Pharmaceuticals for Human Use (ICH). However, this conventional process modeling approach has a challenge with respect to 1) the resources required to conduct experiments for DoE based modeling and 2) the prediction accuracy and the predictable range of the process model when multicollinearity is involved. The reason for the first challenge, i.e., huge resources required to develop a DoE based process model, is because most industrial processes show high scalability and hence typically DoE runs for design space and Normal Operating Range (NOR) setting need to be performed at commercial scale. The second challenge is also common in the industrial process and relates to multicollinearity, that cannot be described properly using DoE based process modeling, where the species and the ranges of the input parameters are limited if. These two challenges are addressed separately in the four case studies in this thesis.

In case studies 1 and 2 a computer-aided process simulation utilizing Discrete Element Method (DEM) was demonstrated to address the first challenge in a blending process to reduce the process development cost by substituting actual experiments with in-silico experiments. Quantitative prediction of the blend uniformity was successfully demonstrated, opening up the possibility to reduce the number of experiments in process development. To address the second challenge alternative statistical process modeling was applied for a process involving multicollinearity in case studies 3 and 4 where tablet shape had to be optimized in order to reduce the risk of physical defects and coating process optimization to assure the proper appearance of film-coated tablets. Process models were built based on Partial Least Squares Regression (PLSR), which can cope with mutually correlated parameters by using latent variables. The response surfaces were in good agreement with the verification study results, suggesting a high prediction accuracy for a process involving multicollinearity and a potential to develop a design space and NORs ensuring the desired quality.

While the advantages and applicability were demonstrated in the four case studies, the computer-aided process simulation and the alternative statistical process modeling approach also showed limitations and revealed the need to further facilitate effective and efficient process modeling. In the case studies 1 and 2 the DEM simulation was applied neglecting the existence of fluid/gas and elasto-plastic deformation. Hence to reproduce a process where solid particles are conveyed by fluid/gas and solid particle show plastic deformation, coupled numerical methods such as Computational Fluid

Dynamics (CFD)-DEM, DEM-Finite Element Method (FEM), and an extended DEM to incorporate the elasto-plastic deformation in DEM calculations are considered as a next step. With regard to the statistical process modeling as an alternative to the DoE based approach, the PLSR based modeling applied in case studies 3 and 4 has its limits when it comes to processes involving nonlinearity. Concluding, practicable process development approaches that can cope with both multicollinearity and nonlinearity need to be further developed to facilitate reliable process modeling for a broader variety of processes.

Kurzfassung

Um die Qualität der Arzneimittel in der Massenproduktion für den kommerziellen Vertrieb sicherzustellen, ist das Prozessverständnis und die Prozesssteuerung basierend auf einem Prozessmodell eine übliche und wichtige Prozessentwicklungsaktivität in der pharmazeutischen Industrie. Eines der gängigsten Verfahren ist die Entwicklung eines Prozessmodells mit Hilfe eines Design of Experiments (DoE), wie es von der International Conference on Harmonisation of Technical Requirements for Registration of Pharmaceuticals for Human Use (ICH) empfohlen wird. Der übliche Prozessmodellierungsansatz ist jedoch problematisch im Hinblick auf 1) die erforderlichen Ressourcen zur Durchführung von Experimenten für DoE-basierte Modellierung und 2) die Vorhersagegenauigkeit und dem vorhersagbaren Bereich des Prozesssmodells, wenn Multikollinearität vorliegt. Der Grund für die erste Herausforderung, nämlich dass große Ressourcen verbraucht werden, um ein DoE-basiertes Prozessmodells zu entwickeln, liegt darin, dass - wenn der Prozess wie die meisten industriellen Prozesse eine hohe Skalierbarkeit aufweist,- typischerweise DoE-Läufe für die Festlegung von Design Space und Normal Operating Ranges im kommerziellen Maßstab durchgeführt werden müssen. Die zweite Herausforderung kommt in industriellen Prozessen häufig vor und ist mit dem Problem der Multikollinearität verknüpft, die mit einem DoE basierten Prozessmodel nicht adäquat beschrieben werden kann, da Art und Bereiche der Inputvariablen limitiert sind. Diese beiden Herausforderungen werden in den vier Fallstudien dieser Arbeit gesondert behandelt.

In den Fallstudien 1 und 2 wurde an einem Mischprozess gezeigt, dass die erste Herausforderung durch eine computergestützte Prozesssimulation unter Verwendung von DEM adressiert werden kann, mit dem Ziel, die Prozessentwicklungskosten zu reduzieren, indem tatsächliche Experimente durch In-Silico-Experimente ersetzt wurden. Die quantitative Vorhersagbarkeit der Gleichmäßigkeit der Mischung wurde erfolgreich gezeigt, was die Möglichkeit eröffnet, die Anzahl der Experimente in der Prozessentwicklung zu reduzieren. Um der zweiten Herausforderung zu begegnen, wurde in den Falbeispielen 3 und 4 eine alternative statistische Prozessmodellierung für einen Prozess mit Multikollinearität angewandt, bei dem die Tablettenform im Hinblick auf die Vermeidung physikalischer Defekte und im Hinblick auf die anschließende Coatingprozedur sowie das Aussehen der überzogenen Tabletten optimiert werden sollte. Prozessmodelle wurden auf der Basis von Partial Least Squares Regression (PLSR) erstellt, die die miteinander korrelierten Parameter mithilfe von latenten Variablen bewältigen können. Die Response Surface Plots stimmten gut mit den Ergebnissen der Verifizierungsstudie überein, was auf eine hohe Vorhersagegenauigkeit für einen Prozess hindeutet, bei dem Multikollinearität existiert, und auch auf ein Potential zur Entwicklung von Design Space und NOR, die die gewünschte Qualität sicherstellen.

Während die Vorteile und Anwendbarkeit von Prozessmodellen in den vier Fallstudien gezeigt wurden, zeigten die computergestützte Prozesssimulation und der alternative statistische

Prozessmodellierungsansatz auch Einschränkungen und ließen die Notwendigkeit offenbar werden, die Prozessmodellierung im Hinblick auf Effektivität und Effizienz weiterzuentwickeln.. In den Fallstudien 1 und 2 wurde die DEM-Simulation angewendet, bei der das Vorhandensein von Flüssigkeit/Gas und elasto-plastischer Verformung vernachlässigt wird. Ein nächster Schritt, um Prozesse zu reproduzieren, bei dem feste Partikel durch ein Fluid oder Gas gefördert werden und feste Partikel plastische Verformung zeigen, wären daher an DEM gekoppelte numerische Verfahren wie z. B Computational Fluid Dynamics (CFD)-DEM, DEM-Finite Element Method (FEM) und ein erweitertes DEM zur Berücksichtigung der elasto-plastischen Verformung in der DEM-Berechnung. Im Hinblick auf die statistische Prozessmodellierung als Alternative zum DoE-basierten Ansatz weist die PLSR-basierte Modellierung, die in den Fallstudien 3 und 4 gezeigt wurde, eine Einschränkung bei der Modellierung nicht linearer Systeme auf. Zusammenfassend gilt es,in der Zukunft, Ansätze zu entwickeln, die sowohl Multikollinearität als auch Nichtlinearität bewältigen, um eine zuverlässige Prozessmodellierung für eine breite Palette von Prozessen zu ermöglichen.

Erklärung nach § 9 der Promotionsordnung

Hiermit erkläre ich gemäß § 9 der Promotionsordnung der Mathematisch-Naturwissenschaftlichen Fakultät der Christian-Albrechts-Universität zu Kiel, dass ich die vorliegende Arbeit, abgesehen von der Beratung durch meinen Betreuer, selbstständig und ohne fremde Hilfe verfasst habe. Weiterhin habe ich keine anderen als die angegebenen Quellen oder Hilfsmittel benutzt und die den benutzten Werken wörtlich oder inhaltlich entnommenen Stellen als solche kenntlich gemacht. Die vorliegende Arbeit ist unter Einhaltung der Regeln guter wissenschaftlicher Praxis entstanden und wurde bei keiner anderen Universität zur Begutachtung eingereicht. Mir wurde kein akademischer Grad entzogen.

Shuichi Tanabe

Acknowledgement

It is my pleasure to express my gratitude to all those who helped and supported me during my PhD.

First of all, I would like to express my sincere gratitude to Prof. Dr. Regina Scherlieβ for this precious opportunity to accomplish my PhD thesis under her supervision, for her patience, motivation, and kind support. I received generous guidance from her in writing this thesis.

I am also heartily thankful to PD Dr. Nora A. Urbanetz for her elaborated guidance, considerable encouragement, and invaluable discussion. Without her guidance and persistent help this dissertation would not have been possible.

Further thanks go to Dr. Tomoyuki Watanabe, Dr. Hiroshi Nakagawa, and Dr. Srikanth R. Gopireddy for their valuable cooperation in my research. Discussions with them have been insightful and make my research achievement great. I am also very grateful to my seniors in Daiichi Sankyo Co., Ltd. and Daiichi Sankyo Europe GmbH for making my PhD study possible by the financial support and consideration.

Finally, I would like to extend my indebtedness to my family, Naomi, Yoichi, and Yurika for their endless love, understanding, support, encouragement, and sacrifice throughout my study. Thank you for giving me freedom and support at the right time.